Fermilab

FERMILAB-THESIS-1996-58

Università degli Studi di Pavia

Dipartimento di Fisica Nucleare e Teorica

Dottorato di Ricerca in Fisica – VIII Ciclo

Fragmentation phenomena in perturbative QCD: Fragmentation Functions Approach and Parton Shower

Ph.D. Thesis of

Simona Rolli

Tutor: **Prof. Mario Greco**

Academic Year 1994/95

Index

Introduction

This is a phenomenological thesis dealing with fragmentation phenomena in perturbative QCD.

In the study of large p_t phenomena, depending on the kind of variables or distributions one is interested in, two different approaches are available for theoretical predictions: one is the analytical calculation of Parton Level (PL) amplitudes, convoluted with distribution functions describing intial and final state emission (structure and fragmentation functions) the other is the so called Parton Shower (PS) which describes in complete fashion the final state providing observable particles and allowing the generated events to be interfaced to a detector simulation.

In this thesis we will use in a complementary way both the methods, in order to study some fragmentation phenomena of interest like the inclusive single particle production at letpon and hadron colliders, jet fragmentation at hadron colliders, gluon radiation in jets physics.

The outline of the thesis is the following: after giving some brief re-

minds on QCD and deep inelastic phenomena in **Chapter I** we will describe the formalism of Fragmentation Functions in **Chapter II** along with the procedure used to extract them from e^+e^- data for light mesons to next-to-leading order. Two different approaches have been used: the first one based on NLO fit to data and the other one based on the use of a Parton Shower MonteCarlo. The agreament between the two approaches is indeed very good.

In **Chapter III** and **Chapter IV** we apply the formalism of Fragmentation Functions to study the inclusive single particle production at hadron-hadron and lepton-hadron colliders in a complete NLO formalism, giving predictions and comparing the results to data when available.

Finally in **Chapter V** we use the Parton Shower interfaced to a Parton Level matrix element calculation in order to study the production of $Wb\bar{b}$ plus jets.

References:

- a) M.Greco, S.Rolli, *Next-to-leading-order eta production at hadron colliders*, Zeitschrift für Physik C, 60 (1993) 169;
- b) P. Chiappetta, M. Greco, J.Ph. Guillet, S. Rolli, M. Werlen, *Next-to-leading-order determination of pion fragmentation functions*, Nuclear Physics B 412 (1994) 3;
- c) M. Greco , S. Rolli, A. Vicini,*Inclusive single particle photoproduction to next-to-leading order*, Zeitschrift für Physik C, 65 (1995) 277;
- d) M.Greco, S.Rolli, *Light mesons production at the Tevatron to next-to-leading order* Fermilab Pub-94-324-A, in press on Phys. Rev.D;
- e) L. Galtieri, M. Garcia-Sciveres, J. Lys, W.-M. Yao, S. Rolli, *Gluon radiation studies using the $W+ \geq 1$ jet sample*

CDF/ANAL/TOP/CDFR/3253;

- f) S. Rolli, *Production of Wbb plus jets*,
  CDF/DOC/MONTECARLO/CDFR/3321;

Chapter 1

Introduction to QCD

1.1 Introduction

In the Standard Model strong interactions are described by Quantum Cromo Dynamics (QCD) [1].

In this chapter we will briefly analyze some characteristics of this theory that explains with some accuracy several of the phenomenological aspects of processes in which we deal with hadron and their elementary constituents: quarks and gluons.

We will analyze the theoretical frame starting from the parton model successively improved with QCD corrections. We will consider in particular the concepts of asymptotic freedom and running coupling constant. Perturbative QCD (pQCD) will be shown to be a very good theory to

describe high transferred momentum processes. In the second part of the chapter we will consider the phenomenology of some basilar processes like deep inelastic scattering, e^+e^- annihilation into hadrons and hadron-hadron collisions.

1.1.1 Asymptotic freedom

Non abelian gauge theory without spontaneous symmetry breaking are renormalizable and asymptotically free. [1]

This property is quite crucial, and for this reason pQCD is a very good candidate to be the theory describing strong interactions, owing the fact that it incorporates and extends the description of deep inelastic scattering phenomena.

In this section we will give a simple introduction to the problem of scaling and its breaking: we will see renormaliztion group equations and running coupling constant and define an asymptotically free theory.

Asymptotic scaling and renormalization group equations

We will start considering a renormalizable theory with just one adimensional coupling constant. For large values of the external momenta ($p_i^2 = -x_i Q^2,\ Q^2 \to \infty$) one expects that physical observables become independent on mass term (in the limit to disregard all the terms of powers of mass divided by the scale of external momenta and when one is far from thresholds and all the observables are finite in the infrared limit, or with the mass going to zero -massless limit-) owing the fact that in the theory dimensional scale parameters are not left.

[1] We remember indeed that in the electroweak sector of the Standard Model this is not true and the running coupling constant grows when the scale is growing, contrary to what happens in QCD

As we know our theory is not completely specified by the bare Lagrangian, but we need a renormalization procedure in order to avoid ultraviolet divergences. This can be achieved for example via dimensional regularization, ie the reduction of space-time dimension to $n < 4$

$$\frac{d^4k}{(2\pi)^4} \to (\mu)^{2\epsilon}\frac{d^{4-2\epsilon}k}{(2\pi)^{4-2\epsilon}} \tag{1.1}$$

where $\epsilon = 2 - \frac{n}{2}$. Loop integrals (of type $\frac{d^nk}{(k^2+m^2)^2}$) will show poles at $\epsilon = 0$ and these singularities will be absorbed into the theory parameters. The μ scale is the point where the divergences are subtracted and the way we subtract them defines the rinormalization scheme.

We can choose to subtract just the pole $\frac{1}{\epsilon}$ and this is the Minimal Scheme (MS) of subtraction. Or we can subtract the combination:

$$\frac{1}{\epsilon} + \ln(4\pi) - \gamma_E \tag{1.2}$$

where γ_E is the Eulero constant, and this defines the modified minimal subtraction scheme ($\overline{MS}$). We will denote this convention as $\frac{1}{\bar{\epsilon}}$.

When we introduce the new scale μ to define a renormalized coupling constant, renormalized fields and so on, we introduce a different scale for the momenta, breaking the original scale invariance and making the physical quantities depending on the ratio Q/μ in the asymptotic limit.

Now let us consider in more detail one adimensional physical quantity S depending on a single parameter Q in a massless theory. As we saw before after the renormalization S will be function of $\frac{Q^2}{\mu}$ and α (it is itself function of μ). So, if we introduce:

$$t = \ln\left(\frac{Q^2}{\mu^2}\right), \tag{1.3}$$

we will have in general

$$S = S(t, \alpha). \tag{1.4}$$

The fact that S must not depend on the value of μ puts some stringent constraints on the functional form of S. Asking for invariance in respect to variation of the parameter μ is equivalent to establish the following Renormalization Group Equations (RGE):

$$\left[\frac{\partial}{\partial\mu^2} + \frac{\partial\alpha}{\partial \ln \mu^2}\frac{\partial}{\partial\alpha}\right] S(t,\alpha) = 0 \tag{1.5}$$

that, introducing the β-function

$$\beta(\alpha) = \frac{\partial\alpha}{\partial \ln \mu^2} \tag{1.6}$$

become:

$$\left[\frac{\partial}{\partial \ln \mu^2} + \beta(\alpha)\frac{\partial}{\partial\alpha}\right] S(t,\alpha) = 0 \tag{1.7}$$

and whom general solution is:

$$S(t,\alpha) = S(0,\alpha(t)), \tag{1.8}$$

where $\alpha(t)$ is the running coupling constant defined by:

$$t = \int_{\alpha}^{\alpha(t)} \frac{dx}{\beta(x)}. \tag{1.9}$$

We can say that RGE's imply that all the Q^2 dependence of S is manifested via $\alpha(t)$

For a generic Green function, , , RGE's are slightly complicated than (5). The relation between bare Green function (as calculated from the appropriate Feynman diagrams in terms of bare quantities and some cut-off M) and the renormalized ones is the following:

$$, _{UNR}(\frac{Q}{M}, x_i, \alpha_0) = Z_{\Gamma}, _{REN}(\frac{Q}{\mu}, x_i, \alpha), \tag{1.10}$$

where Q is the energy scale and x_i are fixed ratios of invariants in respect to variation of the scale, $\alpha_0(\alpha_s)$ is the bare (renormalized) coupling constant and Z_Γ is in general the product of renormalization factors for the fields.

RGE's for the Green function , are given by:

$$\left[-\frac{\partial}{\partial t}+\beta(\alpha)\frac{\partial}{\partial \alpha}+\gamma_\Gamma(\alpha)\right], _{REN}(t,x_i,\alpha)=0 \tag{1.11}$$

where $\gamma_\Gamma(\alpha)=\frac{1}{Z_\Gamma}\frac{\partial Z_\Gamma}{\partial \ln \mu^2}$ is the anomalous dimension. The solution is given by:

$$, (t,x_i,\alpha)= , (0,x_i,\alpha(t))exp\int_\alpha^{\alpha(t)}\frac{\gamma_\Gamma(x)}{\beta(x)}dx. \tag{1.12}$$

In order to evaluate (12) one needs to know $\beta(\alpha)$, $\gamma_\Gamma(\alpha)$ and $, (0,x_i,\alpha(t))$

Actually these quantities are known only in perturbation theory. We can build an asymptotic expansion for , in the case very important where $\alpha(t)\to 0$ per $t\to\infty$.

This is what we call Asymptotic Freedom, and a theory asymptotically free is the one where the running coupling constant tends to be zero for $t\to\infty$.

We will now briefly show the perturbative expansion for $\beta(\alpha)$ and the corresponding expressions for the running coupling constant.

We have:

$$\beta(\alpha)=-b\alpha_s^2(1+b'\alpha_s+O(\alpha_s^2)) \tag{1.13}$$

with

$$b=\frac{(33-2N_f)}{12\pi} \tag{1.14}$$

$$b'=\frac{153-19N_f}{2\pi(33-2N_f)} \tag{1.15}$$

where N_F is the number of flavors and the coefficients of the β-function are extracted from higher order corrections to quark-gluon and gluon-gluon vertices.

From equation (13) we derive

$$\frac{\partial \alpha_s(Q^2)}{\partial t} = -b\alpha_s^2(Q^2)[1 + b'\alpha_s(Q^2) + O(\alpha_s^2(Q^2))]. \tag{1.16}$$

We can solve (16) perturbatively. At first order (leading logarithm approximation) α_s is given by:

$$\alpha_s(Q^2) = \frac{\alpha_s(\mu)}{1 + \alpha_s(\mu)bt}, \tag{1.17}$$

while if we include even the second term (next-to-leading logarithm approximation) α_s is given by:

$$\alpha_s(Q^2) = \frac{2\pi}{b_0 \ln\left(\frac{Q^2}{\Lambda^2}\right)} \left(1 - \frac{b_0' \ln\left[\ln\left(\frac{Q^2}{\Lambda^2}\right)\right]}{b_0 \ln\left(\frac{Q^2}{\Lambda^2}\right)}\right), \tag{1.18}$$

where

$$b_0 = \frac{11}{6}N - \frac{1}{3}N_f \tag{1.19}$$

$$b_0' = \frac{17}{6}N^2 - \frac{5}{6}NN_f - \frac{1}{2}C_f N_f \tag{1.20}$$

$N = 3$ is the number of colors and N_f is the number of flavors with $C_f = \frac{(N^2-1)}{2N}$ and the asymptotically free regime is defined for $Q^2 >> \Lambda^2$.

The Λ parameter defined by:

$$\ln \frac{Q^2}{\Lambda^2} = -\int_{\alpha(t)}^{\infty} \frac{dx}{\beta(x)}, \tag{1.21}$$

represents the scale where the coupling becomes strong: it a universal parameter of QCD and its numerical value depends on the approximation used to calculate α_s from the effective number of flavors and the renormalization scheme. From phenomenology of deep inelastic processes we have $\Lambda = \mathrm{O}(200\ \mathrm{Mev})$ for $N_F = 5$.

1.2 Deep inelastic scattering

1.2.1 The naif parton model

Let us consider deep inelastic scattering of a photon of large invariant mass Q on a hadronic target (ie a proton). If k and k' are the four-momenta of ongoing and outgoing leptons and $q = k - k'$ is the transferred four-momentum and p is the four-momentum of the proton, we have the following variables describing the kinematics:

$$Q^2 = -q^2, \quad p^2 = M^2, \tag{1.22}$$

$$x = \frac{Q^2}{2pq} = \frac{Q^2}{2M(E - E')}, \tag{1.23}$$

$$y = \frac{q \cdot p}{k \cdot p} = 1 - \frac{E}{E'}, \tag{1.24}$$

where the energies are defined in the reference frame where the proton is at rest.

The differential cross section is given by:

$$\frac{d\sigma}{dxdy} = \frac{8\pi\alpha^2}{Q^2 y}\left[\frac{y^2}{2}W_1(x, Q^2) + (1 - y)\frac{Q^2 W_2(x, Q^2)}{4x^2}\right], \tag{1.25}$$

where we disregard the initial hadronic mass , and W_1 and W_2 are the structure functions. At large Q^2, in the first experiments at SLAC [2], it was shown that F_1 and F_2 can be derived from W_1 and W_2 and they were approximatively independent on Q^2:

$$W_1(x, Q^2) \to F_1(x), \tag{1.26}$$

$$\nu W_2(x, Q^2) \to F_2(x). \tag{1.27}$$

This is the so called Bjorken scaling, valid in a simple parton model where we are not considering internal interactions in the hadron. In this model if we sit in the frame where the impulse is infinite, and we consider the photon scattering on a pointlike quark with charge e_q and proton impulse fraction ξ, we obtain for the effective cross section (we are disregarding the masses) the following expression:

$$\frac{d\sigma}{dxdQ^2} = \frac{4\pi\alpha^2}{Q^4}[1+(1-y)^2]\frac{e_q^2}{2}\delta(x-\xi) \tag{1.28}$$

from this we can derive the expressions for the structure functions:

$$F_2 = xe_q^2\delta(x-\xi) = 2xF_1. \tag{1.29}$$

If we define $q(\xi)d\xi$ as the probability for a quark q to have a fraction of the impulse in the range between ξ and $\xi + d\xi$ and assume incoherent photon scattering on the quark, we obtain:

$$F_2 = \sum_q \int_0^1 d\xi q(\xi) x e_q^2 \delta(x-\xi) = \sum_q e_q^2 x q(x) \tag{1.30}$$

1.2.2 QCD corrections

In QCD, the original scale invariance is broken by logarithmic terms of the type $\ln Q^2$.

Indeed, if we consider corrections of order α_s to the reaction $eq \to eq$, i.e. the virtual and real emission of a gluon, we obtain in the $\overline{MS}$ scheme:

$$\frac{1}{u}F_2^q(u,M^2) = e_q^2[\delta(1-u) + \frac{\alpha_s}{2\pi}\theta(1-u)(P_{qq}(u)(-\frac{1}{\bar{\epsilon}}) + \\ + P_{qq}(u)\ln(\frac{Q^2}{M^2}) + c_{qq}(u))], \tag{1.31}$$

$$\frac{1}{u}F_2^g(u,M^2) = \sum_q e_q^2[\frac{\alpha_s}{2\pi}\theta(1-u)(P_{qg}(u)(\frac{1}{\bar{\epsilon}}) + \\ +P_{qg}(u)\ln\frac{Q^2}{M^2}) + c_{qg}(u))], \tag{1.32}$$

where F_2^g and F_2^q are the two terms of the structure function corresponding to a electron-quark diffusion and electron-gluon one, $u = x/\xi$ and M will be defined below. P_{qq}, P_{qg}, c_{qq}, c_{qg} are calculable in the frame of perturbative theory and they will be specified below. Integrals containing infrared and collinear divergences has been regularized and the singularities appear as poles in $1/\epsilon$. If we we should not use dimensional regularization but for examples we should introduce a little mass for the gluon in order to regularize the singolarities divergencies should appear as logarithms of the regularizing masses.

Let us now introduce distribution functions for quarks, $q(\xi)$, and gluons, $g(\xi)$. If we choose to define the distribution functions in order they are independent on the scale M we have:

$$F_2(x,M^2) = \sum_q e_q^2 x q(x,M^2), \tag{1.33}$$

and equations (31) and (32) gives rise to the following relations:

$$q(x,M^2) = q(x) + \frac{\alpha_s}{2\pi}\int_x^1 \frac{d\xi}{\xi}q(\xi)[P_{qq}(\frac{x}{\xi})(-\frac{1}{\epsilon} + \ln\frac{Q^2}{M^2}) + c_{qq}(\frac{x}{\xi})] + \\ +\frac{\alpha_s}{2\pi}\int_x^1 \frac{d\xi}{\xi}g(\xi)[P_{qg}(\frac{x}{\xi})(-\frac{1}{\epsilon} + \ln(\frac{Q^2}{M^2}) + c_{qg}(\frac{x}{\xi})]. \tag{1.34}$$

The $\epsilon \to 0$ limit is interpreted in the following way: we absorb the collinear singularities into the bare, non measurable, distribution $q(x)$ in order to define a physical quantity $q(x,M^2)$, to the factorization scale M, that is the analogous of the renormalization scale μ we saw above. P_{ij}

have a simple probabilistic meaning and for this we address the reader to Appendix A.

PQCD does not give absolute predictions for the renormalized distributions $q(x,Q^2)$, nevertheless we can define the Q^2 evolution. If we define $t = \ln \frac{Q^2}{M^2}$ we obtain:

$$\frac{d}{dt}q(x,t) = \frac{\alpha_s(t)}{2\pi}\int_x^1 \frac{d\xi}{\xi}[q(\xi,t)P_{qq}(\frac{x}{\xi}) + g(\xi,t)P_{qg}(\frac{x}{\xi})]. \tag{1.35}$$

This equation is the analogous of the one describing the evolution of α_s with Q^2 and it has been known as Lipatov-Altarelli-Parisi equation [3].

More in general evolution equations are of the following form:

$$\frac{d}{dt}\begin{pmatrix} q(x,t) \\ g(x,t) \end{pmatrix} = \frac{\alpha_s(t)}{2\pi}\times \tag{1.36}$$

$$\int_x^1 \frac{d\xi}{\xi}\begin{pmatrix} P_{qq}(\frac{x}{\xi},\alpha(t)) & P_{qg}(\frac{x}{\xi},\alpha(t)) \\ P_{gq}(\frac{x}{\xi},\alpha(t)) & P_{gg}(\frac{x}{\xi},\alpha(t)) \end{pmatrix}\begin{pmatrix} q(\xi,t) \\ g(\xi,t) \end{pmatrix}. \tag{1.37}$$

At Born level kernels have the following perturbative development:

$$P_{ij}(z,\alpha_s) = P_{ij}^0(z) + \frac{\alpha_s}{2\pi}P_{ij}^{(1)}(z) + \ldots \tag{1.38}$$

Physically P_{ij} rappresent the probability to find a parton of type i inside a parton of type j with impulse fraction x and negligible transverse momentum in respect to the scale M.

For sake of clarity we should say that the probabilistic interpretation for splitting functions is valid just at Born level (leading logs approximation) To this order kernels are given by:

$$P_{qq}^0(x) = C_F\left[\frac{1-x^2}{(1-x)_+} + \frac{3}{2}\delta(1-x)\right], \tag{1.39}$$

$$P_{qg}^0(x) = T_R[x^2 + (1-x)^2] \quad con \;\; T_R = \frac{N_F}{2}, \tag{1.40}$$

$$P^0_{gq} = C_F \left[\frac{1-(1-x)^2}{x} \right], \tag{1.41}$$

$$P^0_{gg}(x) = 2N \left[\frac{x}{(1-x)_+} + \frac{1-x}{x} + x(1-x) \right] + \delta(1-x) \frac{11N - 4T_R}{6}, \tag{1.42}$$

where +distribution are defined as:

$$\int_0^1 dx f(x)[g(x)]_+ = \int_0^1 dx [f(x) - f(1)]g(x), \tag{1.43}$$

Finally $c_{ij}(u)$-functions defined in equations (31) (32) (34) rappresent finite factors in the parton distributions and they depend on the process chosen to define the structure functions.

1.3 e^+e^- annihilation into hadrons

Let us consider the inclusive hadron production:

$$e^+e^- \to H + X. \tag{1.44}$$

In the naif parton model, if we don't consider effects due to weak interactions, the differential cross sections in θ and E is given by:

$$\sigma^H(z, \cos\theta) = \frac{3}{8}(1 + \cos^2\theta)\sigma^H_T(z) + \frac{3}{4}(1 - \cos^2\theta)\sigma^H_L(z), \tag{1.45}$$

where in the center of mass frame θ is the angle of the hadron with the beam and z is proportional to the energy of the hadron.

If we considering p as the four-momentum of the hadron and q as the four-momentum of the photon we have:

$$q^2 = Q^2, \qquad z = \tfrac{2pq}{Q^2}.$$

In the parton model, after integration over θ one has:

$$\sigma_L^H(z) = 0 \tag{1.46}$$

and

$$\sigma_T^H(z) = 3\sigma_0 \sum_{a=1}^{f} [D_{0q_a}^H(z) + D_{0\bar{q}_a}^H(z)], \tag{1.47}$$

where $D_{0q_a}^H(z)$ is the type H hadron density inside the quark q_a with fraction z of energy of the quark and

$$\sigma_0 = \frac{4\pi\alpha^2}{3Q^2} \tag{1.48}$$

is the total $e^+e^- \to \mu^+\mu^-$ cross section.

If we want to take into account the QCD corrections, to first order in α_s we have to consider the tree level reaction $e^+e^- \to q\bar{q}g$ and the one-loop reaction $e^+e^- \to q\bar{q}$.

The naif parton model relations are modified and we assist to logarithmic violation to the original scaling. Defining $t = \ln(\frac{Q^2}{M_f^2})$ where M_f is the fragmentation scale (analogous to the factorization scale) we obtain:

$$\sigma_L^H(z) = 3\sigma_0 \frac{4}{3}\frac{\alpha_s}{2\pi}\left[\int_z^1 \frac{dy}{y}(\sum_{a=1}^{f} e_a^2[D_{0q_a}^H(\frac{z}{y}) + D_{0\bar{q}_a}^H(\frac{z}{y})] + \sum_{a=1}^{f} e_a^2 D_{0g}^H(\frac{z}{y})\frac{(1-y)4}{y})\right], \tag{1.49}$$

and

$$\sigma_T^H(z,t) = 3\sigma_0 \int_z^1 \frac{dy}{y}\sum_{a=1}^{f} e_a^2[D_{0q_a}^H(\frac{z}{y}) + D_{0\bar{q}_a}^H(\frac{z}{y})][\delta(1-y) + \frac{\alpha_s}{2\pi}tP_{qq}(y) + \alpha_s d_q(y)] + 2\sum_{a=1}^{f} e_a^2 D_{0g}^H(\frac{z}{y})[\frac{\alpha_s}{2\pi}tP_{gq}(y) + \alpha_s d_g(y)], \tag{1.50}$$

where d_g and d_q are the subleading finite terms given in Appendix D.

As for the case of deep inelastic scattering, singularities are absorbed in bare fragmentation functions in order to define a renormalized fragmentation function to the scale M_f. In this case too the factorization schemes can be different. The relation between bare fragmentation functions and renormalized ones is the following:

$$D_q^H(z,t) = \int_z^1 \frac{dy}{y}\left(D_{0q}^H(y)[\delta(y-1) + \frac{\alpha}{2\pi}tP_{qq}(y) + \alpha_s d_q(y)] + \right. \\ \left. + D_{0G}^H\left(\frac{z}{y}\right)\left[\frac{\alpha_s}{2\pi}tP_{Gq}(y) + \alpha_s d_G(y)\right]\right). \quad (1.51)$$

Starting from the previous equation one can demonstrate that the fragmentation functions evolve with the scale M_f in accordance to the following equations:

$$\frac{\partial D_q^H(z,M_f^2)}{\partial \ln(M_f^2)} = \frac{\alpha_s(M_f^2)}{2\pi}\int_z^1 \frac{dy}{y}\left[P_{qq}^T(y,\alpha_s(M_f^2))D_q^H(\frac{z}{y},M_f^2) \right. \\ \left. + P_{gq}^T(y,\alpha_s(M_f^2))D_g^H(\frac{z}{y},M_f^2)\right] \quad (1.52)$$

$$\frac{\partial D_g^H(z,M_f^2)}{\partial \ln(M_f^2)} = \frac{\alpha_s(M_f^2)}{2\pi}\int_z^1 \frac{dy}{y}\left[P_{qg}^T(y,\alpha_s(M_f^2))D_q^H(\frac{z}{y},M_f^2) \right. \\ \left. + P_{gg}^T(y,\alpha_s(M_f^2))D_g^H(\frac{z}{y},M_f^2)\right]. \quad (1.53)$$

We note that the fragmentation functions evolution equations kernels are different from the ones of structure functions: the equality is valid just at leading order.

Let us see now how it is possible to maintain a relation of the type of (47) and how it is possible to relate fragmentation functions to physically measurable quantity like a cross-section. [4]

Let us consider equations (49) and (50). From the first one, remembering the sum rules for the momenta, we can deduce:

$$\sum_H \int_0^1 dz \frac{1}{2} z \sigma_L^H(z) = 3\sigma_0 (\sum_{a=1}^{f} e_a^2) \frac{\alpha_s}{\pi}. \tag{1.54}$$

If we consider that the cross section for $e^+e^- \rightarrow$ hadrons is given by:

$$\sigma_{TOT} = 3\sigma_0 \sum_{a=1}^{f} e_a^2 (1 + \frac{\alpha_s}{\pi}), \tag{1.55}$$

we can see that the entire correction to the cross section σ_{TOT} is given totally by σ_L^H and then:

$$\sum_H \int_0^1 dz \frac{1}{2} \sigma_T^H(z,t) = 3\sigma_0 \sum_{a=1}^{f} e_a^2, \tag{1.56}$$

without corrections of order α_s.

In the same way as for the leptoproduction, where we required that the relation between structure functions and quark distribution functions was the same as in the naif parton model, here we will define effective fragmentation functions in terms of physical measurable quantities. We adopt the following description:

$$\sigma_T^H(z,t) = 3\sigma_0 \sum_{a=1}^{f} e_a^2 [D_{q_a}^H(z,t) + D_{\bar{q}_a}^H(z,t)] \tag{1.57}$$

without corrections of order α_s.[2]

[2] This definition corresponds to interpret the entire transverse cross section as due to two-jets events. We could indeed choose the effective fragmentation functions in a different way. If we have:

$$\sigma^H(z,t) = 3\sigma_0 \sum_{a=1}^{f} e_a^2 [1 + \frac{\alpha_s(t)}{\pi}] (\bar{D}_{q_a}^H(z,t) + \bar{D}_{\bar{q}_a}^H(z,t)) \tag{1.58}$$

we can see that both the sum rules for charge and momentum conservation are not

We immediately obtain the formula for σ_L in terms of the effective fragmentation functions, trading the coupling constant with the running one and the bare fragmentation functions with the renormalized ones, which depend on t:

$$\sigma_L^H(z,t) = 3\sigma_0 \frac{4}{3}\frac{\alpha_s(t)}{2\pi}\left[\int_z^1 \frac{dy}{y}(\sum_{a=1}^{f} e_a^2[D^H_{0q_a}(\frac{z}{y},t) + D^H_{0\bar{q}_a}(\frac{z}{y},t)] + \sum_{a=1}^{f} e_a^2 D^H_{0g}(\frac{z}{y},t)\frac{(1-y)4}{y})\right]. \quad (1.59)$$

1.4 Hadron-hadron collisions

Let us consider high transfer momentum reactions, in which we have intial state hadrons. These kind of reactions give rise to jets production or single particle production of large momentum and are described by QCD in the following way.

The effective two hadrons scattering cross section can be written in this way:

$$\sigma(P_1,P_2,\theta) = \sum_{i,j}\int dx_1 dx_2 F_i(x_1,M)F_j(x_2,M)d\sigma_{ij}(p_1,p_2,\alpha(\mu),Q), \quad (1.60)$$

P_1 and P_2 are the four-momenta of the incoming hadrons; $p_1 = x_1P_1$ and $p_2 = x_2P_2$ are the four momenta of the partons participating to the hard subprocess, $F_i(x,M)$ are the distribution functions defined by the

affected by order α_s correction (as it was before for the charge sum rule). Nevertheless from an aestethical point of view the first choice tells us that a fraction of events to order α_s is actually due to three-jets events, and the angular distribution for σ_T^H $(1+\cos^2\theta)$ is more appropriate for $q\bar{q}$ production.

factorization scale M, and Q is the characteristic process scale (eg the transverse momentum of the jet). μ is an arbitrary parameter chosen of order of Q scale characterizing the parton parton interaction and σ_{ij} is the cross section for the hard interaction between partons i and j.

The latter can be developed as a perturbative series in powers of α_s: at leading log approximation is given by the parton model effective cross section, while to next-to-leading order it is given by adding corrections due to real and virtual gluon emission, where the intial state singularities are factorized in the effective structure functions, while the final state singularities are factorized in the fragmentation functions, in the case of high p_t single particle hadro-production.

1.4.1 Elementary hard subprocesses in QCD

Cross sections for elementary subprocesses at order α_s are given by the following expression:

$$\frac{d\sigma_{ij\to kl}}{dt} = \frac{\alpha_s^2}{s^2}|M|^2_{ij\to kl}. \tag{1.61}$$

In Table I we show the matrix elements expressions $|M|^2$ as functions of Mandelstam variables and the values of the matrix element at $\theta = 90$ degrees.

We see that for low values of x ($x = 0.1$) the two subrocesses:

$$gg \to gg, \tag{1.62}$$

$$gq(\bar{q}) \to gq(\bar{q}), \tag{1.63}$$

start to dominate, owing the fact that the gluon distribution functions are comparable to the quark ones.

In Figure 1, we show the inclusive jet cross section at CDF as function of p_t and the comparison with the theoretical calculations by Ellis, Kunzst and Soper [6] to next-to-leading order, obtained using MRSD0' set of

structure functions. As we see the agreement is very good on more than seven orders of magnitude.

We remind that to order α_s is very strong the sensibility to the choices of scales and to the value of Λ, and only with the order α_s^3 corrections this uncertainty can be reduced to no more than 20-30% [5].

Process	$\|M\|^2$	F_M
$qq' \to qq'$	$\frac{4}{9}\frac{s^2+u^2}{t^2}$	2.22
$\bar{q}q' \to \bar{q}q'$		
$qq \to qq$	$\frac{4}{9}\left(\frac{s^2+u^2}{t^2}+\frac{s^2+t^2}{u^2}\right)-\frac{8}{27}\frac{u^2}{st}$	3.26
$\bar{q}q \to \bar{q'}q'$	$\frac{4}{9}\frac{t^2+u^2}{s^2}$	0.22
$qq \to qq$	$\frac{4}{9}\left(\frac{s^2+u^2}{t^2}+\frac{t^2+u^2}{s^2}\right)-\frac{8}{27}\frac{u^2}{st}$	2.59
$\bar{q}q \to gg$	$\frac{32}{27}\frac{u^2+t^2}{ut}-\frac{8}{3}\frac{u^2+t^2}{s^2}$	1.04
$gg \to \bar{q}q$	$\frac{1}{6}\frac{u^2+t^2}{ut}-\frac{3}{8}\frac{u^2+t^2}{s^2}$	0.15
$qg \to qg$	$\frac{4}{9}\frac{u^2+s^2}{us}+\frac{u^2+s^2}{t^2}$	6.11
$gg \to gg$	$\frac{9}{2}\left(3-\frac{ut}{s^2}-\frac{us}{t^2}-\frac{st}{u^2}\right)$	30.04

Table I

1.4.2 Inclusive single particle production

The cross section for inclusive single particle production is obtained as a convolution of partonic cross section, structure and fragmentation functions, evolved in the appropriate way.

For a h particle we have:

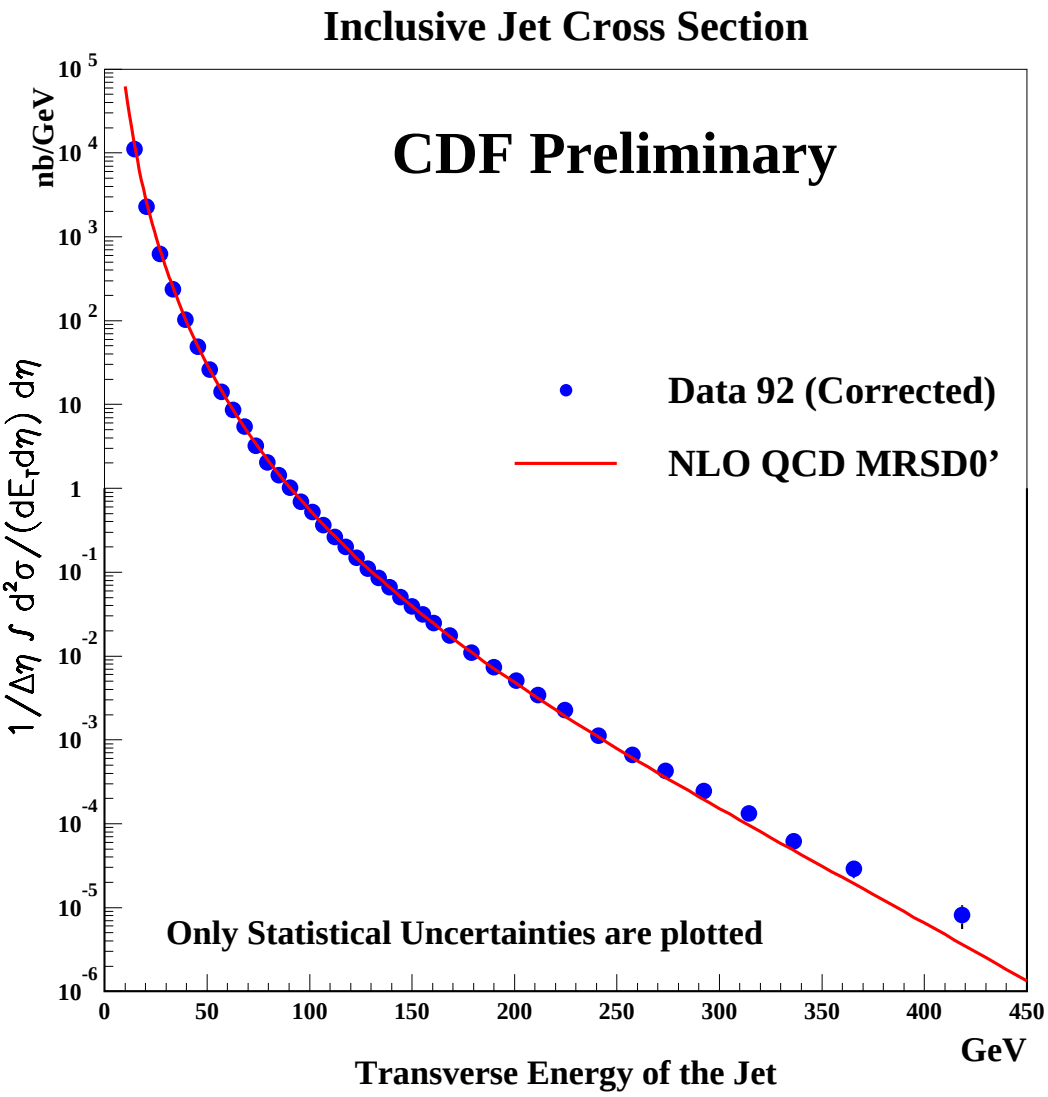

Figure 1.1: NLO inclusive jet production at CDF compared with the data

$$E\frac{d^3\sigma}{dP^3} = \sum_{a,b,c}\int dx_1 dx_2 dz \frac{1}{\pi z} F_a(x_1, Q^2) F_b(x_2, Q^2) \frac{d\sigma^{ab\to c}}{dt} D_c^h(z, Q^2) \quad (1.64)$$

where $D_c^h(z, Q^2)$ is the fragmentation function for the parton c (quark or gluon) into an hadron h with z fraction of longitudinal momentum of the particle.

The multiplicity to produce n particles of type h coming form the fragmentation of c-parton is given by:

$$< N_h >= \int_0^1 D_c^h(z) dz. \quad (1.65)$$

One can show the validity of the following sum rules:

a. momentum conservation

$$\sum_h \int_0^1 z D_c^h(z) dz = 1; \quad (1.66)$$

b. charge conservation

$$\sum_h e_h \int_0^1 dz [D_c^h(z) - D_{\bar{c}}^h(z)] = 1. \quad (1.67)$$

Appendix A

1.5 Splitting functions in Altarelli-Parisi equations

We saw that the evolution equations which describe the evolution of parton densities with the scale Q can be written as follows:

$$\frac{dq^i}{dt}(x,t) = \frac{\alpha}{2\pi}\int_x^1 \frac{dy}{y}[\sum_{j=1}^{2f} q^i(y,t)P_{q^iq^j}(\frac{x}{y}) + G(y,t)P_{q^iG}(\frac{x}{y})], \qquad (1.68)$$

$$\frac{dG}{dt}(x,t) = \frac{\alpha}{2\pi}\int_x^1 \frac{dy}{y}[\sum_{j=1}^{2f} q^i(y,t)P_{Gq^j}(\frac{x}{y}) + G(y,t)P_{GG}(\frac{x}{y})], \qquad (1.69)$$

where indexes i and j are for different flavors.

The quarks number varies via two principal mechanism: a high energy quark can loose part of its energy via the emission of a gluon, or a gluon inside the proton can produce a $q\bar{q}$ pair. In the same way the number density of gluons inside a proton can change via radiation of a gluon from quark or because a gluon can split into a $q\bar{q}$ pair or gg pair.

The latter is typical for non abelian theory where we see triple bosons vertices.

The $P(z)$ functions that we saw as kernels of the evolution equations are known as splitting functions and some of their properties are immediately derived from the fact that flavour and color commute.

First of all, we have that $P_{q_iq_j}$ is diagonal in the quark index, owing the fact that a gluon exchange conserves the flavour.

$$P_{q_iq_j} = \delta_{ij}P_{qq}. \qquad (1.70)$$

Indeed when we disregard the masses, the gluon emission probability is the same for every flavour:

$$P_{Gq_i} = P_{Gq} \qquad (independent\ on\ i) \tag{1.71}$$

Finally a gluon gives rise to a $q\bar{q}$ massless pair with equal probability for every flavour:

$$P_{q_iG} = P_{qG} \qquad (independent\ on\ i) \tag{1.72}$$

We can rewrite (68) and (69) without indexes i and j.

$$\frac{dq}{dt}(x,t) = \frac{\alpha}{2\pi}\int_x^1 \frac{dy}{y}[q(y,t)P_{qq}(\frac{x}{y}) + G(y,t)P_{qG}(\frac{x}{y})] \tag{1.73}$$

$$\frac{dG}{dt}(x,t) = \frac{\alpha}{2\pi}\int_x^1 \frac{dy}{y}[\sum_{i=1}^{2f} q^i(y,t)P_{Gq}(\frac{x}{y}) + G(y,t)2fP_{GG}(\frac{x}{y})] \tag{1.74}$$

The matrix

$$\int_0^1 dz z^{n-1}\begin{pmatrix} P_{qq}(z) & 2fP_{qG}(z) \\ P_{Gq}(z) & P_{GG}(z)\end{pmatrix} = \begin{pmatrix} A_n^{NS} & 4T(R)A_n^{qG} \\ A_n^{Gq} & A_n^{qG}\end{pmatrix} \tag{1.75}$$

gives the logarithm exponents for every n as they are given in Literature [3].

For every value of n the matrix has to be diagonalized in order to obtain eigenvalues and eigenvectors of evolution equations.

The non diagonal functions $\frac{\alpha}{2\pi}P_{Gq}(z)$ and $\frac{\alpha}{2\pi}P_{qG}(z)$ may be interpreted as probability densities: $\frac{\alpha}{2\pi}P_{Gq}(z)$ as the probability to find to order α_s a gluon inside a quark (antiquark) with fraction z of the longitudinal momentum of the parent parton and $\frac{\alpha}{2\pi}P_{qG}(z)$ as the probability to find to the same order a quark (antiquark) inside a gluon.

For the diagonal functions the interpretation is not immediate, owing the fact that we have δ-singularities at $z = 1$.

The probability densities are given in this case by:

$$\mathcal{P}_{qq} + d\mathcal{P}_{qq} = \delta(1-z) + \frac{\alpha}{2\pi} P_{qq}(z) dt, \tag{1.76}$$

$$\mathcal{P}_{GG} + d\mathcal{P}_{GG} = \delta(1-z) + \frac{\alpha}{2\pi} P_{GG}(z) dt, \tag{1.77}$$

so we can see that only for $z < 1$ we can give a probabilistic interpretation.

Momentum conservation at splitting vertices imposes further constraints on P: indeed for $z < 1$ we have:

$$P_{qq}(z) = P_{Gq}(1-z), \tag{1.78}$$

$$P_{qG}(z) = P_{qG}(1-z) \qquad z < 1, \tag{1.79}$$

$$P_{GG}(z) = P_{GG}(1-z). \tag{1.80}$$

Previous equations are derived from the fact that when a quark radiates a gluon with fraction z of the momentum this is also equivalent to radiate a quark with fraction $1-z$ and so on. The presence of δ-singularities alters the form of these relations. Nevertheless it remains valid that:

$$\int_0^1 dz z [P_{qq}(z) + P_{Gq}(z)] = 0, \tag{1.81}$$

$$\int_0^1 dz z [2f P_{qG}(z) + P_{GG}(z)] = 0, \tag{1.82}$$

in order to guarantee that the total momentum of the proton is conserved.

$$\frac{d}{dt} \int_0^1 dx x [\sum_{i=1}^{2f} q_i(x,t) + G(x,t)] = 0. \tag{1.83}$$

Splitting functions are calculable directly from simple QCD vertices. We have then:

$$P_{Gq}(z) = C_F \frac{1+(1-z)^2}{z}, \tag{1.84}$$

$$P_{qq}(z) = C_F \frac{1+z^2}{1-z} \qquad (z<1), \tag{1.85}$$

with $C_2(R) = \frac{N^2-1}{2N}$.

In the same way:

$$P_{qG}(z) = \frac{1}{2}[z^2+(1-z)^2]. \tag{1.86}$$

and finally:

$$P_{GG}(z) = 2N\left[\frac{1-z}{z} + \frac{z}{1-z} + z(1-z)\right] \qquad (z<1). \tag{1.87}$$

These expressions have to be regularized at $z=1$ interpreting them in distributional sense, or better the terms $\frac{1}{1-z}$ which become $\frac{1}{(1-z)_+}$,where "plus" distributions are defined as follows:

$$\int_0^1 \frac{dz f(z)}{(1-z)_+} = \int_0^1 \frac{dz[f(z)-f(1)]}{(1-z)} = \int_0^1 dz \ln(1-z)\frac{d}{dz}f(z). \tag{1.88}$$

We can then add to $P_{qq}(z)$ and $P_{gg}(z)$ the δ-terms with coefficients determined by (78)-(79):

$$P_{qq}(z) = C_F\left[\frac{1+z^2}{(1-z)_+} + \frac{3}{2}\delta(1-z)\right], \tag{1.89}$$

$$P_{GG}(z) = 2N\left[\frac{1-z}{z} + \frac{z}{(1-z)_+} + z(1-z) + \left(\frac{11}{12} - \frac{1}{3}\frac{T(R)}{C_2(G)}\right)\delta(1-z)\right]. \tag{1.90}$$

Chapter 2

Perturbative fragmentation functions

2.1 Introduction

In the prevoiuos chapter we have seen how some deep inelastic phenomena are described by perturbative QCD.

In this chapter we will analyze in more detail the fragmentation phenomenon and see how it is described in the frame of perturbative fragmentation functions.

2.1.1 Q^2 dependence of fragmentation functions

As we saw in the first chapter, pQCD redefines parton model fragmentation functions introducing a Q^2 evolution [7]. It is possible to technically calculate the Q^2 dependence and then the evolution and the method is clearly based on the evolution equations, as we saw in the previous chapter. In this chapter we will see in more detail how we can solve the evolution equations via their transformation in momentum space.

We can rewrite, for reader's convenience, the evolution equations for FF:

$$\frac{\partial D_q^H(z,M_f^2)}{\partial \ln(M_f^2)} = \frac{\alpha_s(M_f^2)}{2\pi}\int_z^1 \frac{dy}{y}\left[P_{qq}^T(y,\alpha_s(M_f^2))D_q^H(\frac{z}{y},M_f^2) + P_{gq}^T(y,\alpha_s(M_f^2))D_g^H(\frac{z}{y},M_f^2)\right] \quad (2.1)$$

$$\frac{\partial D_g^H(z,M_f^2)}{\partial \ln(M_f^2)} = \frac{\alpha_s(M_f^2)}{2\pi}\int_z^1 \frac{dy}{y}\left[P_{qg}^T(y,\alpha_s(M_f^2))D_q^H(\frac{z}{y},M_f^2) + P_{gg}^T(y,\alpha_s(M_f^2))D_g^H(\frac{z}{y},M_f^2)\right]. \quad (2.2)$$

A quark can fragment into a hadron directly or it can radiate a gluon that successively will fragment into hadrons. In the same way a gluon can fragment into a hadron or it can produce a $q\bar{q}$ pair , where one of the quarks will later fragment. Finally it can produce a gg pair, one of them will fragment.

We can solve the system given by (1) and (2). These can be rewrite in terms of the momenta of the distribution functions:

$$\frac{dM_{q_i}^h}{dt}(n,t) = \frac{\alpha(t)}{2\pi}[A_{qq}^n M_{q_i}^h(n,t) + A_{Gq}^n M_G^h(n,t)], \quad (2.3)$$

$$\frac{dM_G^h}{dt}(n,t) = \frac{\alpha(t)}{2\pi}[A_{qG}^n \sum_{i=1}^{2f} M_{q_i}^h(n,t) + A_{GG}^n M_G^h(n,t)], \tag{2.4}$$

where

$$M_a^h(n,t) = \int_0^1 dz z^{n-1} D_a^h(z,t), \tag{2.5}$$

$$A_{ij}^n = \int_0^1 dz z^{n-1} P_{ij}(z). \tag{2.6}$$

These equations are easily solved if we introduce the functions: $D_{NS}^h(z,t)$ and $D_S^h(z,t)$, which correspond to non-singlet and singlet terms

$$D_i^-(z,M_f^2) \equiv \frac{1}{2}\left(D_{q_i}^H(z,M_f^2) - D_{\bar{q}_i}^H(z,M_f^2)\right) \tag{2.7}$$

$$D_i^+(z,M_f^2) \equiv \frac{1}{2}\left(D_{q_i}^H(z,M_f^2) + D_{\bar{q}_i}^H(z,M_f^2)\right) - \frac{1}{2N_f} D_S(z,M_f^2) \tag{2.8}$$

$$D_S(z,M_f^2) \equiv \sum_{i=1}^{N_f}\left(D_{q_i}^H(z,M_f^2) + D_{\bar{q}_i}^H(z,M_f^2)\right). \tag{2.9}$$

In the evolution equations the singlet part D_S is coupled to the gluon fragmentation function whereas the non-singlet parts D^- and D^+ are decoupled.

Solutions are complicated by the fact that singlet and non-singlet term are mixed in the same way as they are for the structure functions. The resulting expressions for momenta are given by:

$$M_{NS}^h(n,t) = M_{NS}^h(n,t) e^{A_{qq}^n s/2\pi b}, \tag{2.10}$$

$$M_S^h(n,t) = \frac{e^{\lambda_+^n s}[\sigma_-^n M_s^h(n,t_0) - M_G^h(n,t_0)]}{(\sigma_-^n - \sigma_+^n)} + \\ + \frac{e^{\lambda_-^n s}[-\sigma_+^n M_s^h(n,t_0) - M_G^h(n,t_0)]}{(\sigma_-^n - \sigma_+^n)}, \tag{2.11}$$

$$M_G^h(n,t) = \frac{e^{\lambda_+^n s}[\sigma_+^n \sigma_-^n M_s^h(n,t_0) - \sigma_+^n M_G^h(n,t_0)]}{(\sigma_-^n - \sigma_+^n)} + \\ + \frac{e^{\lambda_-^n s}[-\sigma_+^n \sigma_-^n M_s^h(n,t_0) + \sigma_+^n M_G^h(n,t_0)]}{(\sigma_-^n - \sigma_+^n)}, \tag{2.12}$$

where $s = \ln \frac{t}{t_0}$ $\sigma_{+-}^n = [A_{22}^n - A_{11}^n \pm \sqrt{(A_{22}^n - A_{11}^n)^2 + 4A_{12}^n A_{21}^n}]/2A_{12}^n$ and $t_0 = \ln \frac{Q_0^2}{\Lambda^2}$ $\lambda_{+-}^n = A_{11}^n + A_{12}^n \sigma_{+-}^n$, $A_{11}^n = A_{qq}^n/2\pi b$, $A_{12}^n = 2f A_{Gq}^n/2\pi b$, $A_{21}^n = A_{qG}^n/2\pi b$, $A_{GG}^n/2\pi b$ $b = \frac{33-2f}{12\pi}$.

Given a certain set of input momenta at the scale Q_0^2 equations (3)-(4) give the momenta at the desired Q^2 scale. Fragmentation functions are obtained simply applying an inverse Mellin transformation.

Momentum conservation gives rise to the following equations:

$$\sum_h \int dz z D_G^h(z,t) = 1, \tag{2.13}$$

$$\sum_h \sum_i \int dz z D_{q_i}^h(z,t) = \sum_h \int dz z D_S^h(z,t) = 2f, \tag{2.14}$$

which become for the splitting functions:

$$\int dz z [P_{qq}(z) + P_{Gq}(z)] = 0, \tag{2.15}$$

$$\int dz z [2f P_{qG}(z) + P_{GG}(z)] = 0. \tag{2.16}$$

Fragmentation functions evolution can be done at several orders of the perturbative series. We know infact that the running coupling constant and the splitting functions can be developed at different orders of the perturbative expansion. During our study we used a FORTRAN code that is able to perform a leading logarithm approximation evolution or a next-to-leading logarithm one.

Next-to-leading evolution is performed in the same scheme developed to study heavy quark fragmentation and production [8]. In this case we have very large logarithm to all orders in the perturbative expansion and at first sight the perturbative approximation seems to fail. Nevertheless it is possible resum all these logarithms to order next-to-leading-log and the method is based on the factorization theorem which assures that the cross section for heavy quark production can be written as a convolution of the fragmentation function and the partonic cross section. This one is calculable in QCD as an expansion in powers of the running coupling constant, where the mass of the parton regularize the collinear divergences coming from gluon emission, while infrared divergences are regularized in the usual way of summing real and virtual contributions.

We then have:

$$\frac{d\hat{\sigma}}{dx}(x,Q,m) = \sum_{i=0}^{\infty} a^{(i)}(x,Q,m)\left(\frac{\alpha_s(Q)}{2\pi}\right)^i. \tag{2.17}$$

If we write the cross section at order $\alpha_s(Q)$ as

$$\frac{d\sigma}{dx}^{(1)}(x,Q,m) = a^{(0)}(x) + a^{(1)}(x,Q,m)\frac{\alpha_s(Q^2)}{2\pi}, \tag{2.18}$$

the diagrams contributing are the ones of real and virtual gluon emission: if one disregards terms of the order of powers of quark mass, then one has the following contributions:

$$\frac{d\sigma}{dx}^{(1)}(x,Q,m) = \delta(1-x) + \frac{\alpha_s(Q^2)}{2\pi}a^{(1)}(x,Q,m), \tag{2.19}$$

where

$$a^{(1)}(x,Q,m) = C_F + C_F\left[\ln\frac{Q^2}{m^2}\left(\left(\frac{1}{1-x}\right)_+(1+x^2) + \frac{3}{2}\delta(1-x)\right)\right.$$
$$\left. +2\frac{1+x^2}{1-x}\ln x - \left(\frac{\ln(1-x)}{1-x}\right)_+(1+x^2)\right.$$

$$+\frac{1}{2}\left(\frac{1}{1-x}\right)_+(x^2-6x-2)+(\frac{3}{2}\pi^2-\frac{5}{2})\delta(1-x)\Bigg] \quad (2.20)$$

As we can see $a^{(1)}$ contains logarithms of $(\frac{Q^2}{m^2})$ and then in the limit of high energy it becomes large: this is the manifestation of collinear singularities due to gluons emission. We can forsee that collinear singularities are due to all orders in perturbation theory and the coefficients $a^{(n)}(x,Q,m)$ behave as $\ln(\frac{Q^2}{m^2})^n$ for large Q.

Factorization theorem, along with the Altarelli-Parisi equations, allows to extract logarithmic terms from the partonic cross section and use them to define an effective fragmentation function for quarks and gluons satisfying Altarelli-Parisi equations, with kernels given by the following expression:

$$P_{ij}(x,\alpha_s(\mu)) = P_{ij}^{(0)}(x) + (\frac{\alpha_s(\mu)}{2\pi})P_{ij}^{(1)}(x) + O(\alpha_s^3) \quad (2.21)$$

which contains leading e next to leading contributions.

If one solves the evolution equations using the zero-th order for $P(x)$, then $D(x,\mu)$ will include the correct $\alpha_s^n(\mu)\ln^n(\frac{\mu}{\mu_0})$ powers (leading logarithms approximation), while if one uses the α_s order expression for $P(x)$ subleading terms are also considered of the type: $\alpha_s^{n+1}(\mu)\ln^n(\frac{\mu}{\mu_0})$.

Now we will see some technical details of the FF calculation at next to leading order. In momentum space, evolution equation has the following form (we are considering for sake of simplicity, just the non-singlet part):

$$\frac{d\hat{D}_{NS}(\mu)}{d\ln\mu^2} = A_N^{(2)}\hat{D}_{NS}(\mu) \quad (2.22)$$

$$A_N^{(2)} = \frac{\alpha_s(\mu)}{2\pi}\left[P_N^{(0)} + \frac{\alpha_s(\mu)}{2\pi}P_N^{(1)}\right]. \quad (2.23)$$

where $A_N^{(2)}$ is the Mellin transformation for the splitting functions, at next to leading order.

Of course $\alpha_s(\mu)$ has to be accurate at the same order.

If we introduce

$$t = \frac{1}{2\pi b_0} \ln \frac{\alpha_s(\mu_0)}{\alpha_s(\mu)} \tag{2.24}$$

after some algebra we have:

$$\begin{aligned} \hat{D}_{NS}(\mu) &= \hat{D}_{NS}(\mu_0) exp \left[P_N^{(0)} t + \frac{1}{4\pi^2 b_0} (\alpha_s(\mu_0) - \alpha_s(\mu)) \right. \\ &\left. \times (P_N^{(1)} - \frac{2\pi b_1}{b_0} P_N^{(0)}) \right] . \end{aligned} \tag{2.25}$$

Kernels in momentum space are given in Appendix B.

Our evolution code is based on the procedure described above and the result is the evolution of fragmentation functions at every scale we desirer.

During out analysis we used data obtained at Q_0^2=30 GeV as input to evolve at scales of interest covering all the range going from fixed target experiment to hadron and lepton colliders.

In order to extract the phenomenological input we adopted three different strategies in the case of π^0 production. Cross checks between the three showed the intrinsic consistency of the methods, so we choose to use the method based on use of a parton shower MonteCarlo to extract the fragmentation functions for all the other light mesons: η, $\pi^{\pm}$, $K^{\pm}$, K_s^0.

2.2 π^0 fragmentation functions

2.2.1 Extraction of π^0 fragmentation functions

Selection of experimental data.

We first discuss the experimental data we will use to extract the π^0 fragmentation functions. We first consider e^+e^- collisions. The JADE collaboration [9] has published data at $\sqrt{S}$ = 14, 22.5 and 34.4 GeV. We

use the data at 34.4 GeV, covering mainly the low z_H range (up to $z_H = 0.209$). Data from the TPC collaboration [10] at $\sqrt{S} = 29$ GeV are given as $\frac{1}{\sigma_{had}}\frac{d\sigma}{\beta dz_H}$, therefore a value of R=4.00 is assumed to bring them to the usual form $\frac{S}{\beta}\frac{d\sigma}{dz_H}$. Data from the TASSO collaboration [11] at $\sqrt{S} = 34.6$ GeV extend up to $z_H = 0.728$. The broadest z_H range is covered by data from the CELLO collaboration, extending from $z_H = 0.049$ to $z_H = 0.919$ at $\sqrt{S} = 35$ GeV [12] and from $z_H = 0.094$ to $z_H = 0.847$ at $\sqrt{S} = 22$ GeV [13]. Data from experiments at DORIS are not used, as hardly any point survive with the cut on the lower energy of the π^0 at 2 GeV. Data obtained at LEP are for the moment not constraining. However, cross checks have been performed with the 2 points surviving the cut of data from the Argus collaboration [14] at $\sqrt{S} = 10$ GeV and the 4 points from the L3 collaboration [15] at $\sqrt{S} = 91$ GeV.

Fragmentation functions from HERWIG.

We first consider the π^0 inclusive production in e^+e^- annihilation at $M_{f0} = \sqrt{S} = 30$ GeV, as simulated by the Monte Carlo generator HERWIG. As well known, this event generator includes the QCD parton shower to leading and next to leading accuracy - in particular the kinematical corrections due to the phase space boundaries are summed up to all orders - as well as the hadronisation of the color singlet clusters into the physical particles. Furthermore HERWIG has been shown [16] to describe with good accuracy the observed features of PETRA and LEP data. Then we will use the π^0 distribution generated by each quark flavor which originates from the photonic vertex, as a realistic description of the quark fragmentation into π^0. Owing to the symmetry of quarks and antiquarks fragmenting into π^0 we extract the quark fragmentation functions from:

$$\frac{d\sigma_{e^+e^-\rightarrow\pi^0}}{dz_H}(z_H, M_{f0}^2) \sim 6\sigma_0 \sum_q e_q^2 D_q^{\pi^0}(z_H, M_{f0}^2), \qquad (2.26)$$

where the pointlike cross section σ_0 is given by:

$$\sigma_0 = \frac{4\pi\alpha^2}{3Q^2},$$

. The reaction $e^+e^- \to \pi^0 + X$ has been therefore decomposed into each contribution $e^+e^- \to u\bar{u}$, $d\bar{d}$, $s\bar{s}$, $c\bar{c}$ and $b\bar{b}$. The generated distributions are parameterized as

$$D_i^{\pi^0}(z, M_{f0}^2) = N_i z^{\alpha_i}(1-z)^{\beta_i} \tag{2.27}$$

and analyzed using the minimization procedure MINUIT. The coefficients N_i are constrained by the normalization condition:

$$\int_{\frac{2m_\pi}{M_{f0}}}^1 dz\ D_i(z, M_{f0}^2) = \langle n_\pi \rangle_i, \tag{2.28}$$

where the average values $\langle n_\pi \rangle_i$ are given by HERWIG for each quark flavor, in agreement with the total observed multiplicity $\langle n_\pi \rangle$. The parameters N_i, α_i and β_i are extracted from the π^0 inclusive distribution generated, for each flavor, in the x range $.025 \leq z_H \leq .95$ and shown in table I. As can be inferred from this table the statistical error on the parameters is less than 5%.

As an illustration of the accuracy of the method and also of its limitations, the π^0 inclusive cross-section obtained from eqs. (2.26) and (2.27), together with the results of table I , are compared in figure 1 with the CELLO data [12] at $\sqrt{S} = 35$ GeV. The agreement is reasonable in the range $z_H \leq .5$. So far we have not included the contribution from the gluon fragmentation function. Indeed from the analysis of the three jet events it would be possible, in principle, to extract from HERWIG the appropriate information. The corresponding accuracy is however unsatisfactory, due to the limited sensitivity to hard gluon effects in e^+e^- annihilation.

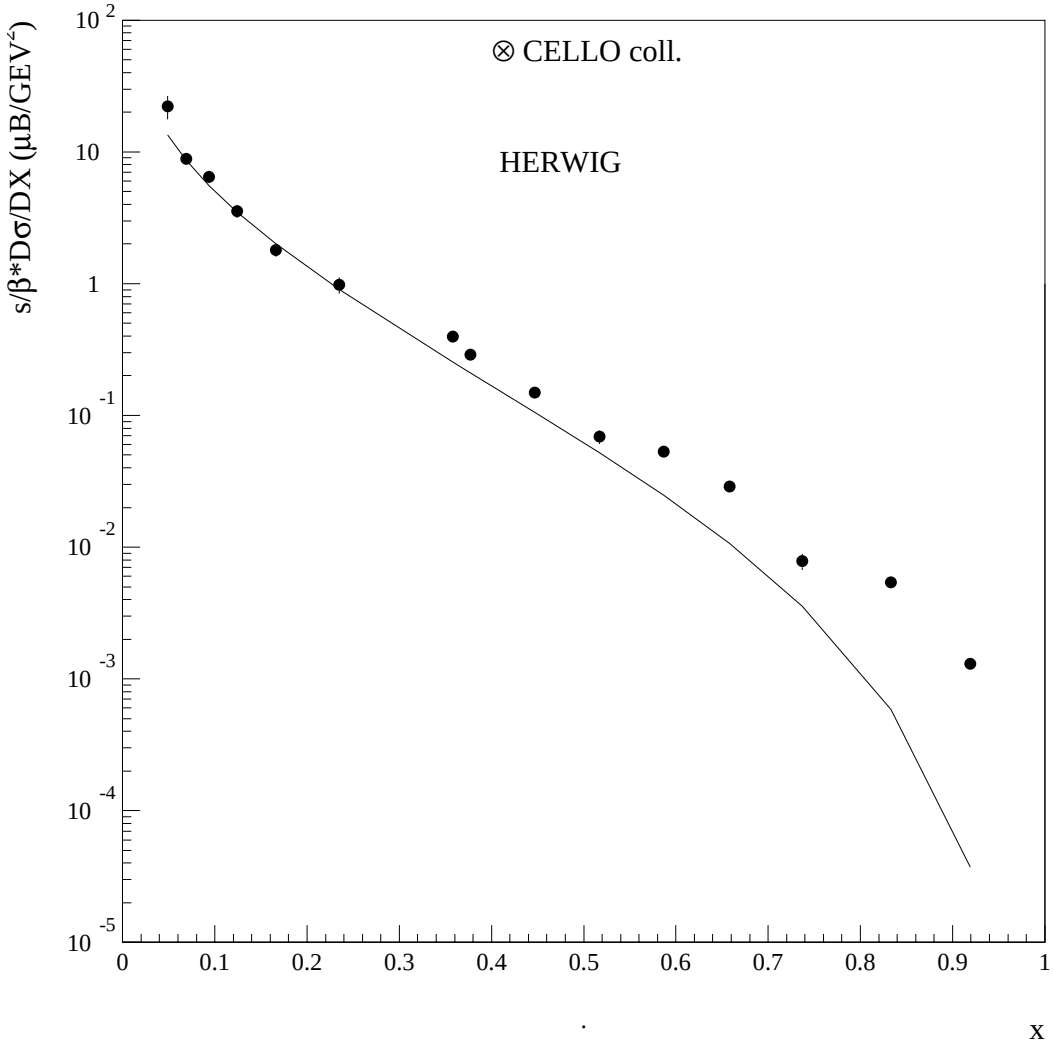

Figure 2.1: LO inclusive π^0 production in e^+e^- annihilation with the quarks HERWIG FF

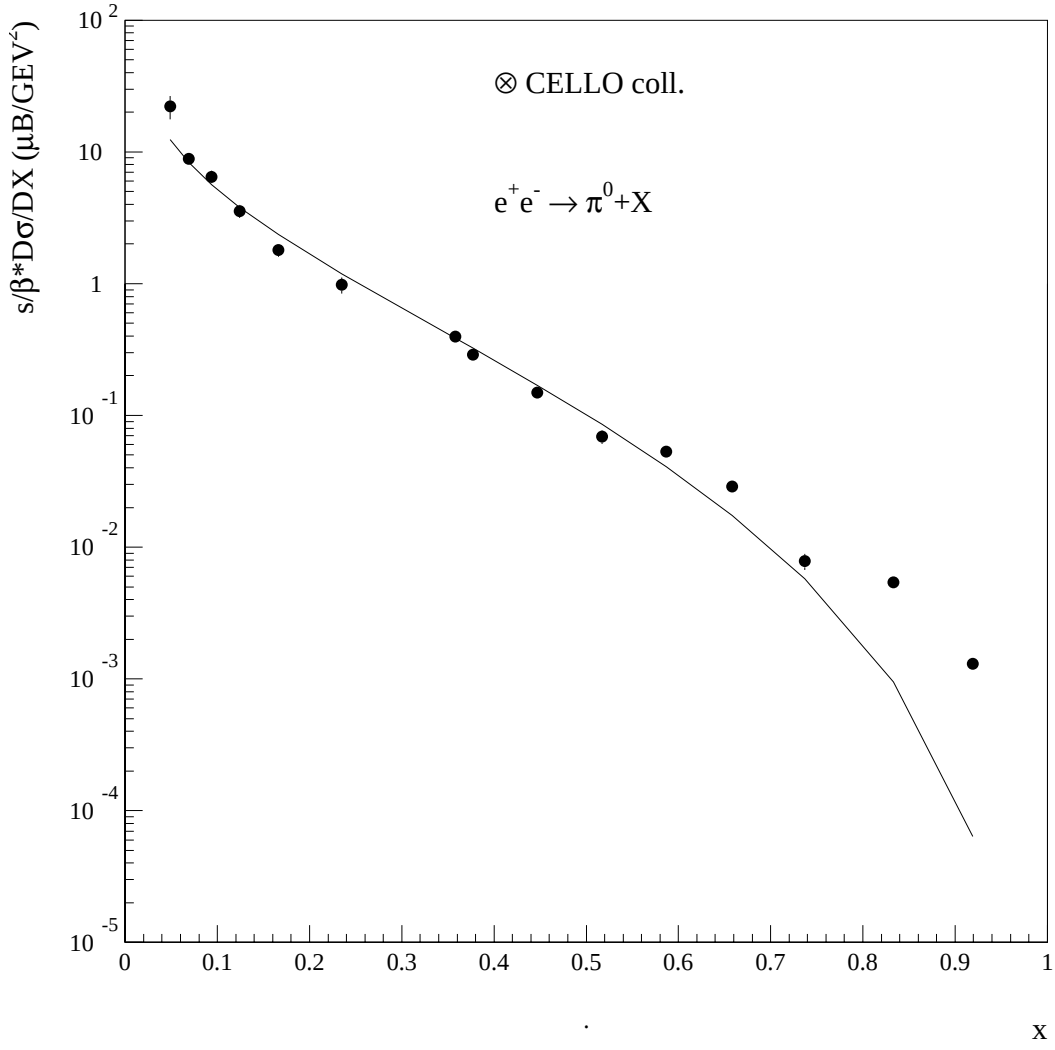

Figure 2.2: NLO inclusive π^0 production in e^+e^- annihilation with the evolved HERWIG FF

For this reason we have followed a different approach. To extract the gluon fragmentation function from HERWIG we have analyzed the subprocess $gg \to gg \to \pi^0 + X$ from $p\bar{p}$ annihilation at $M_{f0} = \sqrt{s} \sim 30$ GeV, in analogy to the quark case. In order to eliminate the background from the fragmentation of the spectator partons we have considered the pions lying only within a cone of semi aperture $\delta = .35 - .40$ rad around the direction of the parent gluons emitted at 90 deg. The value of δ is found by an appropriate angular study of the generated distribution. With a parameterization of the form (2.27) we find the values of the parameters N_g, α_g and β_g given in table II. After inclusion of the gluon fragmentation function and use of NLO evolved fragmentation functions together with NLO terms in the π^0 inclusive cross section the agreement with CELLO data is improved as can be inferred from figure 2 up to $z_H \simeq 0.7$

In the next chapter we will compare our predictions at NLO to experimental data from hadronic colliders, while in the next subsection we will extract the π^0 fragmentation functions at next to leading order using two different hypotheses at the reference scale $M_{f0}^2 = 2$ GeV^2.

Set I: fragmentation functions with natural scales.

For this set, we take α_s as given by:

$$\alpha_s(\mu^2) = \frac{1}{b \ln(\mu^2/\Lambda^2)} \left[1 - \frac{b'}{b} \frac{\ln\ln(\mu^2/\Lambda^2)}{\ln(\mu^2/\Lambda^2)}\right]. \qquad (2.29)$$

and $\Lambda = 190$ MeV, corresponding to the set of structure functions we will use [17,18].

Definition

We assume for this case an SU(2) symmetry:

$$D_u^{\pi^0}(z, M_{f0}^2) = D_{\bar{u}}^{\pi^0}(z, M_{f0}^2) = D_d^{\pi^0}(z, M_{f0}^2) = D_{\bar{d}}^{\pi^0}(z, M_{f0}^2) =$$

$$D_V(z, M_{f0}^2) + D_S(z, M_{f0}^2). \quad (2.30)$$

Then, we take

$$D_s^{\pi^0}(z, M_{f0}^2) = D_{\bar{s}}^{\pi^0}(z, M_{f0}^2) = D_c^{\pi^0}(z, M_{f0}^2) == D_{\bar{c}}^{\pi^0}(z, M_{f0}^2) = D_S(z, M_{f0}^2), \quad (2.31)$$

and

$$D_g^{\pi^0}(z, M_{f0}^2) = D_G(z, M_{f0}^2). \quad (2.32)$$

We parameterize the different functions of z as follows

$$\begin{aligned} D_V(z, M_{f0}^2) &= N_v\,(1-z)^{\beta_v} & (2.33)\\ D_S(z, M_{f0}^2) &= N_s\,(1-z)^{\beta_s} & (2.34)\\ D_G(z, M_{f0}^2) &= N_g\,(1-z)^{\beta_g}. & (2.35) \end{aligned}$$

At the initial scale M_{f0}, we start with four flavors. The b quark contribution is taken into account in the evolution. Fixing the threshold at 4 m_b^2, so we have:

$$D_b^{\pi^0}(z, M_f^2) = \begin{cases} 0 & \text{if } M_f^2 < 4m_b^2 \\ N_s\,(1-z)^{\beta_s} & \text{if } M_f^2 = 4m_b^2 \end{cases} \quad (2.36)$$

So we are left with six parameters to be determined with the help of experimental data.

Choice of the scale

We use the standard approach to fix all the scales to the same value which is some natural scale of the problem. More precisely, for e^+e^- collisions, we take $\mu = M_f = \sqrt{S}$ whereas for p p collisions, we set the three scales equal and proportional to the transverse momentum of the π^0:

$$\mu = M = M_f = cP_t$$

where c is a constant to be fixed by the fit to experimental data .

Results for set I

First of all, for e^+e^- collisions, we limit ourselves to a π^0 energy greater than 2 GeV because we don't trust perturbation theory for low π^0 energies. Therefore for $\sqrt{S} \simeq 30$ GeV, we will only use z values greater than 0.1. As it can be inferred from eqs (25-27) we have not used a factor z^α in the input parameterizations since in this z range it does not improve the fit but only leads to correlations. With six parameters, a big correlation still occurs between N_v and β_v, so we fix $\beta_v = 1$. Then N_s, N_g and β_g remain slightly correlated. A good fit to CELLO [12], TASSO [11], TPC [10] and JADE [9] data leading to a $\chi^2 = 26.3$ for 29 points is obtained for values of the parameters given in table III (systematic errors have been added in quadrature to statistical errors).

Set II: fragmentation functions with optimized scales.

For this set, we take the numerical solution of the following equation equation of α_s:

$$\frac{1}{\alpha_s(\mu^2)} + b' \ln\left(\frac{b'\alpha_s(\mu^2)}{1 + b'\alpha_s(\mu^2)}\right) = b \ln\left(\frac{\mu^2}{\Lambda^2}\right), \tag{2.37}$$

with:

$$b = \frac{33 - 2N_f}{12\pi}, \quad b' = \frac{153 - 19N_f}{24\pi^2},$$

which is more appropriate than eq.citeapalfa for small scales μ. Indeed for large μ the two definitions agree but for small μ they can differ by more than 20 %. $\Lambda = 230$ MeV, since we will use the ABFOW set of structure functions [19] .

Definition

We assume also for this case an SU(2) symmetry:

$$D_u^{\pi^0}(z,M_{f0}^2) = D_{\bar{u}}^{\pi^0}(z,M_{f0}^2) = D_d^{\pi^0}(z,M_{f0}^2) = D_{\bar{d}}^{\pi^0}(z,M_{f0}^2) = D_u(z,M_{f0}^2). \tag{2.38}$$

Then we take:

$$D_s^{\pi^0}(z,M_{f0}^2) = D_{\bar{s}}^{\pi^0}(z,M_{f0}^2) = D_s(z,M_{f0}^2), \tag{2.39}$$

$$D_c^{\pi^0}(z,M_{f0}^2) = D_{\bar{c}}^{\pi^0}(z,M_{f0}^2) = D_c(z,M_{f0}^2), \tag{2.40}$$

and

$$D_g^{\pi^0}(z,M_{f0}^2) = D_g(z,M_{f0}^2). \tag{2.41}$$

We parameterize these different functions of z in the following way:

$$D_u(z,M_{f0}^2) = N_u\, z^{-1}\,(1-z)^{\beta_u} \tag{2.42}$$

$$D_s(z,M_{f0}^2) = N_s\, z^{-1}\,(1-z)^{\beta_s} \tag{2.43}$$

$$D_c(z,M_{f0}^2) = N_c\, z^{-1}\,(1-z)^{\beta_c} \tag{2.44}$$

$$D_g(z,M_{f0}^2) = N_g\, z^{-1}\,(1-z)^{\beta_g}. \tag{2.45}$$

So we are left with eight parameters to be determined with the help of experimental data. Since we will use the optimized procedure for the determination of the scales, it is much simpler not to change the number of flavors. So, in this case, we will neglect the b contribution. This assumption is motivated by the fact that $\sigma(e^+\,e^- \to \gamma^* \to b\,\bar{b}) = 1/4\,\sigma(e^+\,e^- \to \gamma^* \to c\,\bar{c})$ and in $p\,p$ collision the b production is suppressed due to the weak b content of the proton.

A few remarks are in order here. As in the case of set I, the non singlet part D_i^- is always zero due to our assumptions. We did not take $D_s^{\pi^0} = D_c^{\pi^0}$ because in this case the sum over the four flavors of D_i^+ weighted by the square electric charge is zero:

$$\sum_{i=u,d,s,c} e_i^2 \left(D_i^+(z,M^2) + D_{\bar{i}}^+(z,M^2)\right) = 0.$$

So, there is no non-singlet contribution to the cross-section. Therefore we could parameterize directly the singlet and the glue with four parameters only. The e^+e^- data could be correctly described, but the glue is very constrained and it will not be possible to fit hadronic data in the whole energy range.

Choice of the scale

For set II, we use optimized scales according to the procedure of Politzer and Stevenson [20]. Concerning e^+e^- collisions, our approach is the following. Firstly since the scale μ does not appear at lowest order, we cannot optimize with respect to it. Therefore we set $\mu = M_f$ and perform an optimization only with respect to the scale M_f. Therefore, a priori, our optimized scale depends on the choice made for the input fragmentation functions. We have not found a way to get rid from this sensitivity. In practice, the optimized point changes slowly when the input is modified and in addition, since we are in a stable region, it does not matter if we are not exactly on the optimized point. The optimized scale M_f^{opt} is of order of $\sqrt{S}/8$ varying slowly with z. Furthermore, we find no optimization scale for $z \leq .03$ for $\sqrt{S} = 35$ GeV, $z \leq .05$ for $\sqrt{S} = 29$ GeV and $z \leq .1$ for $\sqrt{S} = 22$ GeV. For lower values of $\sqrt{S}$, it is not possible to optimize.

We also use an optimization procedure for hadronic collisions. So we require that:

$$\frac{\partial}{\partial \ln(\mu^2/\Lambda^2)} E_{\pi^0} \frac{d\sigma_{p+p\to\pi^0}}{d^3\vec{P}_{\pi^0}} = 0 \tag{2.46}$$

$$\frac{\partial}{\partial \ln(M^2/\Lambda^2)} E_{\pi^0} \frac{d\sigma_{p+p\to\pi^0}}{d^3\vec{P}_{\pi^0}} = 0 \tag{2.47}$$

$$\frac{\partial}{\partial \ln(M_f^2/\Lambda^2)} E_{\pi^0} \frac{d\sigma_{p+p\to\pi^0}}{d^3\vec{P}_{\pi^0}} = 0. \tag{2.48}$$

The first equation can be computed analytically:

$$\frac{\partial}{\partial \ln(\mu^2/\Lambda^2)} E_{\pi^0} \frac{d\sigma_{p+p\to\pi^0}}{d^3\vec{P}_{\pi^0}} = -\alpha_s^4(\mu^2) b \left\{ 2b'A + 3(1 + b'\alpha_s(\mu^2)) \right.$$
$$\left. \times \left[2bA \ln\left(\frac{\mu^2}{\Lambda^2}\right) + B \ln\left(\frac{M^2}{\Lambda^2}\right) + C \ln\left(\frac{M_f^2}{\Lambda^2}\right) + D \right] \right\} \qquad (2.49)$$

having used

$$\frac{\partial \alpha_s(\mu^2)}{\partial \ln(\mu^2/\Lambda^2)} = -b\ \alpha_s^2(\mu^2)\ (1 + b'\alpha_s(\mu^2)). \qquad (2.50)$$

Note that terms of order of α_s^3 have been cancelled as it should be. Now, we determine the scale μ in order to cancel the right-hand side of eq (2.49). This ensures us that the corrective term K will be negative with a magnitude of roughly 10 % of the lowest order. Then we compute numerically the value of the scales M and M_f which have to fulfill the equations (2.47) (2.48), the scale μ being now a function of M, M_f. We require that the factorization scales must be greater than $\sqrt{2}$ GeV and that the renormalization scale is such that the running coupling constant α_s is less than .34. With these constraints it will be impossible to optimize in low P_t range. More precisely, for low center of mass energies ($\sqrt{S} \leq 63$ GeV), the optimization is not possible for $P_t \leq 5$ GeV. Therefore these regions are not appropriate to apply an optimization procedure.

Results for set II

First we freeze β_s, β_c and β_g according to the counting rules. There are still too many parameters, so we fix N_g and fit to e^+e^- data with four parameters N_u, β_u, N_s and N_c. The fragmentation functions extracted are then used to evaluate hadronic cross sections. Then we vary N_g refitting e^+e^- data and apply the new input to pp data.This procedure is repeated until a reasonable description of hadronic data is reached. Good fits of e^+e^- data (CELLO [13,12], TASSO [11], TPC [10] and JADE [9]) leading to a $\chi^2 \simeq 1$ per d.o.f. are obtained for the two sets - hereafter denoted as

set IIa and set IIb - displayed in Table IV and Table V (see figures 3 and 4 using set IIb). The two sets differ mainly for the gluon normalization. In the following chapter we will analyze the results for colliders.

Process	α	β	N_q	$< n_\pi >$
$e^+e^- \to u\bar{u}$	-0.95 ± 0.02	3.67 ± 0.19	1.20	2.95
$e^+e^- \to d\bar{d}$	-0.95 ± 0.02	3.67 ± 0.15	1.24	2.87
$e^+e^- \to s\bar{s}$	-0.88 ± 0.02	5.32 ± 0.23	1.68	2.73
$e^+e^- \to c\bar{c}$	-0.82 ± 0.02	8.02 ± 0.24	3.09	3.42
$e^+e^- \to b\bar{b}$	-0.95 ± 0.02	10.94 ± 0.29	2.92	4.20

Table I.

δ	α	β	N_g	$< n_\pi >$
0.35 *rad*	-0.28 ± 0.04	6.71 ± 0.39	14.49	3.65
0.4 *rad*	-0.37 ± 0.04	5.79 ± 0.36	12.93	4.55

Table II.

Parton	α_i	β_i	N_i
valence	0.	1.	0.19
sea	0.	5.2	3.5
gluon	0.	2.03	4.9

Table III.

Parton	α_i	β_i	N_i
up	$-1.$	0.94	0.11
strange	$-1.$	3.0	0.55
charm	$-1.$	4.	2.7
gluon	$-1.$	2.	0.55

Table IV.

Parton	α_i	β_i	N_i
up	$-1.$	1.11	0.15
strange	$-1.$	3.0	0.18
charm	$-1.$	4.	2.5
gluon	$-1.$	2.	0.75

Table V.

We are now quite confident of the reliability of the three different methods (for this see also below in chapter 3) and so we can choose one of them to perform the extraction of the fragmentation functions for light mesons.

2.2.2 Fragmentation functions for $\pi^{\pm}$, η, $K^{\pm}$, K_s^0

In this section we report the parameterizations at Q_0= 30 GeV of $\pi^{\pm}$, η, $K^{\pm}$, K_s^0 and the results on NLO fit to the e^+e^- data.

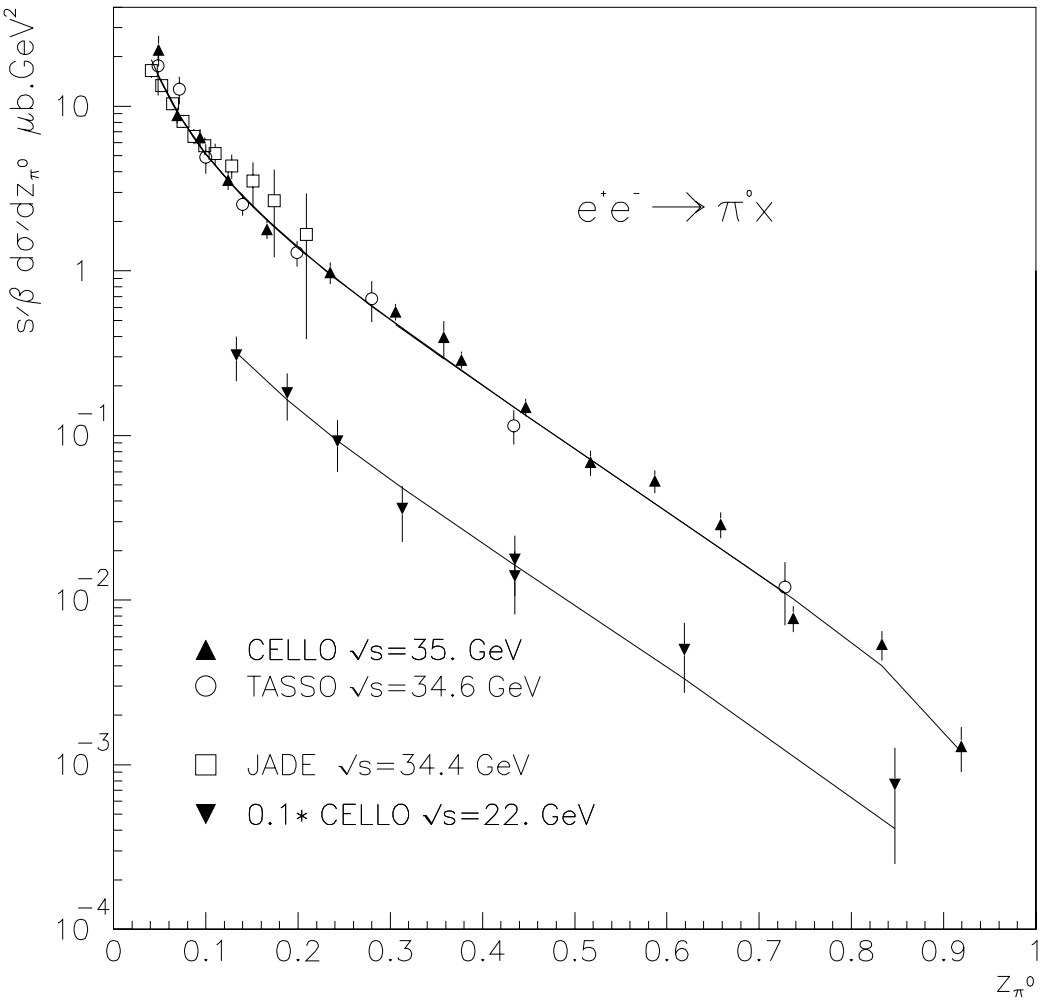

Figure 2.3: NLO inclusive π^0 production in e^+e^- annihilation with set II of FF. $N_g = 0.75$. Data and theory multiplied by 0.1 at 22 GeV

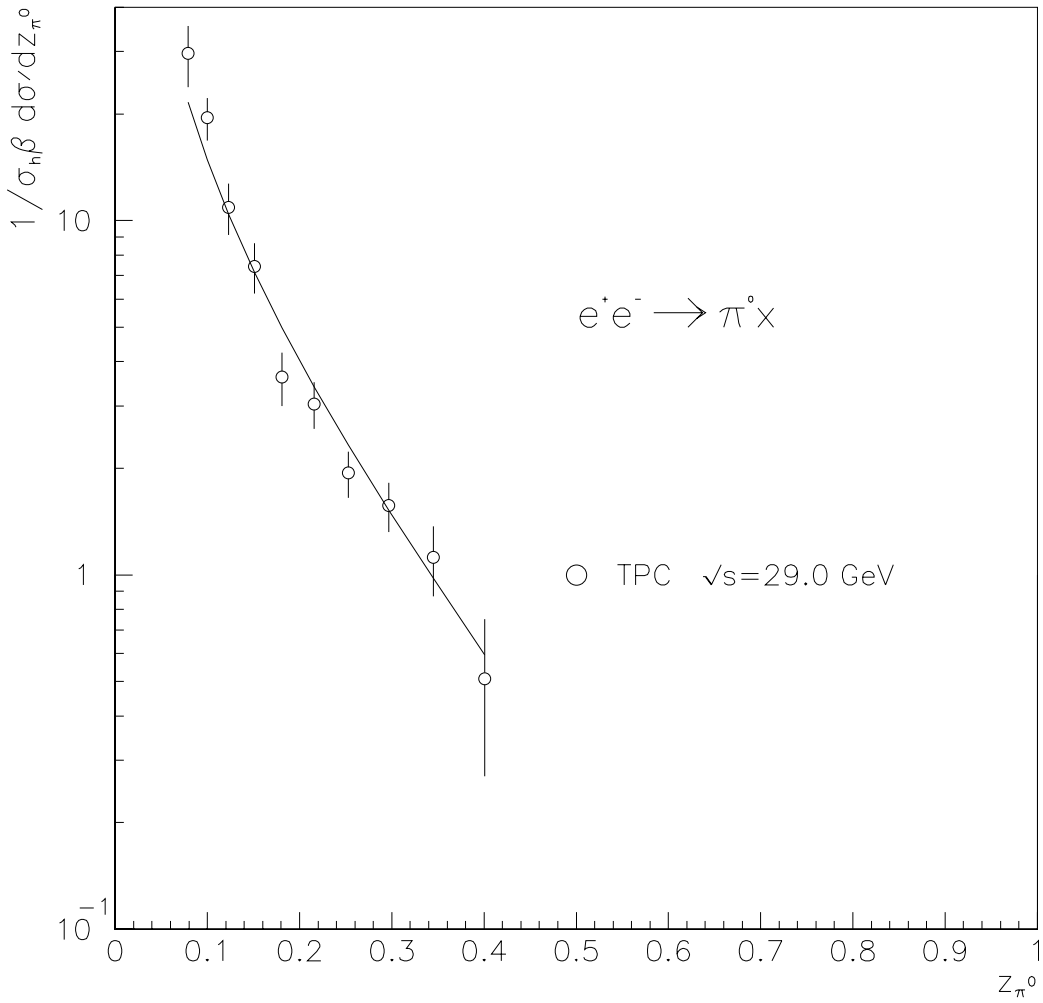

Figure 2.4: Same as fig 9 for TPC data

η

In Table VI we report the parameterization for η fragmentation functions. We show in Figure 5 our results at $\sqrt{S} = 35$ GeV, compared with JADE [9] and CELLO [12] data. The agreement is satisfactory as can be inferred from the figure. The difference between Sets I and II is negligeable . After evolution to $\sqrt{S} = 91.2$ GeV, we also obtain good agreement with L3 [15] LEP data as shown in Figure 6.

Process	α	β	N_q	$< n_\eta >$
$e^+e^- \to u\bar{u}$	-0.91 ± 0.02	2.09 ± 0.07	0.24	0.35
$e^+e^- \to d\bar{d}$	-0.88 ± 0.02	2.14 ± 0.08	0.26	0.36
$e^+e^- \to s\bar{s}$	-0.72 ± 0.02	2.73 ± 0.08	0.37	0.42
$e^+e^- \to c\bar{c}$	0.14 ± 0.03	7.10 ± 0.14	8.73	0.57
$e^+e^- \to b\bar{b}$	-0.20 ± 0.05	11.24 ± 0.31	9.92	0.69

Table VI.

	δ	α	β	N_g	$< n_\eta >$
I	0.35 rad	-0.18 ± 0.06	4.58 ± 0.25	2.52	0.51
II	0.4 rad	-0.43 ± 0.06	3.47 ± 0.26	1.48	0.62

Table VII.

$\pi^\pm$

In Table VIII we report the parameterizations for charge pions. As we can easily see these parameterizations differs from π^0 FF just for a nor-

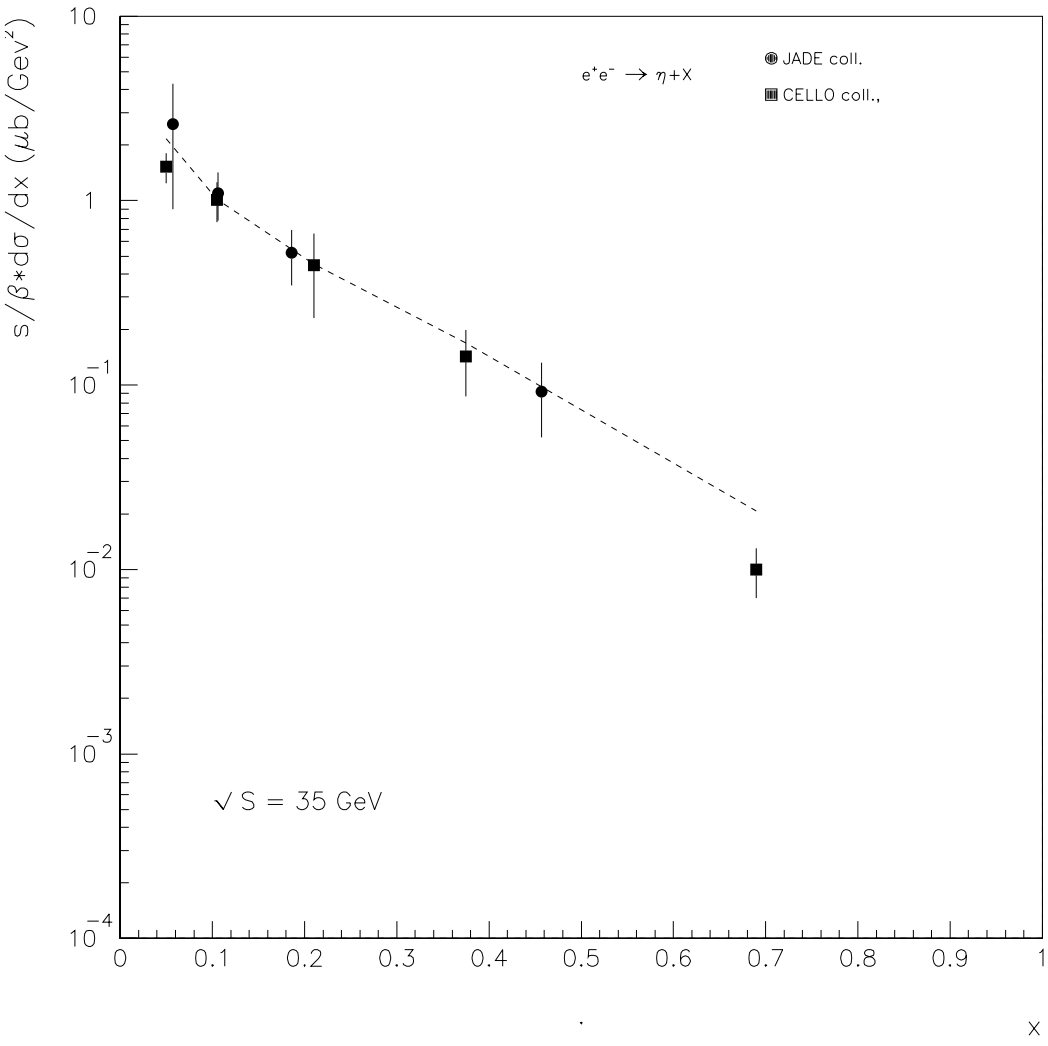

Figure 2.5: NLO inclusive η production in e^+e^- annihilation with evolved HERWIG FF

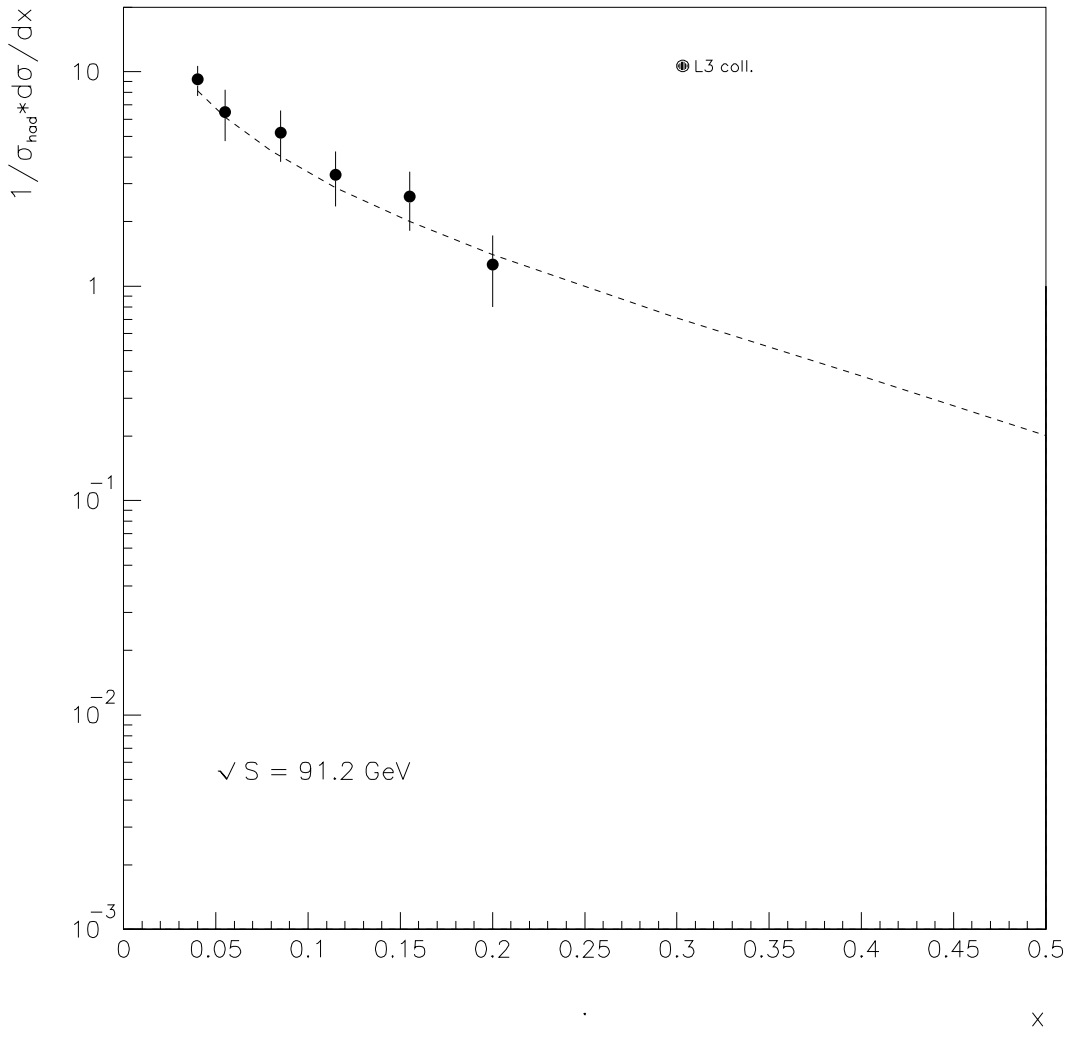

Figure 2.6: NLO inclusive η production in e^+e^- annihilation with the evolved HERWIG FF

malization factor, owing the fact that we can apply a full $SU(2)$ isospin symmetry operation.

Parton	α	β	N_i	$< n_i >$
u	-1.18 ± 0.01	2.32 ± 0.05	0.53	2.83
d	-1.17 ± 0.01	2.41 ± 0.05	0.55	2.82
s	-0.94 ± 0.01	5.83 ± 0.08	1.46	2.66
c	-0.81 ± 0.01	9.01 ± 0.14	3.5	3.41
b	-1.35 ± 0.01	7.16 ± 0.07	1.25	4.19
g	-0.59 ± 0.01	4.43 ± 0.10	4.57	3.52

Table VIII

$K^{\pm}$ and K_s^0

In Table IX e X we report the parameterizations for charge and neutral kaons fragmentation functions. Even in this case we can apply a full $SU(2)$ symmetry operation to the tow sets. In table XIa, b we compare with data from 29 GeV to 90 GeV in the center of mass [21]. As usual the theoretical prediction is affected by an uncertainty of order 30% coming from the factorization/renormalization scales, parton densities, etc.

Parton	α	β	N_i	$< n_i >$
u	-1.42 ± 0.03	1.48 ± 0.13	0.1	0.59
d	-1.10 ± 0.03	4.32 ± 0.05	0.34	0.55
s	-0.83 ± 0.03	2.5 ± 0.03	0.79	0.95
c	-0.70 ± 0.03	3.78 ± 0.08	1.41	1.01
b	-0.77 ± 0.03	7.7 ± 0.18	2.82	1.24
g	-0.39 ± 0.03	4.74 ± 0.08	1.97	0.62

Table IX

$Parton$	α	β	N_i	$< n_i >$
u	-1.06 ± 0.03	4.37 ± 0.13	0.19	0.27
d	-1.39 ± 0.03	1.46 ± 0.05	0.05	0.28
s	-0.84 ± 0.03	2.45 ± 0.03	0.40	0.45
c	-0.80 ± 0.03	3.31 ± 0.08	0.50	0.49
b	-0.63 ± 0.03	8.15 ± 0.18	2.02	0.62
g	-0.56 ± 0.03	4.26 ± 0.08	0.61	0.30

Table X

x	data	our fit
0.105	6.32 ± 0.92	6.5
0.115	5.13 ± 0.61	5.87
0.125	5.13 ± 0.49	5.30
0.135	5.00 ± 038	4.81
0.170	$- - - - -$	3.56
0.190	$- - - - -$	3.05
0.210	$- - - - -$	2.64
0.235	$- - - - -$	2.22
0.275	1.73 ± 0.11	1.71
0.325	1.16 ± 0.073	1.26
0.375	0.842 ± 0.055	0.93
0.425	0.470 ± 0.030	0.69
0.550	0.249 ± 0.020	0.33
0.650	0.090 ± 0.012	0.16
0.8	0.023 ± 0.005	0.04

Table XI a

x	data	our fit
0.035	18.1 ± 0.8	24.5
0.055	13.1 ± 0.6	14.7
0.075	10.1 ± 0.5	10.2
0.095	7.5 ± 05	7.6
0.115	6.4 ± 0.5	5.9
0.135	4.4 ± 0.5	4.8
0.155	4.5 ± 0.5	3.98
0.175	3.4 ± 0.5	3.34
0.195	2.7 ± 0.4	2.84
0.215	2.5 ± 0.5	2.44
0.235	2.2 ± 0.5	2.1
0.255	1.6 ± 0.5	1.8
0.275	1.5 ± 1.1	1.6
0.295	0.8 ± 0.6	1.4
0.355	0.8 ± 0.5	0.9

Table XIIb

2.3 Check with other sets of fragmentation functions

Recently we assist to an increased interest for fragmentation processes and their description via the formalism of fragmentation functions. In particular the DESY group of G. Kramer et al. in some recent papers gave several interesting results regarding the fragmentation functions of light mesons. Their fragmentation functions are extracted performing LO and NLO fit to e^+e^- data in a way very similar to the one described in section 2.1.3 and 2.1.7.

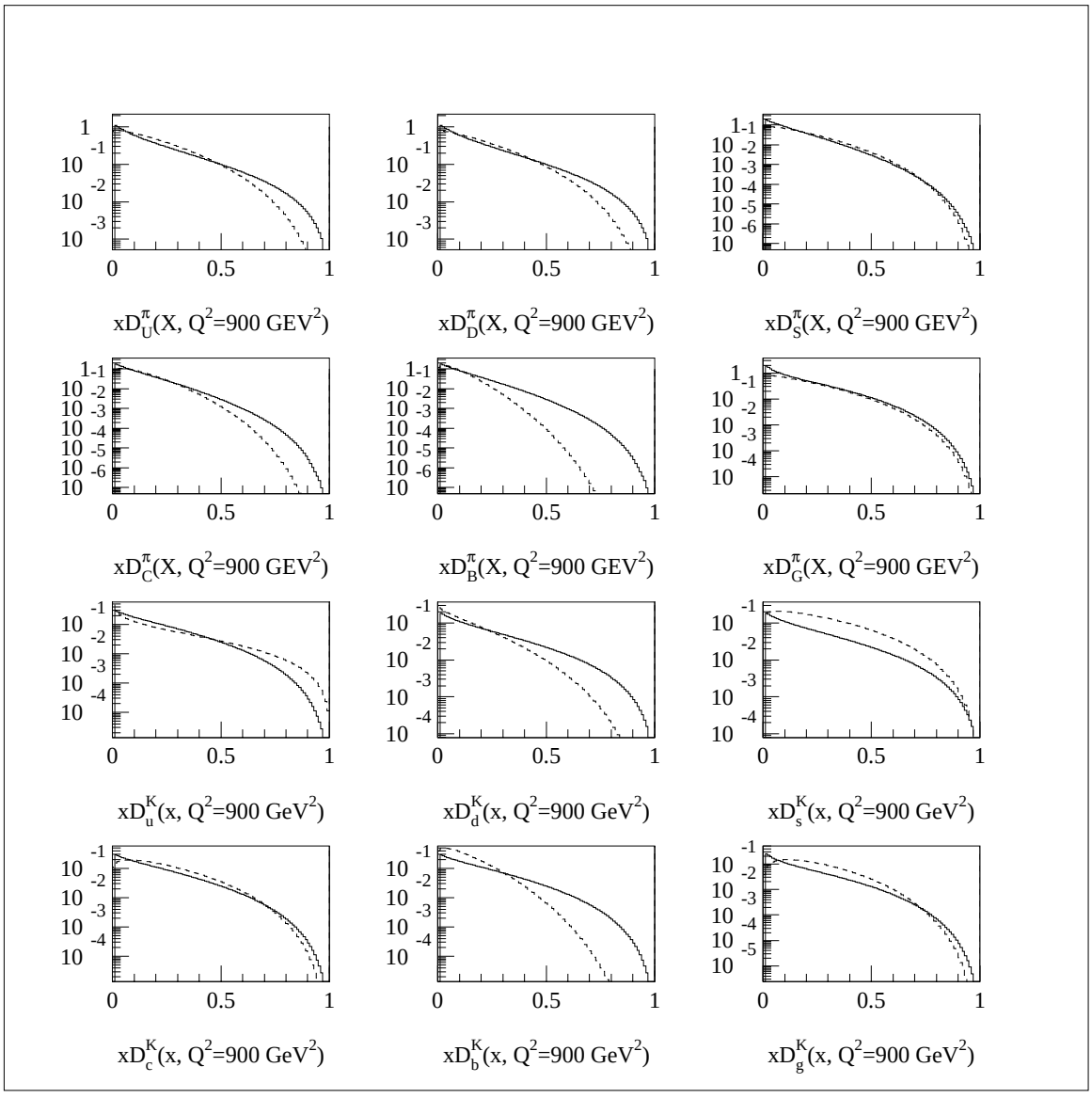

Figure 2.7: HERWIG FF (full line) compared to those by Kramer et al. (dashed line)

In order to better describe the theoretical uncertainty on FF, we performed a detailed check between our sets and the ones from Kramer et al. and in Figure 7 we report the two sets of charged pions and kaons evolved at Q_0^2=900 GeV^2. As we can infer from the figures the agreement is quite good, if we exclude the region of high x where nevertheless the partonic cross sections fall down.

Appendix B

2.4 Splitting functions in momentum space

We saw that $P_{ij}(z)$ momenta are given by the so called anomalous dimensions A^n_{ij} $(i,j = q,G)$ given by the following expressions:

$$-A^n_{ij} = \int_0^1 dz z^{n-1} P_{ij}(z) \tag{2.51}$$

$$A^n_{qq} = \frac{1}{3\pi}\left[1 - \frac{2}{n(n-1)} + 4\sum_{i=2}^{n}\frac{1}{j}\right], \tag{2.52}$$

$$2fA^n_{Gq} = -\frac{4f}{3\pi}\frac{n^2+n+2}{n(n^2-1)} \tag{2.53}$$

$$A^n_{qG} = -\frac{1}{4\pi}\frac{n^2+n+2}{n(n+1)(n+2)}, \tag{2.54}$$

$$A^n_{GG} = \frac{3}{4\pi}\left[\frac{1}{3} - \frac{4}{n(n-1)} - \frac{4}{(n+1)(n+2)} + 4\sum_{j=2}^{n}\frac{1}{j} + \frac{2f}{9}\right]. \tag{2.55}$$

f as usual is the number of flavours.

At next to leading order the splitting functions $P^{(1)}_{qq}(x)$ and its Mellin transformation is given by:

$$P^{(1)}_{qq}(x) = C_F^2 P_F(x) + \frac{1}{2}C_F C_G P_G(x) + C_F N_F T_F P_{N_F}(x), \tag{2.56}$$

where

$$P_F(x) = -2\frac{1+x^2}{1-x}\ln\ln(1-x) - 3\left(\frac{3}{1-x} + 2x\right) \tag{2.57}$$

$$\times \ln x - \frac{1}{2}(1+x)\ln x^2 - 5(1-x) \tag{2.58}$$

$$P_G(x) = \frac{1+x^2}{1-x}\left[\ln x^2 + \frac{11}{3}\ln x + \frac{67}{9} - \frac{1}{3}\pi^2\right] + 2(1+x)\ln x + \frac{40}{3}(1-x) \tag{2.59}$$

$$P_{N_F}(x) = \frac{2}{3}\left[\frac{1+x^2}{1-x}(-\ln x - \frac{5}{3}) - 2(1-x)\right], \tag{2.60}$$

$$P_A(x) = 2\frac{1+x^2}{1+x}\int_{x/(1+x)}^{1/(1+x)} \frac{dz}{z}\ln\frac{1-z}{z} + 2(1+x)\ln x + 4(1-x). \tag{2.61}$$

In momentum space, if we define:

$$P_F(N) = \left(2S_1(N) - \frac{1}{N(N+1)}\right)[2S_2(N) - \frac{1}{-}\pi^2] - \frac{2(2N+1)}{N^2(N+1)^2}S_1(N) \tag{2.62}$$

$$+4S_3(N) - 3S_2(N) + \frac{1}{2}\pi^2 + \frac{3N^3+N^2-1}{N^3(N+1)^3} - \frac{23}{8}, \tag{2.63}$$

$$P_{NF}(N) = \frac{20}{9}S_1(N) - \frac{4}{3}S_2(N) - \frac{1}{6} - 2\frac{11N^2+5N-3}{9N^2(N+1)^2} \tag{2.64}$$

$$P_G(N) = -P_F(N) + S_1(N)\left[-\frac{134}{9} - 2\frac{2N+1}{N^2(N+1)^2}\right] + 4S_1(N)S_2(N) \tag{2.65}$$

$$+S_2(N)\left[\frac{13}{3} - \frac{2}{N(N+1)}\right] + \frac{43}{24} + \frac{151N^4+263N^3+97N^2+3N+9}{9N^3(N+1)^3} \tag{2.66}$$

$$\Delta(N) = 2\left[-2S_1(N) + \frac{3}{2} + \frac{1}{N(N+1)}\right]\left[2S_2(N) - \frac{1}{3}\pi^2 - \frac{2N+1}{N^2(N+1)^2}\right] \tag{2.67}$$

we obtain:

$$P_N^1 = C_F^2(P_F(N) + \Delta(N)) + \frac{1}{2}C_F C_A P_G(N) + C_F N_F T_F P_{NF}(N), \tag{2.68}$$

where, as usual $C_F = \frac{4}{3}$, $C_A = 3$, $T_F = \frac{1}{2}$ and N_f is the number of flavors. $S_{1,2,3}$ are particular combinations of the poligamma functions, defined by:

$$\psi_m = \frac{d^m log,(x)}{dx^m}. \tag{2.69}$$

Chapter 3

One particle inclusive production to next-to-leading order

3.1 Introduction

Let us consider the inclusive production of a hadron H via the generic reaction $A + B \to H$ where A and B stand for hadrons and/or leptons. The cross-section can be written as a convolution of the fragmentation functions $D_l^H(z, M_f^2)$ with the partonic cross-section:

$$E_H \frac{d\sigma_{A+B\to H}}{d^3\vec{P}_H} = \sum_l \int_{z_H}^1 \frac{dz}{z^2} D_l^H(z, M_f^2) E_l \frac{d\sigma_{A+B\to l}}{d^3\vec{P}_l}(\frac{z_H}{z}, \theta, \alpha_s(\mu^2), M_f^2, \cdots), \tag{3.1}$$

where z_H is the reduced energy of the hadron H: $z_H = 2E_H/\sqrt{S}$ and θ is the scattered angle of the parton l. The inclusive production of the parton

l via the reaction $A + B \rightarrow l$ has the following perturbative development:

$$E_l \frac{d\sigma_{A+B\rightarrow l}}{d^3\vec{P}_l}(\frac{z_H}{z}, \theta, \alpha_s(\mu^2), M_f^2, \cdots) = \sigma^0_{A+B\rightarrow l}(\frac{z_H}{z}, \theta)$$
$$+\frac{\alpha_s(\mu^2)}{2\pi}\ \sigma^1_{A+B\rightarrow l}(\frac{z_H}{z}, \theta, M_f^2) + \cdots . \qquad (3.2)$$

Finally $D_l^H(z, M_f^2)$ represents the number of hadrons H inside the parton l carrying the fraction of impulsion z from H, evolved at the scale M_f^2. These fragmentation functions satisfy Altarelli-Parisi type evolution equations as we saw in the previous chapter.

In the LO approximation one keeps only the first order in the perturbative development of the partonic cross-section and in the evolution kernels whereas at NLO one keeps the first and second terms in the perturbative expansion for both partonic cross-section and evolution kernels. Once input fragmentation functions have been specified at some reference scale M_{f0} the evolution equations are solved using an inverse Mellin transform technique.

We will perform an exact NLO calculation valid in the P_t range where perturbative QCD applies. We have not taken into account non perturbative intrinsic transverse momentum effects. Since an extra parton is emitted either from initial or from final parton legs a perturbative contribution to intrinsic transverse momentum due to soft gluon effects is partially included. In addition the inclusion of a non perturbative component would act as an extra parameter and weaken the predictive power of our calculation.

Let us consider now in detail the partonic cross-sections.

3.1.1 $e^+e^- \rightarrow \pi^0$

The partonic cross sections from e^+e^- collisions read at next-to-leading

order:

$$E_{q_i}\frac{d\sigma_{e^+e^-\to q_i}}{d^3\vec{P}_{q_i}}(y,\theta,\alpha_s(\mu^2),M_f^2) =$$
$$\frac{6\,\sigma_0}{\pi Q^2 y}\,e_i^2\left\{\frac{3}{8}(1+\cos^2\theta)\left[\delta(1-y)+\frac{\alpha_s(\mu^2)}{2\pi}\left(P_{qq}^0(y)\ln\left(\frac{Q^2}{M_f^2}\right)+K_q^T(y)\right)\right]\right.$$
$$\left.+\,\frac{3}{4}(1-\cos^2\theta)\frac{\alpha_s(\mu^2)}{2\pi}K_q^L(y)\right\} \tag{3.3}$$

$$E_g\frac{d\sigma_{e^+e^-\to g}}{d^3\vec{P}_g}(y,\theta,\alpha_s(\mu^2),M_f^2) =$$
$$\frac{12\,\sigma_0}{\pi Q^2 y}\sum_{i=u,d,s,c,\ldots}e_i^2\left\{\frac{3}{8}(1+\cos^2\theta)\left[\frac{\alpha_s(\mu^2)}{2\pi}\left(P_{gq}^0(y)\ln\left(\frac{Q^2}{M_f^2}\right)+K_g^T(y)\right)\right]\right.$$
$$\left.+\,\frac{3}{4}(1-\cos^2\theta)\frac{\alpha_s(\mu^2)}{2\pi}K_g^L(y)\right\}, \tag{3.4}$$

where σ_0 is the usual point like cross-section

$$\sigma_0=\frac{4\pi\alpha^2}{3Q^2},$$

α is the QED coupling constant and Q^2 is the invariant mass of the e^+e^- pair. The functions K_q^T, K_q^L, K_g^T and K_g^L have been extracted from the reference [4] (see also [22]).

$$K_q^T(x) = C_F\left\{\frac{3}{2}(1-x)-\frac{3}{2}\frac{1}{(1-x)_+}+2\frac{1+x^2}{1-x}\ln(x)\right.$$
$$\left.+\,(1+x^2)\left(\frac{\ln(1-x)}{1-x}\right)_+ +\left(\frac{2\pi^2}{3}-\frac{9}{2}\right)\delta(1-x)\right\}, \tag{3.5}$$

$$K_g^T(x) = C_F\left\{\frac{1+(1-x)^2}{x}(\ln(1-x)+2\ln(x))-2\frac{1-x}{x}\right\} \tag{3.6}$$

$$K_q^L(x) = C_F \tag{3.7}$$

$$K_g^L(x) = 2\,C_F\,\frac{1-x}{x}. \tag{3.8}$$

In the above equations two scales are involved: the renormalization scale μ at which the running coupling constant α_s is evaluated and the fragmentation scale M_f at which fragmentation functions are evolved. The

choice for these scales is rather arbitrary. Note that for every y, $K_g^T(y)$ is negative, so the choice $M_f^2 = Q^2$ leads to a negative contribution to the partonic cross-section $E_g\, d\sigma_{e^+e^-\to g}/d^3\vec{P}_g$.

The running coupling of QCD α_s is defined at the next-to-leading logarithm approximation by the approximate analytical formula:

$$\alpha_s(\mu^2) = \frac{1}{b\ln(\mu^2/\Lambda^2)}\left[1 - \frac{b'}{b}\frac{\ln\ln(\mu^2/\Lambda^2)}{\ln(\mu^2/\Lambda^2)}\right]. \tag{3.9}$$

As we saw in Chapter 2 we also used for α_s as given by the numerical solution of the equation:

$$\frac{1}{\alpha_s(\mu^2)} + b'\,\ln\left(\frac{b'\alpha_s(\mu^2)}{1+b'\alpha_s(\mu^2)}\right) = b\,\ln\left(\frac{\mu^2}{\Lambda^2}\right), \tag{3.10}$$

with:

$$b = \frac{33-2N_f}{12\pi},\;\; b' = \frac{153-19N_f}{24\pi^2},$$

which is more appropriate than eq.3.9 for small scales μ. Indeed for large μ the two definitions agree but for small μ they can differ by more than 20 %.

3.1.2 $p\,p \to \pi^0$

The partonic cross-sections for hadronic collisions are given by [23]:

$$E_l\frac{d\sigma_{p+p\to l}}{d^3\vec{P}_l}(y,\theta,\alpha_s(\mu^2),M_f^2) = \frac{1}{\pi S}\sum_{i,j}\int_{VW}^{V}\frac{dv}{1-v}\int_{VW/v}^{1}\frac{dw}{w}$$
$$\times\left[F_i^p(x_1,M^2)F_j^p(x_2,M^2)\left(\frac{1}{v}\left(\frac{d\sigma^0}{dv}\right)_{ij\to l}(s,v)\delta(1-w)\right.\right.$$
$$\left.\left.+\frac{\alpha_s(\mu^2)}{2\pi}K_{ij\to l}(s,v,w;\mu^2;M^2,M_f^2)\right) + (x_1\leftrightarrow x_2)\right]. \tag{3.11}$$

The variables V, W are defined by

$$V = 1 - \frac{y}{2}(1-\cos\theta),\;\; W = \frac{y(1+\cos\theta)}{2-y(1-\cos\theta)},$$

and we also have

$$x_1 = \frac{VW}{vw}, \quad x_2 = \frac{1-V}{1-v}$$

and $s = x_1 x_2 S$. At NLO sixteen subprocesses contribute to the cross-section. The terms σ^0 correspond to the lowest order $2 \to 2$ parton scattering subprocesses whereas the terms K contain the one loop corrections to these subprocesses. In the hadronic case, we have three scales: the renormalization scale μ, the factorization scale for the initial state M (the scale of the distribution functions) and the factorization scale for final state M_f (the scale of the fragmentation functions). Schematically, the hadronic cross-section can be written as:

$$\begin{aligned} E_{\pi^0}\frac{d\sigma_{p+p\to\pi^0}}{d^3\vec{P}_{\pi^0}} &= \alpha_s^2(\mu^2)A + \alpha_s^3(\mu^2)\left[2bA\ln\left(\frac{\mu^2}{\Lambda^2}\right) + B\ln\left(\frac{M^2}{\Lambda^2}\right)\right. \\ &\left. + C\ln\left(\frac{M_f^2}{\Lambda^2}\right) + D\right]. \end{aligned} \tag{3.12}$$

We show explicitly the dependence of the hadronic cross-section upon the three scales μ, M and M_f. The four functions A, B, C and D depend on the scales M and M_f via the structure and fragmentation functions. In addition, A, B and C are scheme independent. We always use the $\overline{MS}$ scheme for final factorization whereas the initial factorization scheme is fixed by the set of structure functions used.

Let us discuss now the partonic cross-sections. In order to determine the kinematical region where each partonic reaction dominates we have plotted in figures 1, 2, 3, 4 the partonic cross-sections $E_l \; d\sigma_{p+p\to l}/d^3\vec{P}_l$ for $l = g$, $u + \overline{u} + d + \overline{d}$, $s + \overline{s} + c + \overline{c}$ against P_t at the leading log level for various center of mass energies (WA70, ISR, UA2, LHC). We think it is meaningless to use next-to-leading formulae since the dependence on $\ln(M_f^2)$ is not balanced. We have used ABFOW structure functions [19]. We see that for the low center-of-mass energy experiments WA70 [24] ($\sqrt{S} = 23$ GeV) and E706 [25] ($\sqrt{S} = 31$ GeV) the gluon and the valence

quarks contributions are of the same order at low P_{tl}, whereas when P_{tl} becomes larger, the valence quarks dominate. For ISR experiments [26], [27] ($\sqrt{S} = 63$ GeV) the glue contribution dominates up to $P_{tl} \simeq 10$ GeV. For the UA2 experiment [28], when the pseudo rapidity $\eta = 1.4$, the glue contribution is important up to $P_{tl} \simeq 35$ GeV. Finally for LHC, in the P_{tl} range between 30 and 1000 GeV the glue contribution represents (60 - 80) % of the partonic cross-section. In all cases the "sea" contribution (s,c) is always negligible.

In order to estimate the z range we are sensitive to we will study in table I the integrand of eq. (3.1), i.e.:

$$< z >= \frac{\int \frac{dz}{z} \sum_l D_l^{\pi^0}(z, M_f^2)\ E_l\ \frac{d\sigma_{p+p\to l}}{d^3\vec{P}_l}}{\int \frac{dz}{z^2} \sum_l D_l^{\pi^0}(z, M_f^2)\ E_l\ \frac{d\sigma_{p+p\to l}}{d^3\vec{P}_l}} \tag{3.13}$$

with z varying between $2E_{\pi^0}/\sqrt{S}$ and 1. Note that the partonic cross-sections reach their maximum for z = 1 while the fragmentation functions decrease with z. As we can infer from Table I the large z region is kinematically favored. We have used set I of fragmentation functions which have been discussed before.

$\sqrt{S} = 23$ GeV and $\eta = 0.$		$\sqrt{S} = 63$ GeV and $\eta = 0.$		$\sqrt{S} = 630$ GeV and $\eta = 1.4$	
$P_t^{\pi^0}$	$< z >$	$P_t^{\pi^0}$	$< z >$	$P_t^{\pi^0}$	$< z >$
4.11	0.81	5.25	0.67	13	0.55
4.61	0.82	6.73	0.70	21	0.60
5.69	0.86	8.23	0.73	29.8	0.65
6.69	0.89	10.4	0.77	43.7	0.74

Table I

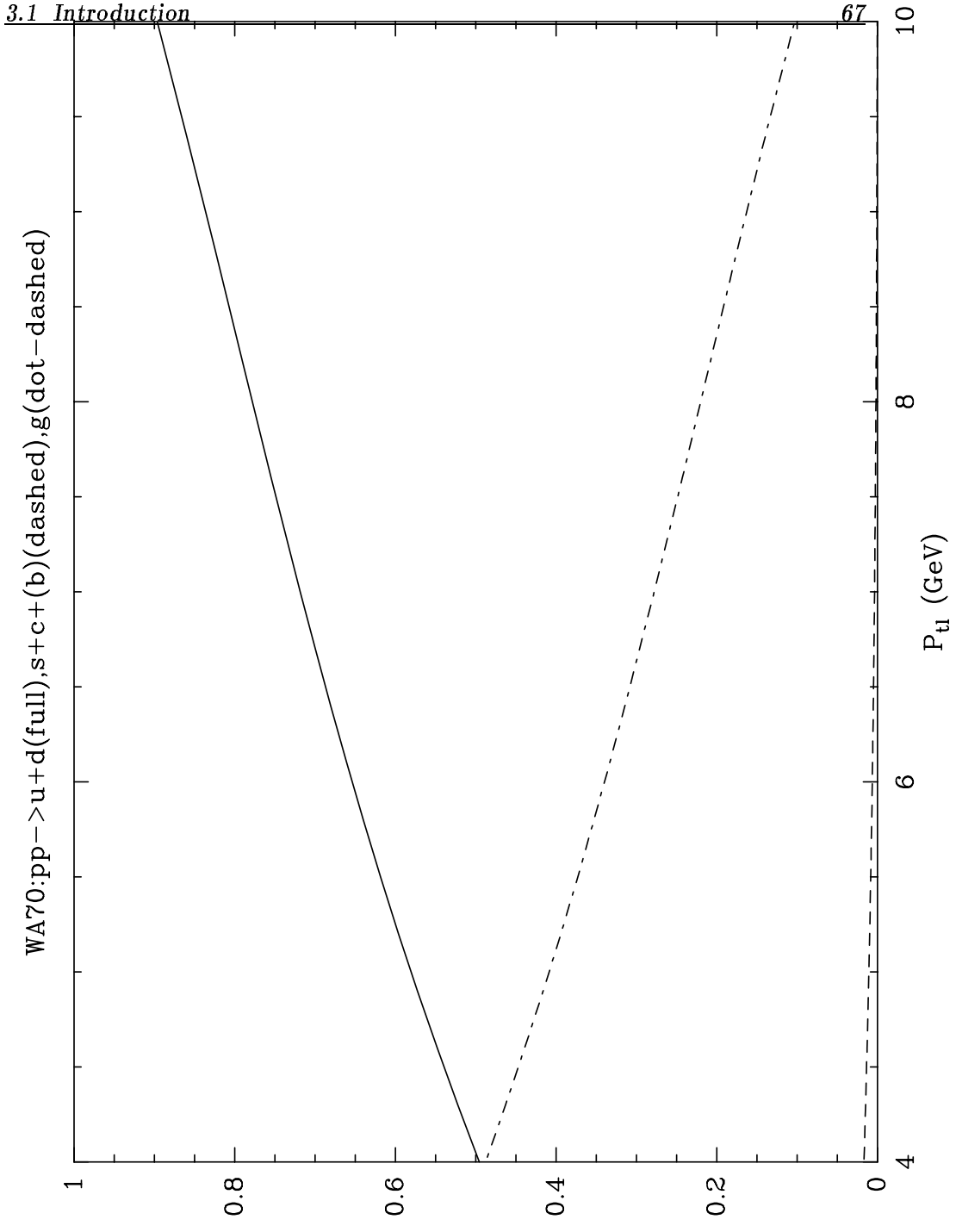
WA70:pp−>u+d(full),s+c+(b)(dashed),g(dot−dashed)
Fraction of E_l $d\sigma/d^3P_l$
P_{tl} (GeV)
1
0.8
0.6
0.4
0.2
0
4
6
8
10

Figure 3.1:

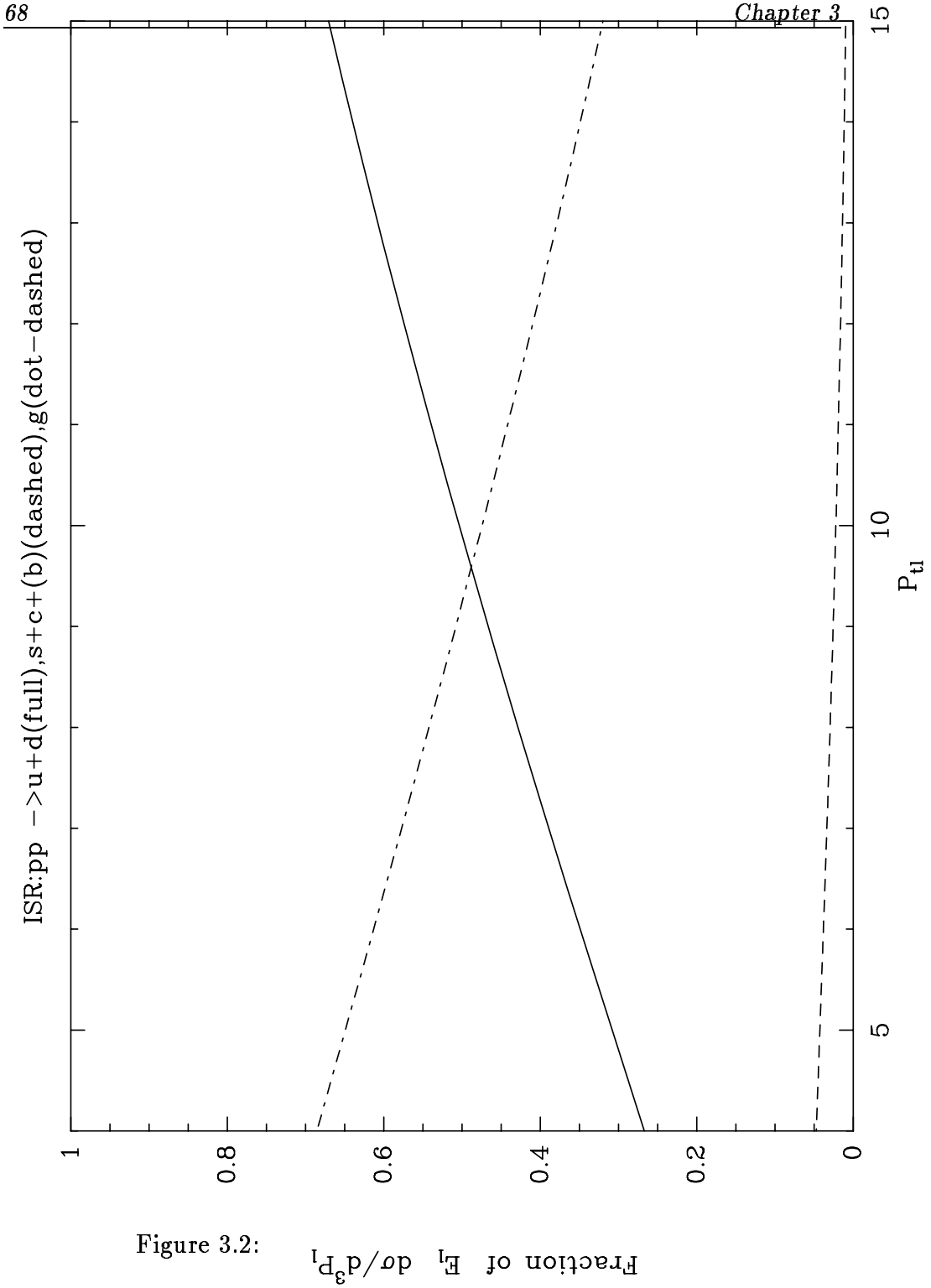
ISR:pp −>u+d(full),s+c+(b)(dashed),g(dot−dashed)
Fraction of E_l dσ/d³P_l
P_tl
0
0.2
0.4
0.6
0.8
1
5
10
15

Figure 3.2:

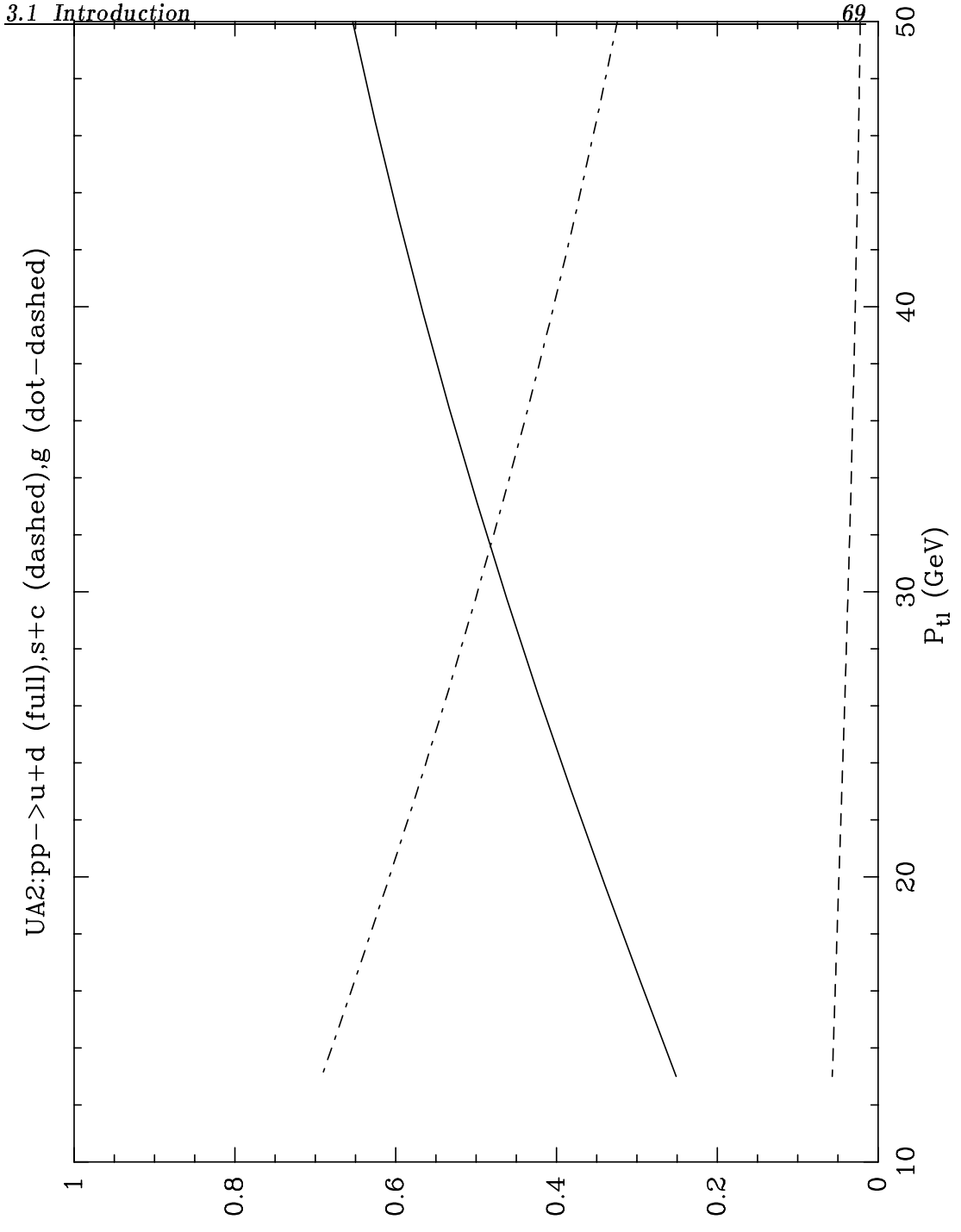
UA2:pp->u+d (full),s+c (dashed),g (dot-dashed)
Fraction of E_1 $d\sigma/d^3P_1$
P_{t1} (GeV)
0
0.2
0.4
0.6
0.8
1
10
20
30
40
50

Figure 3.3:

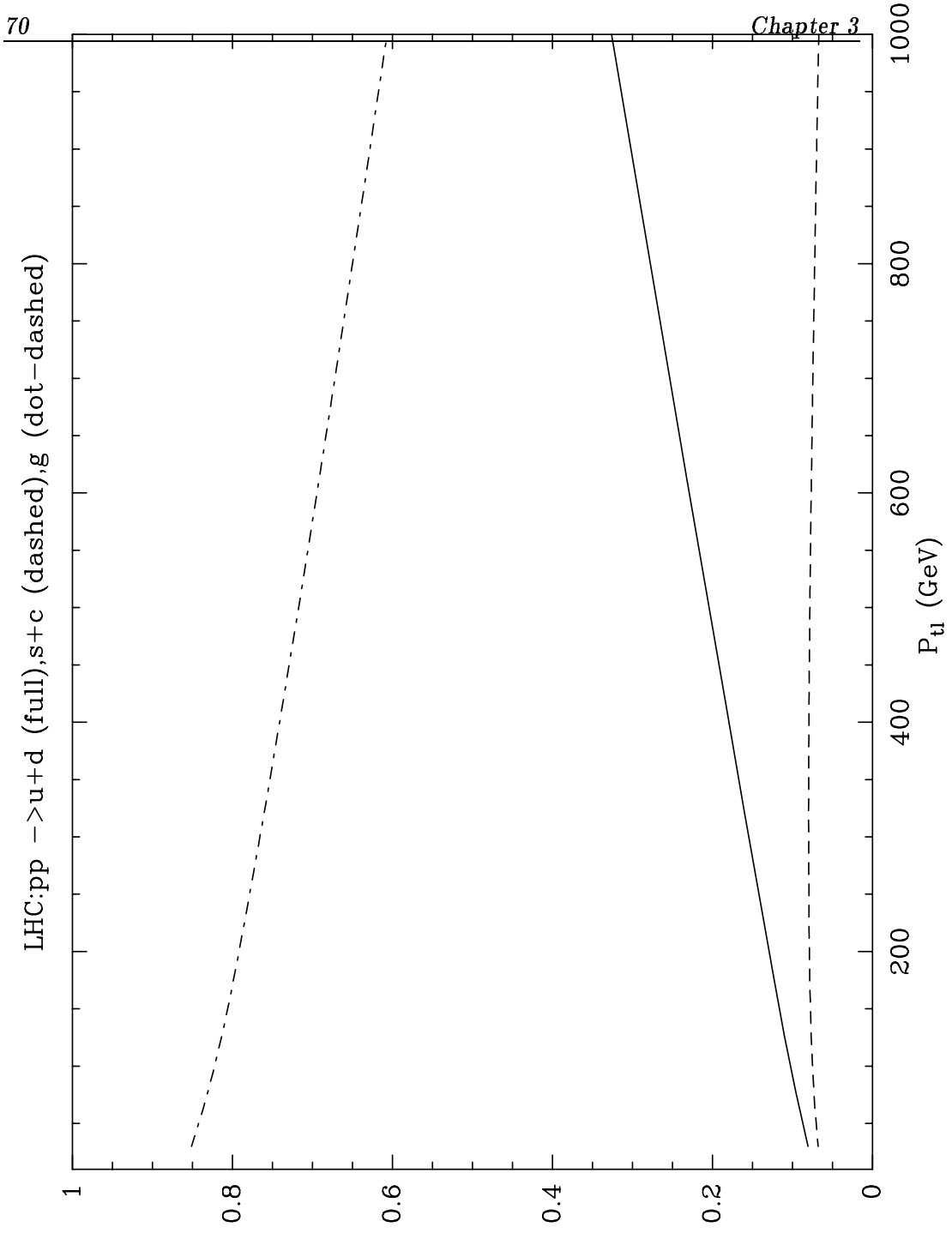
LHC:pp −>u+d (full),s+c (dashed),g (dot−dashed)
Fraction of E_1 $d\sigma/d^3P_1$
P_{t1} (GeV)
0
0.2
0.4
0.6
0.8
1
200
400
600
800
1000

Figure 3.4:

3.2 π^0 production at hadron colliders

Let us first discuss experimental data from hadronic colliders. Data in hadronic reactions have been selected for this study taking into account statistical and systematic accuracy. Whenever possible, reconstructed π^0 are preferred. For SPS fixed target energies, the available data in pp reactions are in reasonable agreement and we will use the data in the central rapidity range at $\sqrt{S} = 23$ GeV, from the WA70 collaboration [24]. The FNAL fixed target range overlaps with the lower ISR energy range. The recent data at $\sqrt{S} = 31$ GeV from pBe reactions obtained by the E706 collaboration [25] are in agreement with some of the ISR results. Resolved π^0 at $\sqrt{S} = 62.8$ GeV taken from table 5 (more precisely data corresponding to the super-retracted geometry) of Kourkoumelis et al. [27] are used. They will be compared with other data available at this energy. We will use also the more recent data from the AFS collaboration [26], which however show a different P_t dependence. At collider energies, the latest data from the UA2 experiment at $\sqrt{S} = 630$ GeV with average pseudo rapidity $\eta = 1.4$ will be used [28]. Cross checks have been made with data at $\sqrt{S} = 540$ GeV with average pseudo rapidity $\eta = 0$ although π^0 are not disentangled from direct photons.

3.2.1 FF from HERWIG

We compare now our predictions at NLO to experimental data from hadronic colliders. We first consider the data from CERN ISR [26, 27], for $\sqrt{S} = 63$ GeV, compared in figures 5 with our predictions for $\mu = M = M_f = P_t$ and $\mu = M = M_f = P_t/2$ using the quark fragmentation functions from table I and the two gluon sets from table II of the previous chapter, with $\delta = 0.35$ and $\delta = 0.40$. The agreement is satisfactory within the theoretical and experimental uncertainties.

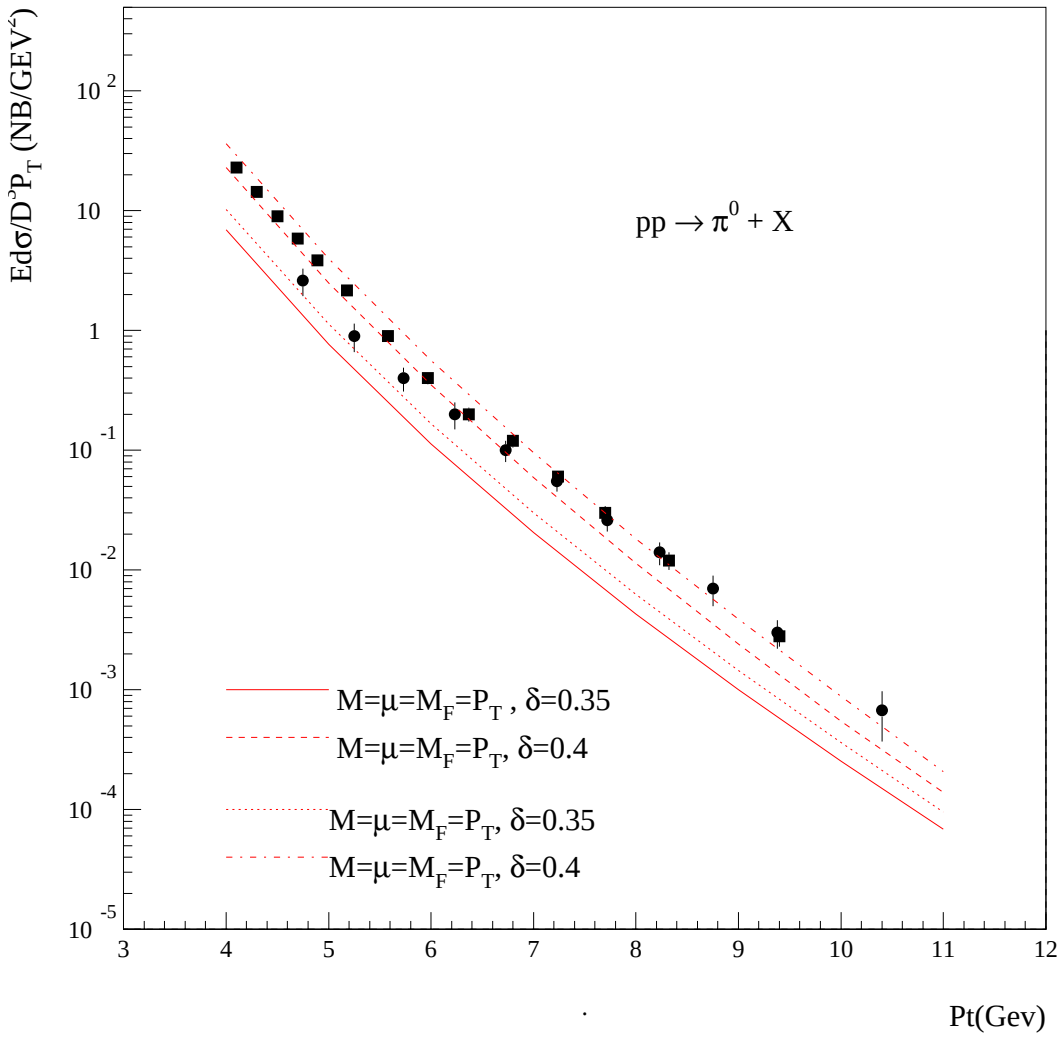

Figure 3.5: π^0 production at ISR at 63 GeV

Let us focus now on the UA2 data at the $Sp\overline{p}S$ collider [28]. We will use two sets of quite precise data, for $P_t \leq 15$ GeV and $\eta \simeq 0$ and, for $15 \leq P_t \leq 45$ GeV and $\eta \simeq 1.4$. The comparison with the theoretical predictions is shown in figures 6 and 7 for $\mu = M = M_f = P_t/2,\ P_t$ and for the two gluon sets of fragmentation functions. The agreement is quite good, and slightly favors the set corresponding to $\delta = 0.35$. The dependence on the renormalization, factorization and fragmentation scales at NLO will be discussed later.

HERWIG fragmentation functions have been used to describe hadronic data at energies higher than ISR one since for fixed target experiments the sensitive z range is above the region where e^+e^- data are correctly fitted.

Furthermore, as can be inferred from fig.2, the glue is already important at $\sqrt{S} = 63$ GeV and its contribution increases with energy. The e^+e^- data constrain essentially quark fragmentation functions in the high z region. This explains why in most of the P_t range (except in high P_t one) HERWIG fragmentation functions describe collider data.

3.2.2 Set I

Using set I of fragmentation functions we will now evaluate the NLO cross-sections for inclusive π^0 production in hadronic collisions and compare them to experimental data from low center of mass energies up to the CERN collider one. Here, the situation is less clear. First, if we keep constant the value of the parameter c it is impossible to obtain a good fit in the whole energy domain. For example, setting $c \simeq 1.5$, the ISR data can be described but the theoretical predictions are by far too low for WA70 and E706 and too high for UA2. A simple solution to this problem is to allow c to vary with the hadronic kinematical variables, in

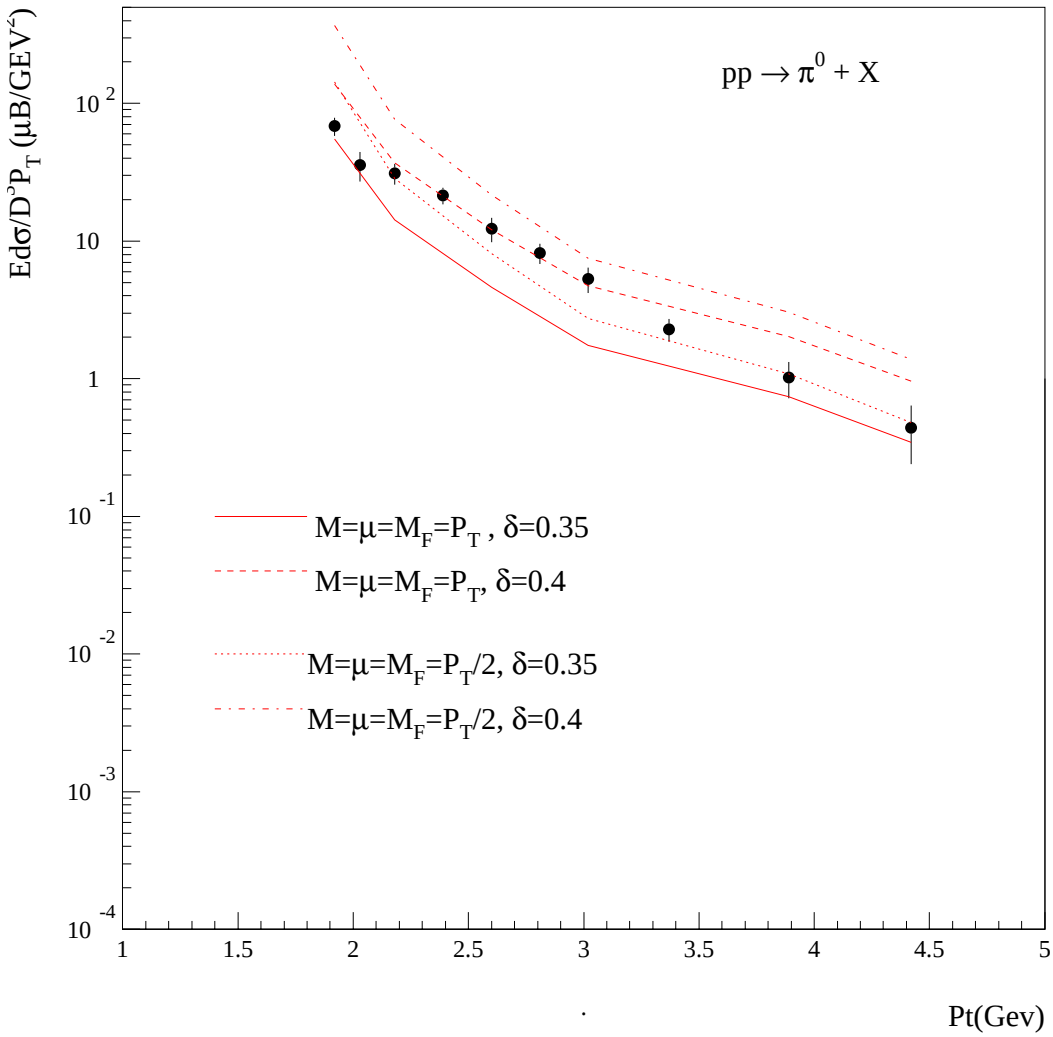

Figure 3.6: π^0 production at UA2 at 540 GeV

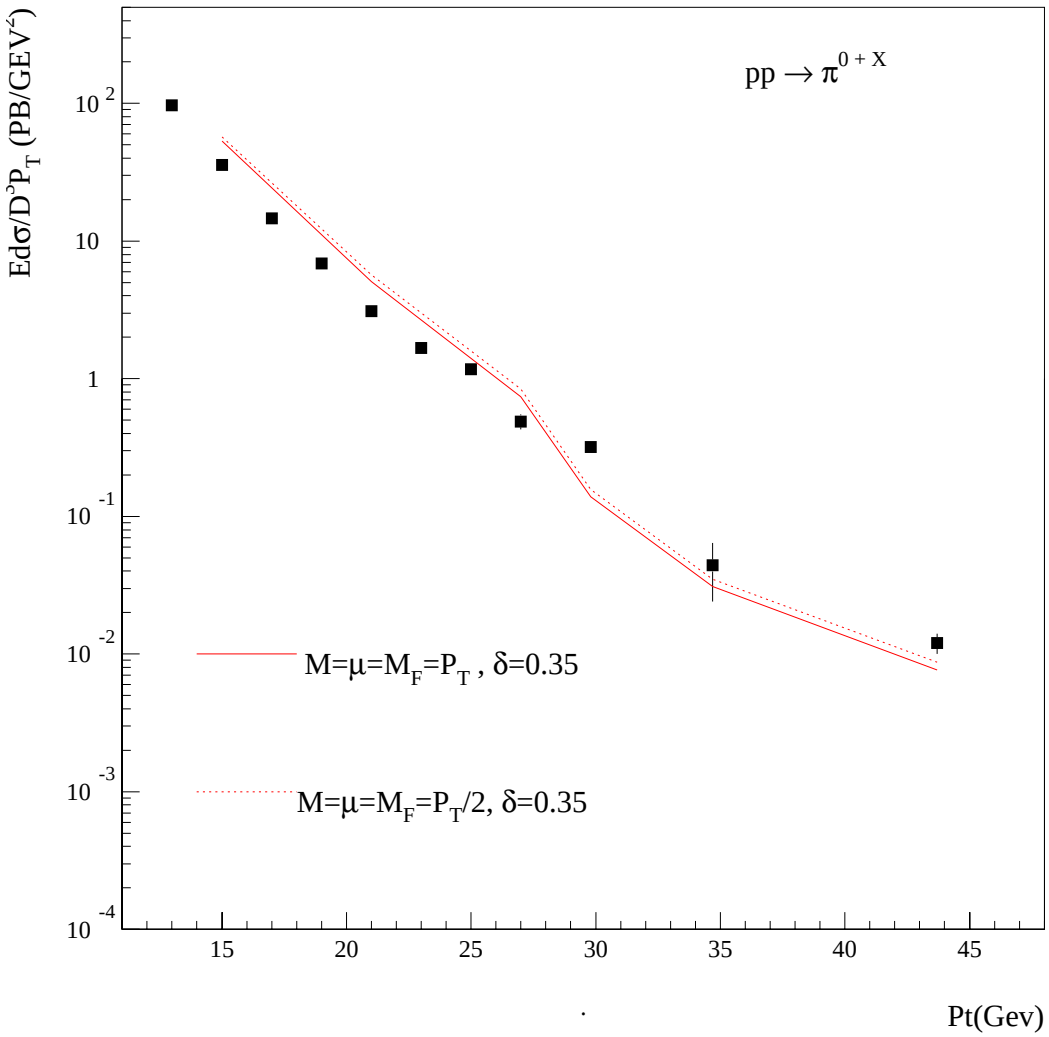

Figure 3.7: π^0 production at UA2 at 630 GeV

particular $\sqrt{S}$. A correct description of the data requires $c \simeq 0.39$ for WA70 [24] (see figure 8), $c \simeq 0.5$ for E706 [25](see figure 9), $c \simeq 1.5$ for ISR experiment [26,27] (see figure 10) and $c \simeq 5.5$ for UA2 [28] (see figure 11).

In particular for the ISR energy range, the data from AFS collaboration [26] are marginally consistent with those of reference [27] since the transverse momentum dependence in the two experiments is different. Therefore it is very difficult to describe both ISR data with high precision. We get rather good fits of data of Kourkoumelis et al. [27] with $\chi^2 = 20.6$ for 14 points using $\mu = M = M_f = 1.3P_t$ and of the AFS collaboration [26] with $\chi^2 = 12.2$ for 11 points using $\mu = M = M_f = 1.6P_t$. Notice that the slope of the UA2 data is not correctly reproduced, with a $\chi^2 = 50.2$ for 11 points. The χ^2 have been calculated with statistical errors, allowing the overall normalization to vary within the systematic error.

A comment is in order here. The approach followed so far is rather simple. When the energy grows up the scales needed to describe data have also to increase. As stated above an acceptable fit of UA2 data [28] in the forward direction can be obtained for the choice of scales $\mu = M = M_f = 5.5P_t$ which is a priori a large scale. The compensation occurring between the leading and next-to-leading terms concerning the scale dependence is much more effective at high energies. At low energy, since we prevent the scale to be less than $M_{f0} = \sqrt{2}$ GeV, this compensation does not occur and the behavior of the leading and next-to-leading cross-sections is quite the same. In other words, we are not in a good region to perform perturbation theory.

A simple scaling form of the type $A(1-x_R)^m P_t^{-n}$, where $x_R = 2P_t \cosh(\eta)/\sqrt{S}$ yields for data in the fixed target and ISR energy range (22 GeV $\leq \sqrt{S} \leq$ 63 GeV) $n \simeq 8$ while for data in the collider energy range (540 GeV $\leq \sqrt{S} \leq$ 630 GeV) $n \simeq 6.5$. Such a simple form fails to describe simultaneously data in the ISR and collider energy range and theoretical

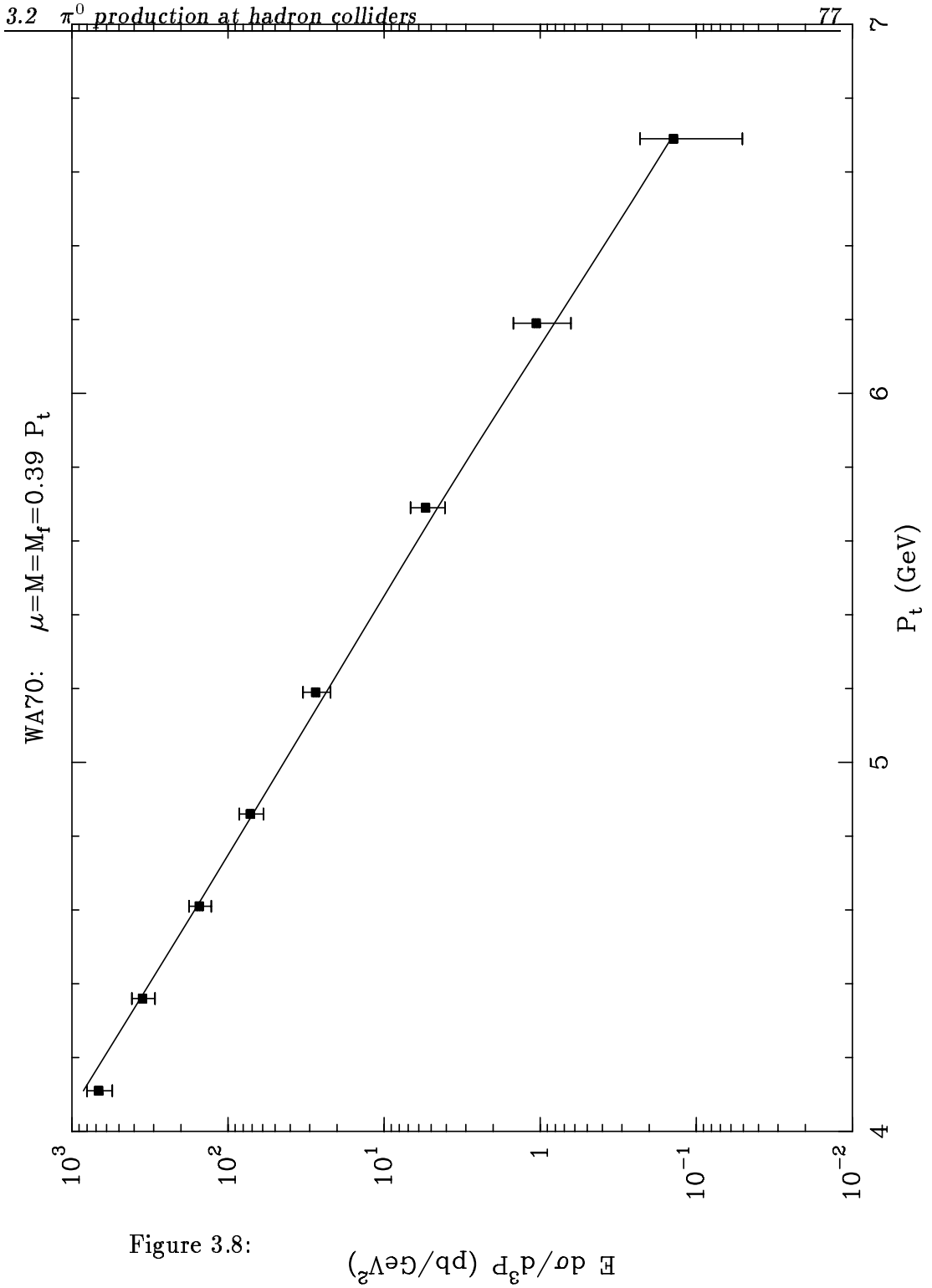
WA70: μ=M=M$_f$=0.39 P$_t$
E dσ/d^{3}P (pb/GeV^2)
P$_t$ (GeV)
10^3
10^2
10^1
1
10^{-1}
10^{-2}
4
5
6
7

Figure 3.8:

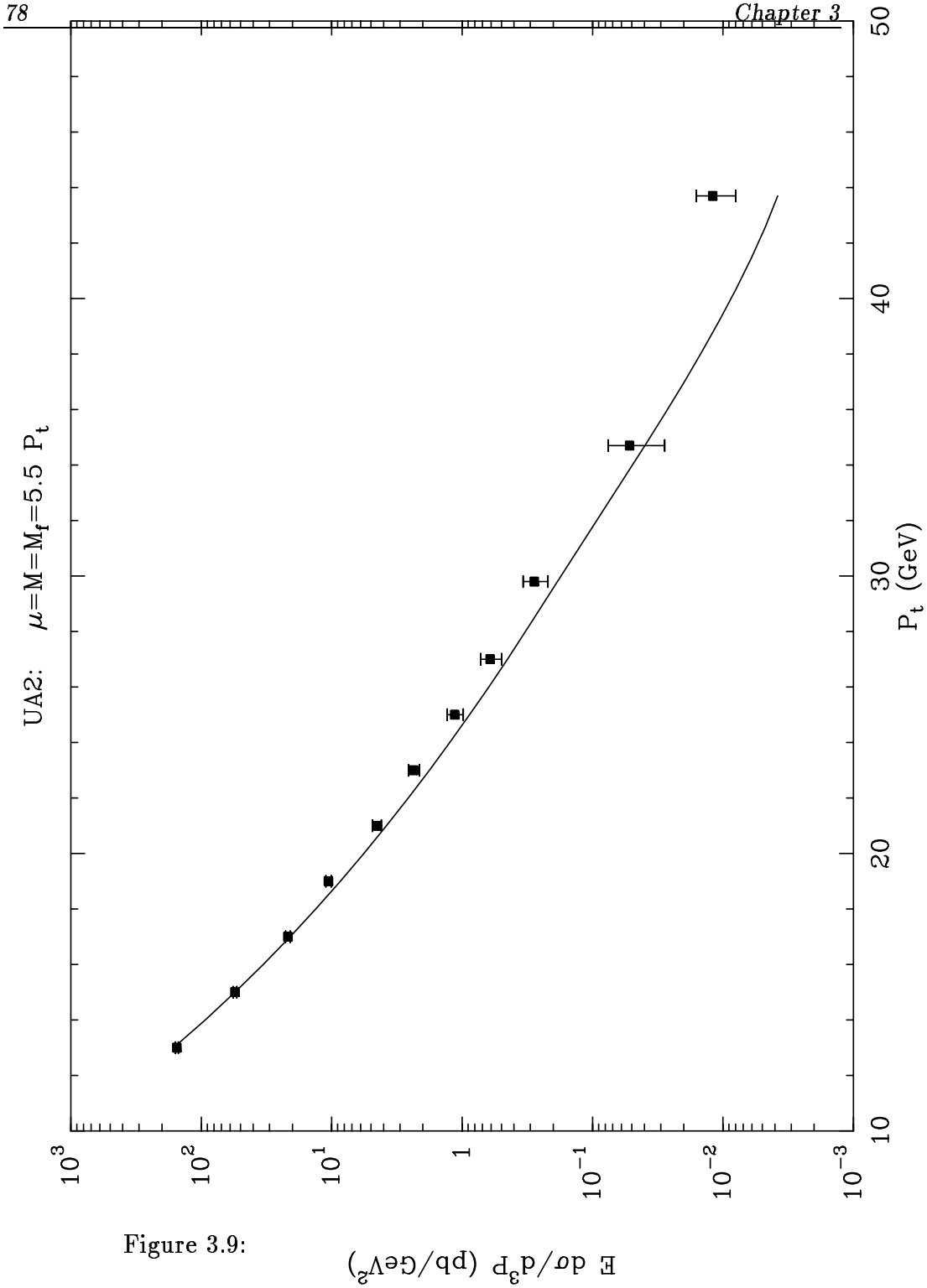
UA2: μ=M=M$_f$=5.5 P$_t$
E dσ/d^{3}P (pb/GeV^2)
P$_t$ (GeV)
10^3
10^2
10^1
1
10^{-1}
10^{-2}
10^{-3}
10
20
30
40
50

Figure 3.9:

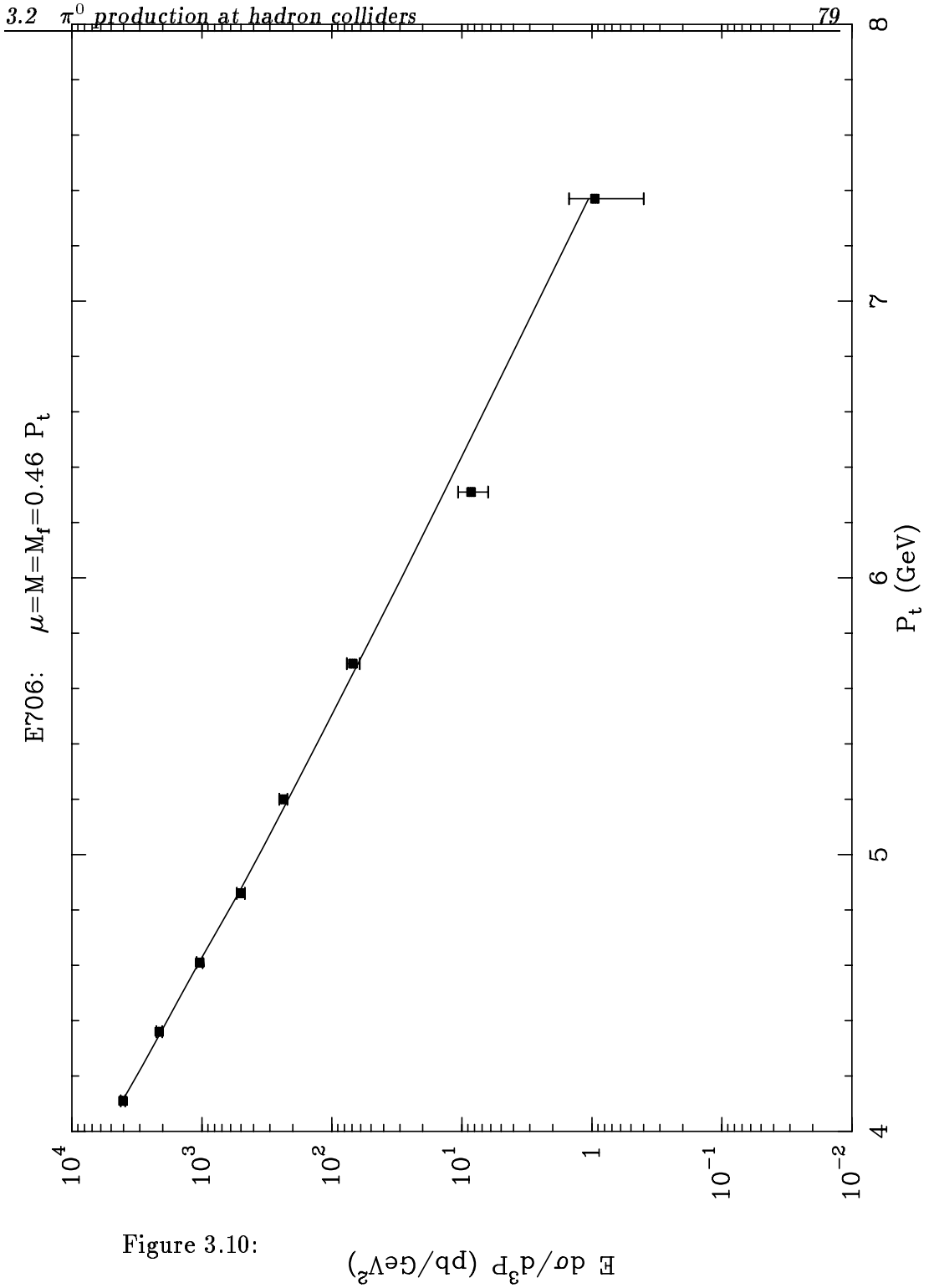
E706: μ=M=M$_f$=0.46 P$_t$
E dσ/d^{3}P (pb/GeV^2)
P$_t$ (GeV)
10^4
10^3
10^2
10^1
1
10^{-1}
10^{-2}
4
5
6
7
8

Figure 3.10:

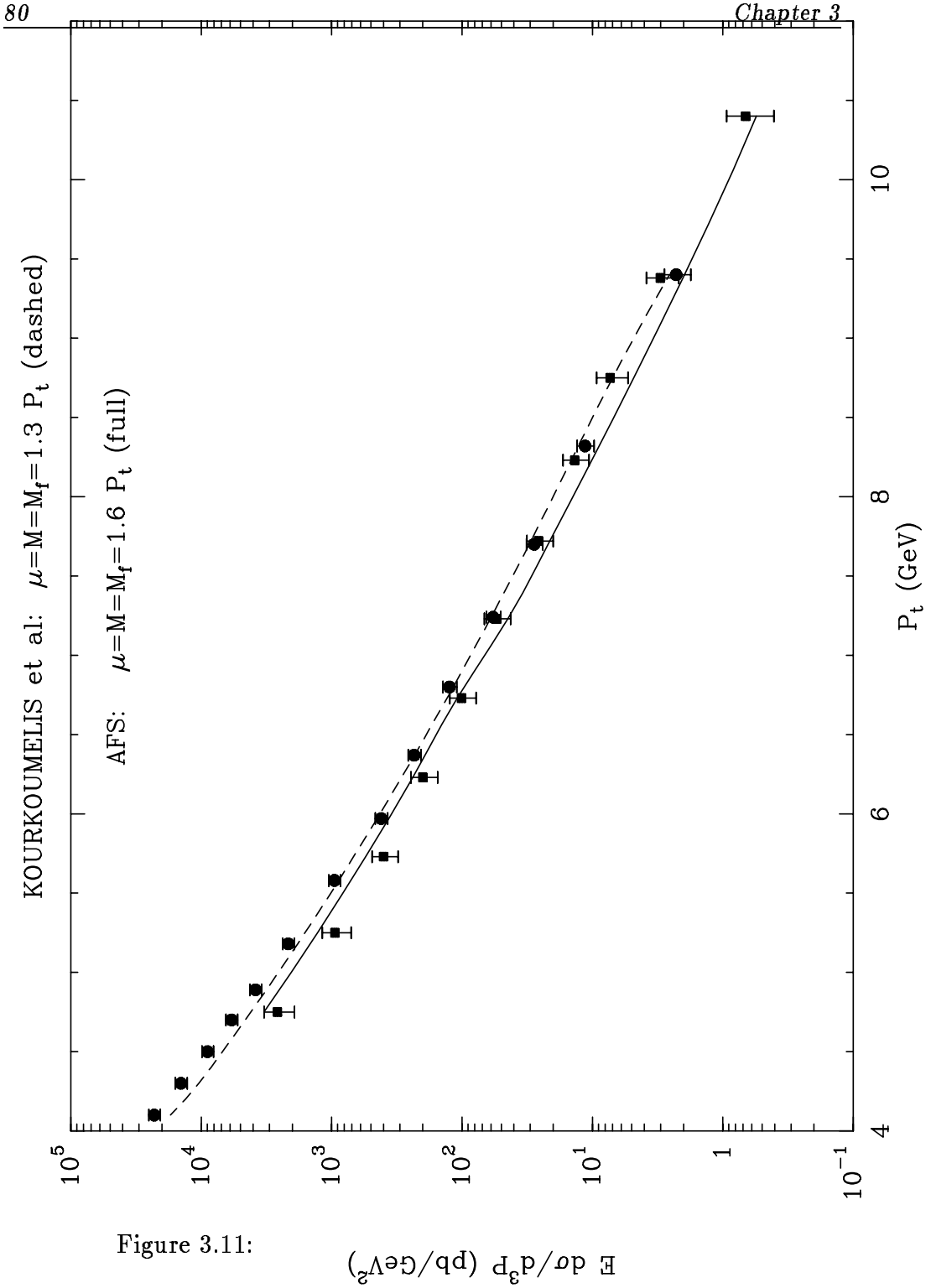
KOURKOUMELIS et al: μ=M=M$_f$=1.3 P$_t$ (dashed)
AFS: μ=M=M$_f$=1.6 P$_t$ (full)
E dσ/d^{3}P (pb/GeV^2)
P$_t$ (GeV)
10^5
10^4
10^3
10^2
10^1
1
10^{-1}
4
6
8
10

Figure 3.11:

predictions in the whole energy range if the scales are independent of $\sqrt{S}$.

Although some care has to be taken on the extraction of the power values due to their sensitivity to the choice of parameterization, the power dependence is difficult to predict analytically in QCD since besides the P_t^{-4} parton subprocesses dependance, factorization and renormalization scales are involved. In addition, since we have arbitrarily set these scales equal, the physical meaning of the increase of the scales with $\sqrt{S}$ is unclear.

This approach might be criticized. Indeed it is not very predictive, since the scales change with the energy. In other words one adds a new parameter which acts as an overall normalization for each experiment. Notice that the normalization of the glue fragmentation function N_g is strongly correlated to the choice made for the scale. More precisely, we could perfectly find a value for N_g which describes the UA2 data with $c = 0.5$. But in this case we couldn't describe the other data at lower energies.

3.2.3 Set II

The two sets differ mainly for the gluon normalization. As can be seen from inspection of figures 12, 13, 14 and 15 a rather good fit of the latest UA2 data at $\sqrt{S} = 630$ GeV [28], AFS [26] and Kourkoumelis et al data [27] can be obtained leading to a $\chi^2 \simeq 50$ for 31 points.

Kourkoumelis et al. data favor the set characterized by the largest glue (set IIb) whereas UA2 data are better fitted by the other set (set IIa). Notice that we have taken into account the systematic errors of the data which affect the overall normalization. The χ^2 are 3.46 (4.28) for the 11 AFS points, 31.54 (23.52) for the 9 Kourkoumelis et al. points and 14.91 (20.00) for the 11 UA2 points with the parameters of set IIa (IIb). Inside the systematic errors we can also describe UA2 data at $\sqrt{S} = 540$ GeV

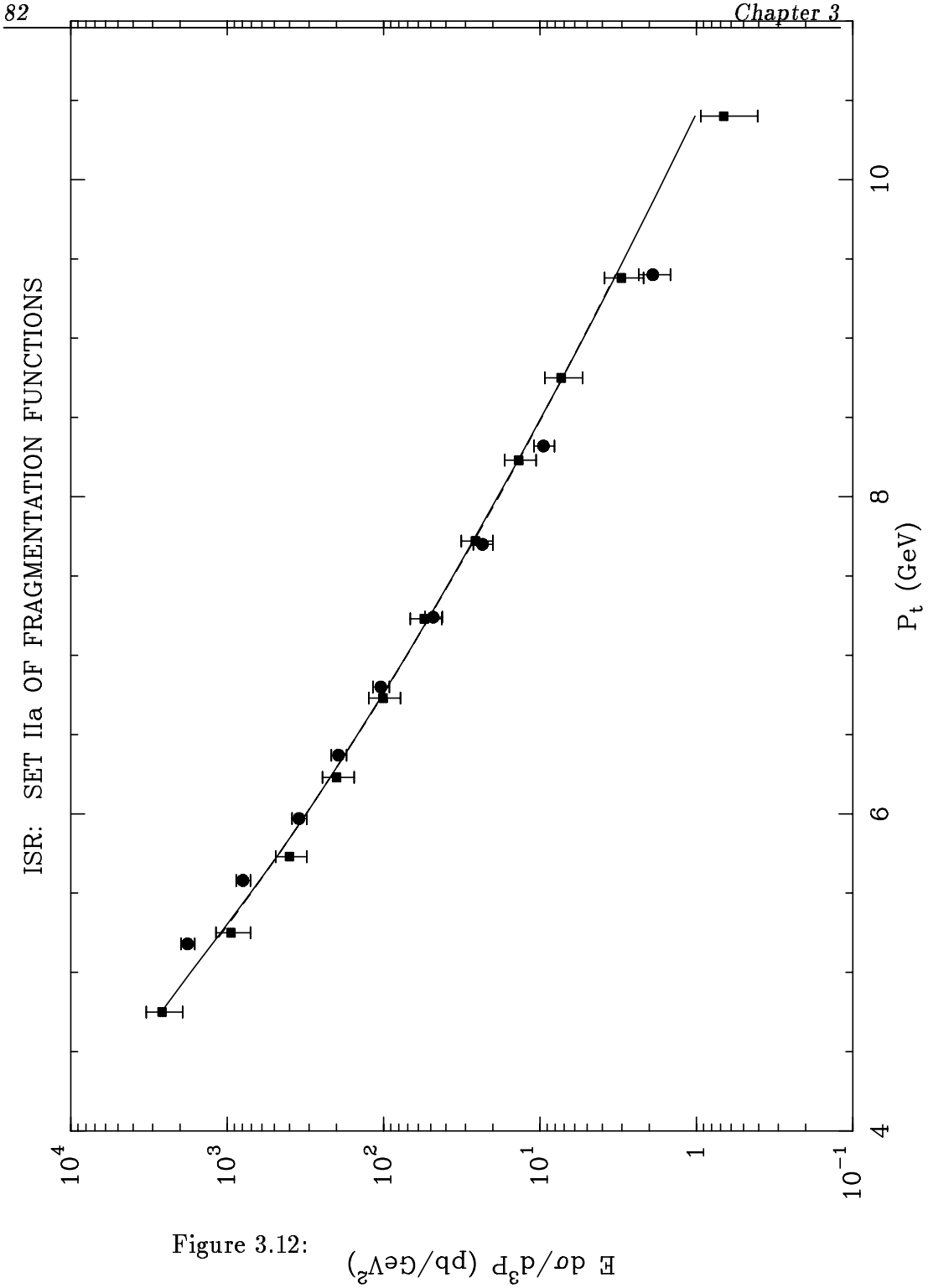
ISR: SET IIa OF FRAGMENTATION FUNCTIONS
E dσ/d³P (pb/GeV²)
P_t (GeV)
10⁴
10³
10²
10¹
1
10⁻¹
4
6
8
10

Figure 3.12:

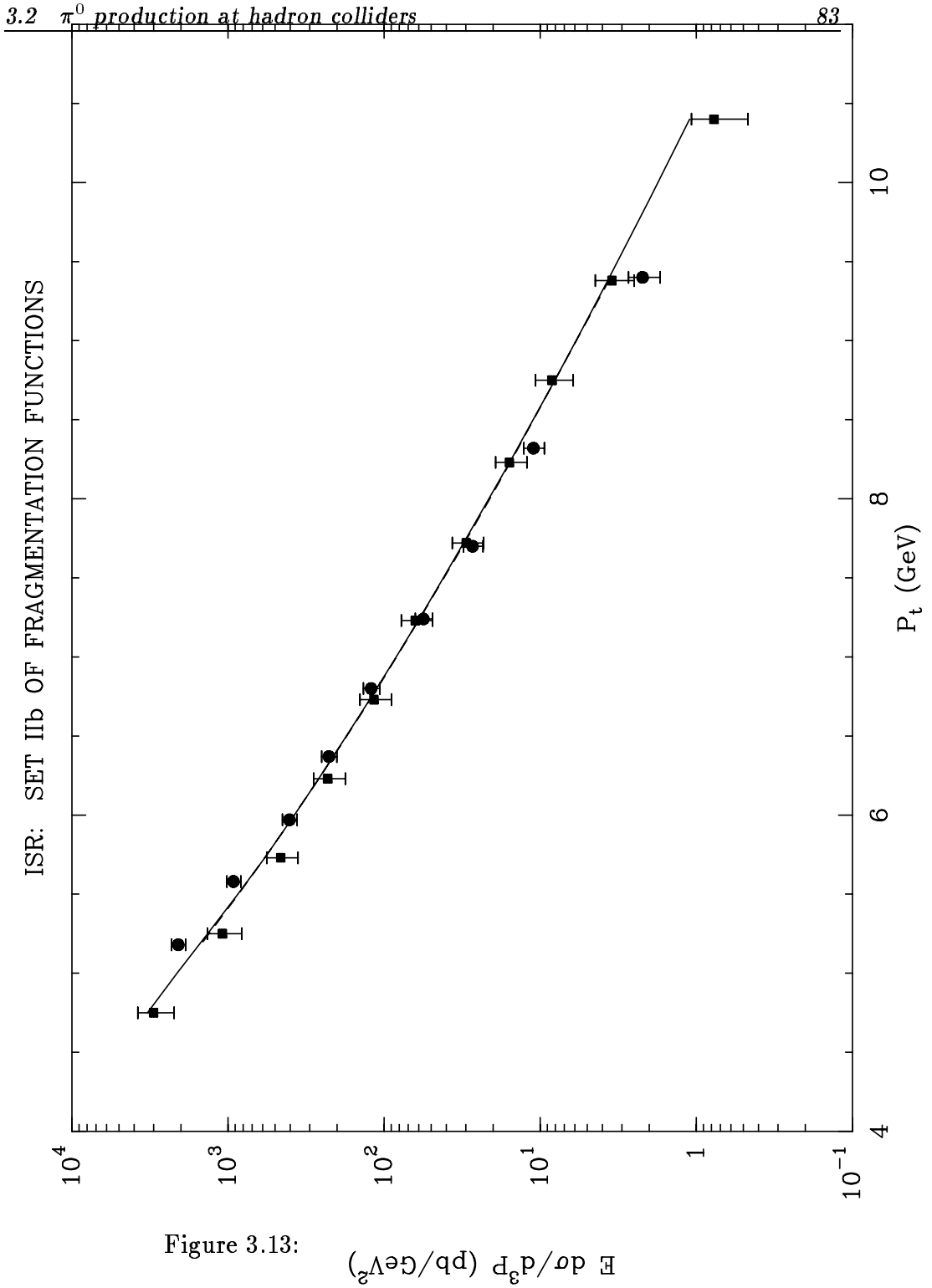
ISR: SET IIb OF FRAGMENTATION FUNCTIONS
$E\ d\sigma/d^3p$ (pb/GeV^2)
P_t (GeV)
10^4
10^3
10^2
10^1
1
10^{-1}
4
6
8
10

Figure 3.13:

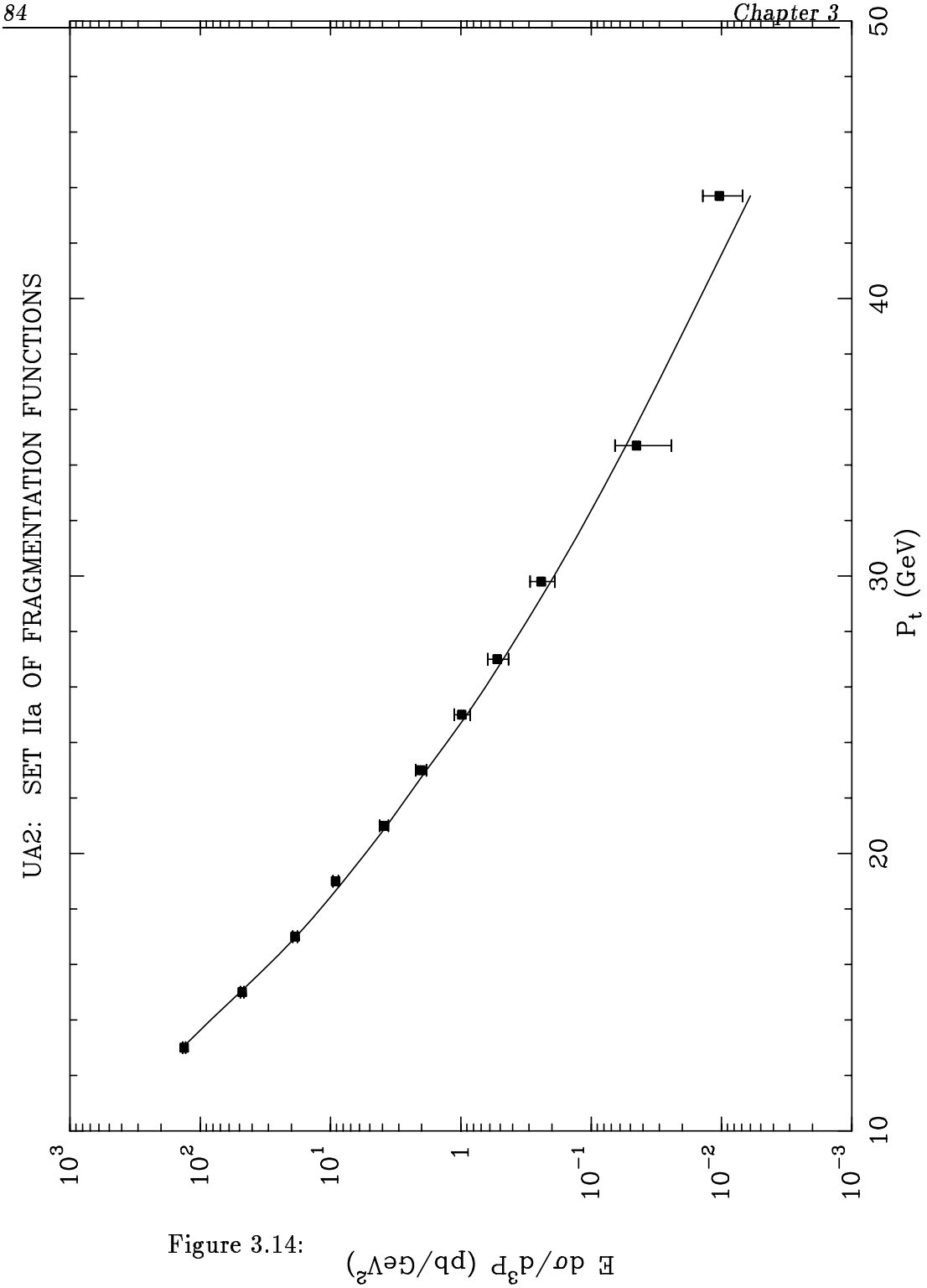
UA2: SET IIa OF FRAGMENTATION FUNCTIONS
E dσ/d³P (pb/GeV²)
P_t (GeV)
10^3
10^2
10^1
1
10^-1
10^-2
10^-3
10
20
30
40
50

Figure 3.14:

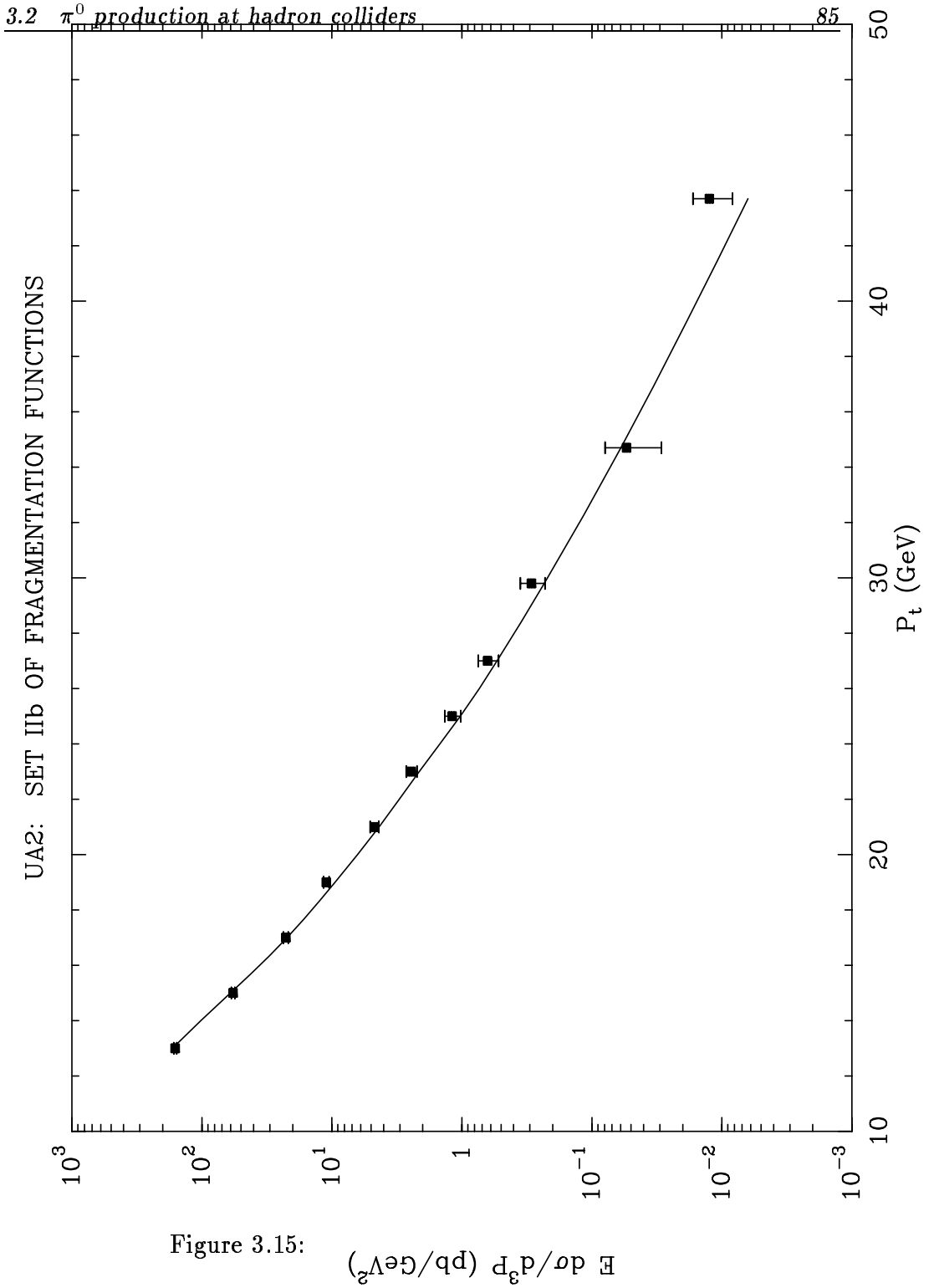
UA2: SET IIb OF FRAGMENTATION FUNCTIONS
E dσ/d³P (pb/GeV²)
P_t (GeV)
10³
10²
10¹
1
10⁻¹
10⁻²
10⁻³
10
20
30
40
50

Figure 3.15:

and $\eta = 1.4$. On the other hand we are not able to describe WA70 and E706 data with the values of N_g found before. This is not very surprising since the corrective term is found to be huge, and although we can find an optimization point this is not very stable suggesting that we are not in the appropriate region to trust perturbation theory.

3.2.4 Predictions at LHC

To our knowledge no global comparison of inclusive π^0 production at hadronic colliders to parton shower MONTE CARLO has been performed. These MONTE CARLO, although based on a leading order calculation, include angular ordering in parton radiation whereas our NLO evaluation does not take into account resummation of large logarithms of kinematical origin. Therefore a comparison of our approach with MONTE CARLO would be interesting for π^0 production at future colliders.

As we have seen present data do not allow to extract the π^0 fragmentation functions unequivocally. To this aim the forthcoming information from ep HERA collider should be very helpful. With these limitations we will now estimate the π^0 rates at LHC using the various sets of fragmentation functions previously derived.

Let us consider first set I of fragmentation functions. In order to describe hadronic data we had to increase the scales $\mu = M = M_f$ from $\frac{P_t}{2}$ at $\sqrt{S} \simeq 20$ GeV up to $5P_t$ at $\sqrt{S} = 630$ GeV. An extrapolation to LHC energy would lead to $\mu = M = M_f \simeq 50P_t$ which seems by far an unnatural scale. To estimate the sensitivity to scales we show in figure 16 the ratio of cross sections at LHC for the two scales $50P_t$ and P_t at $\eta = 0$. As can be inferred from the figure the rates differ by at most a factor of three. To estimate the uncertainty due to structure functions we have taken the set of structure functions of HMRS [18] using the $\overline{MS}$ scheme and the set of Morfing-Tung [17] using the DIS scheme. The predictions

differ by at most 20%. Similarly the ratio of predictions using set II is displayed in figure 17.

The situation is summarized in figure 18 where we show the absolute rates at LHC for $\eta = 0$ from the most plausible sets in the three approaches:HERWIG with $\delta = 0.35$ (full line), set I with $\mu = M = M_f = 100P_t$ (dot-dashed curve) and set II with $N_g = 0.75$ (dashed curve). This gives an estimate of the theoretical uncertainty which is of the order of a factor two. The uncertainty on structure functions is marginal compared to the poor determination of fragmentation functions.

To show the stability of the NLO corrections we display the cross section as a function of the scales μ and $M = M_f$ compared to the LO result for $P_t = 50$ GeV (figures 19-20). We vary the scales between $P_t/5$ and $5P_t$. The NLO cross sections exhibit a saddle point whereas the LO cross sections decrease monotonically when the scales increase.

The uncertainty due to factorization scheme, especially coming from fragmentation functions is expected to be tiny for the two following reasons. Firstly the evaluation done for one jet inclusive cross section has shown[2] that at collider energies its magnitude is of the order of 5% -if done correctly - and we can reasonably expect a same order of magnitude for one hadron inclusive cross section. Secondly a precise estimate doesn't seem mandatory compared to the large uncertainty coming from fragmentation functions.

3.3 η production at hadron colliders

In this section we will show some results regarding the inclusive η production at hadron colliders comparing, whenever possible, the results to experimental data.

We consider now our predictions for inclusive production in hadronic

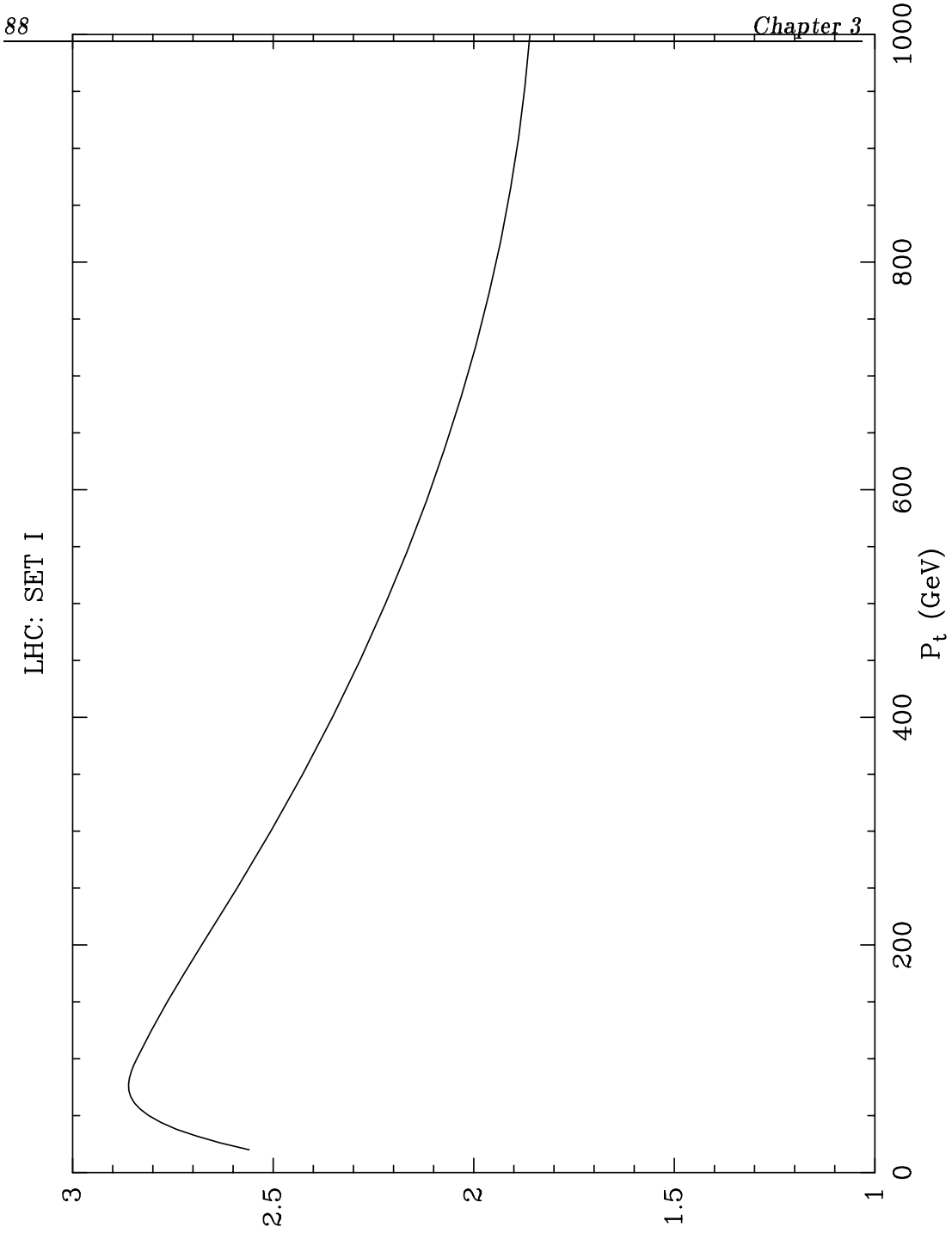
LHC: SET I
RATIO OF CROSS SECTIONS
P_t (GeV)
3
2.5
2
1.5
1
0
200
400
600
800
1000

Figure 3.16:

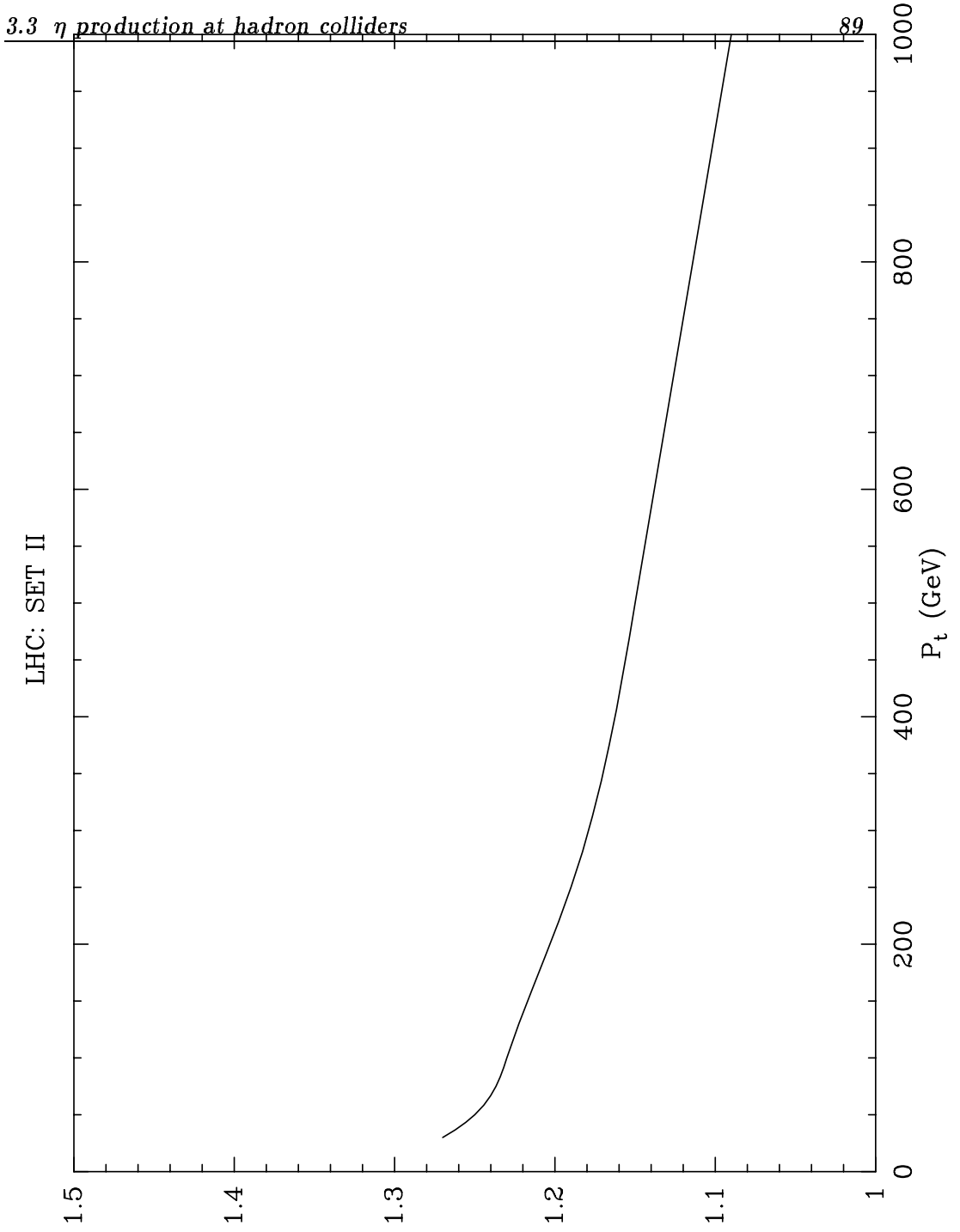
LHC: SET II
RATIO OF CROSS SECTIONS
P_t (GeV)
1.5
1.4
1.3
1.2
1.1
1
0
200
400
600
800
1000

Figure 3.17:

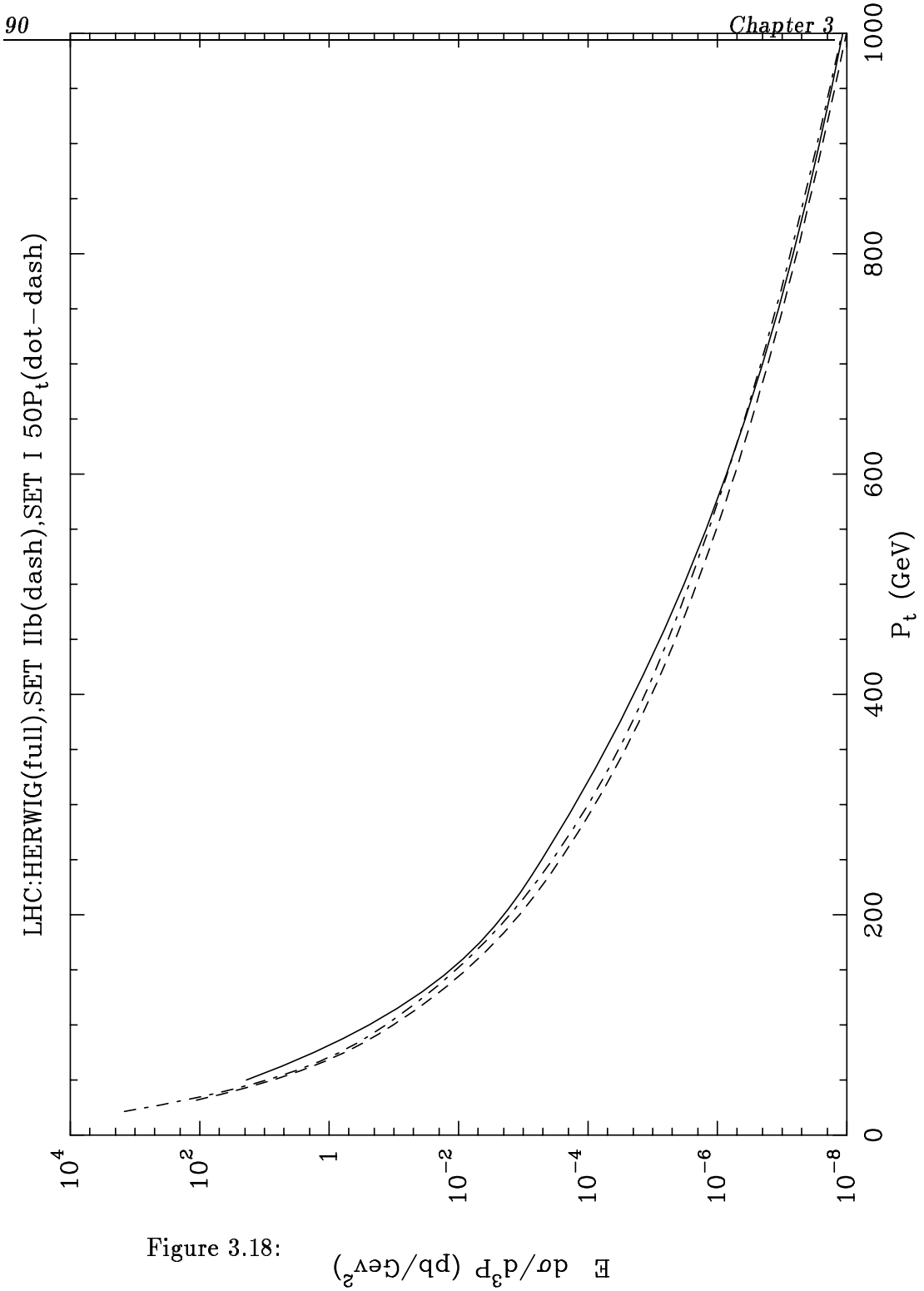
LHC:HERWIG(full),SET IIb(dash),SET I 50P$_t$(dot−dash)
E dσ/d^{3}P (pb/GeV^2)
P$_t$ (GeV)
10^4
10^2
1
10^{-2}
10^{-4}
10^{-6}
10^{-8}
0
200
400
600
800
1000

Figure 3.18:

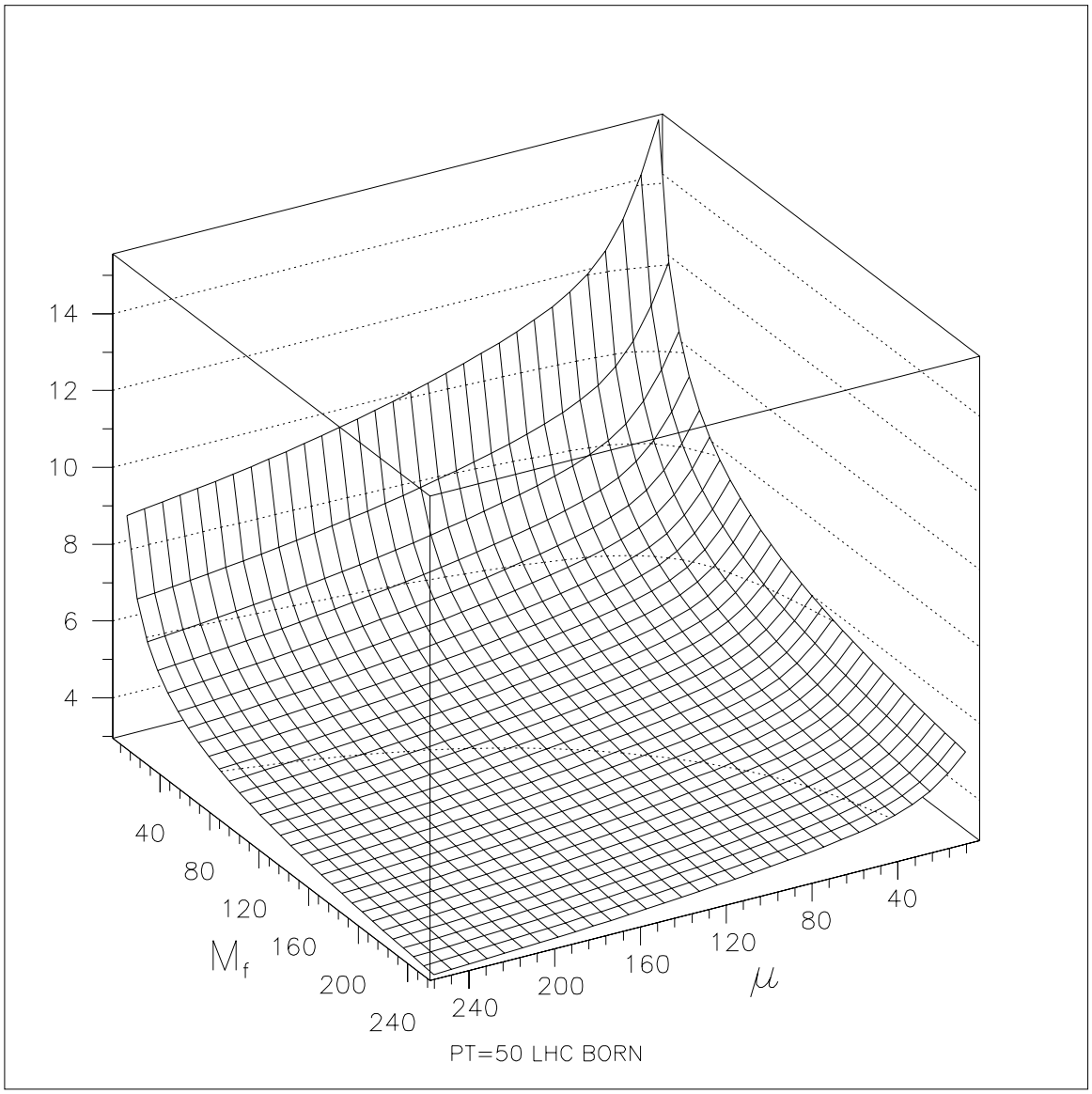

Figure 3.19: π^0 cross sections at LHC in pb using set I of fragmentation functions as a function of the scales μ and $M = M_f$ for $P_t = 50$ GeV and $\eta = 0$. LO prediction

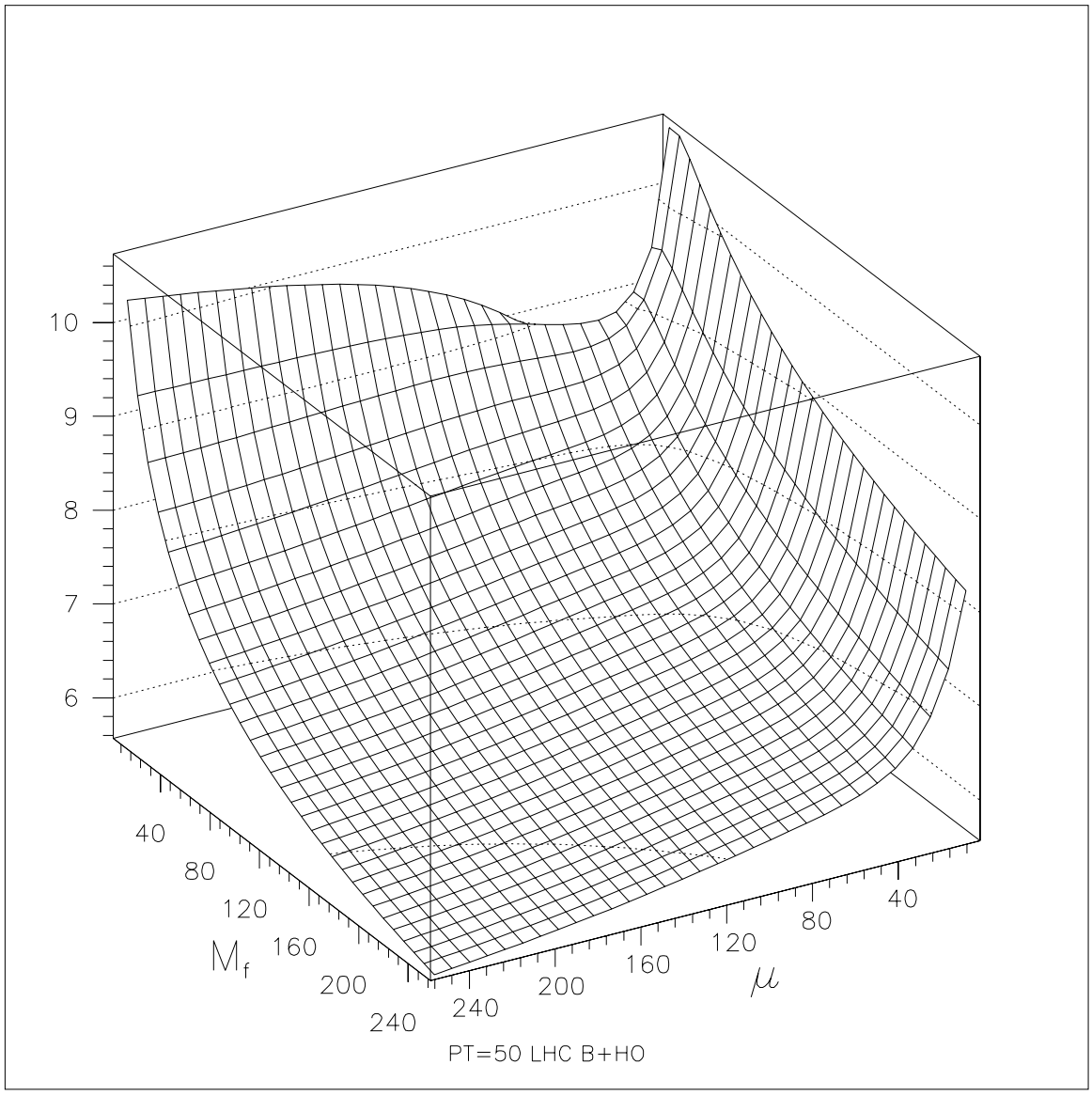

Figure 3.20: Same as Fig.20 but NLO

colliders. We first compare with data from CERN ISR [26], for $\sqrt{S} = 52.7$ GeV and $\sqrt{S} = 62.4$ GeV, as shown in Figures 21 and 22 for $\mu = M = M_f = P_t$ and $\mu = M = M_f = P_t/2$ using the quark fragmentation functions from Table VI and the two gluon solutions from Table VII, for $\delta = 0.35$ (Set I) and $\delta = 0.40$ (Set II). In doing so, in absence of direct data on η production, we have inferred the cross section from π^0 data assuming the experimental [26] η/π^0 ratio R of 0.58 ± 0.05 and 0.55 ± 0.06 respectively, independent from p_t. The agreement is satisfactory within the theoretical and experimental uncertainties.

Let us focus now on the UA2 data at the $Sp\overline{p}S$ collider [28]. We will use two sets of quite precise π^0 data, for $P_t \leq 15$ GeV and pseudorapidity $y \simeq 0$ and for $15 \leq P_t \leq 45$ GeV and $y \simeq 1.4$, and an experimental ratio η/π^0 of 0.5 as obtained from ISR data [26]. The comparison with the theoretical predictions is shown in Figures 23 and 24 for $\mu = M = M_f = P_t/2,\ P_t$ and for the two gluon sets of fragmentation functions. The agreement is quite good at low p_t, and slightly favours set I.

On the other hand we note that at higher p_t the comparison with data suggests a larger value for the ratio η/π^0, and therefore a p_t dependence for this ratio. Indeed from the result of our previous study on inclusive π^0 production, we show in Figure 25 the predicted p_t dependence of $R = \eta/\pi$ at $\sqrt{S}$ =630 GeV, which indeed rises with p_t.

Finally we proceed to the predictions for LHC $\sqrt{S} = 16$ TeV. The cross sections are calculated at LO (Born) and NLO and using HMRS Set of structure functions [18] and are displayed in Fig. 26.[1]

To estimate the theoretical uncertainty we study in Fig. 27 the ratio of the two predictions from the two different choices of gluon fragmentation

[1]The discontinuities in the curves are simply due to CPU time limitation on the number of the data points.

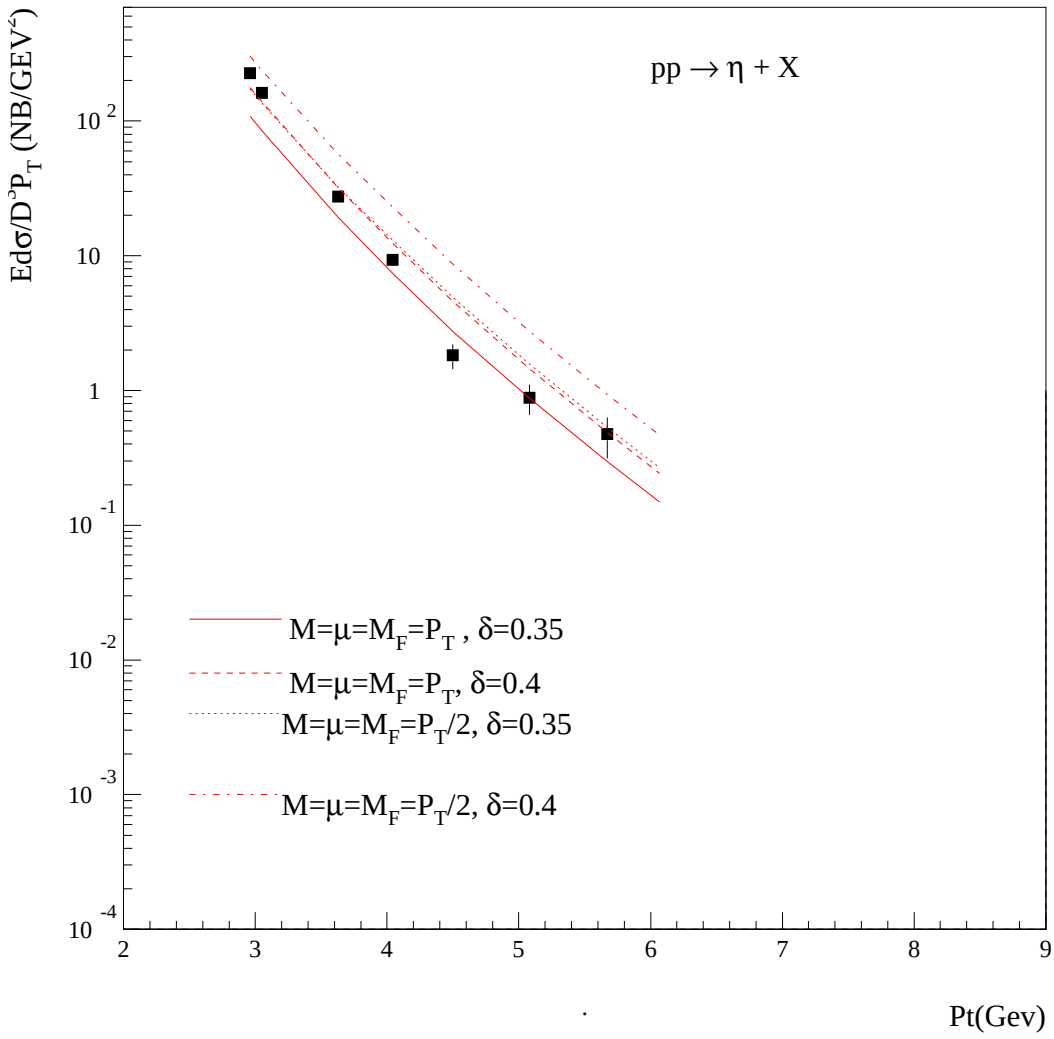

Figure 3.21: η production at ISR at 62.4 GeV

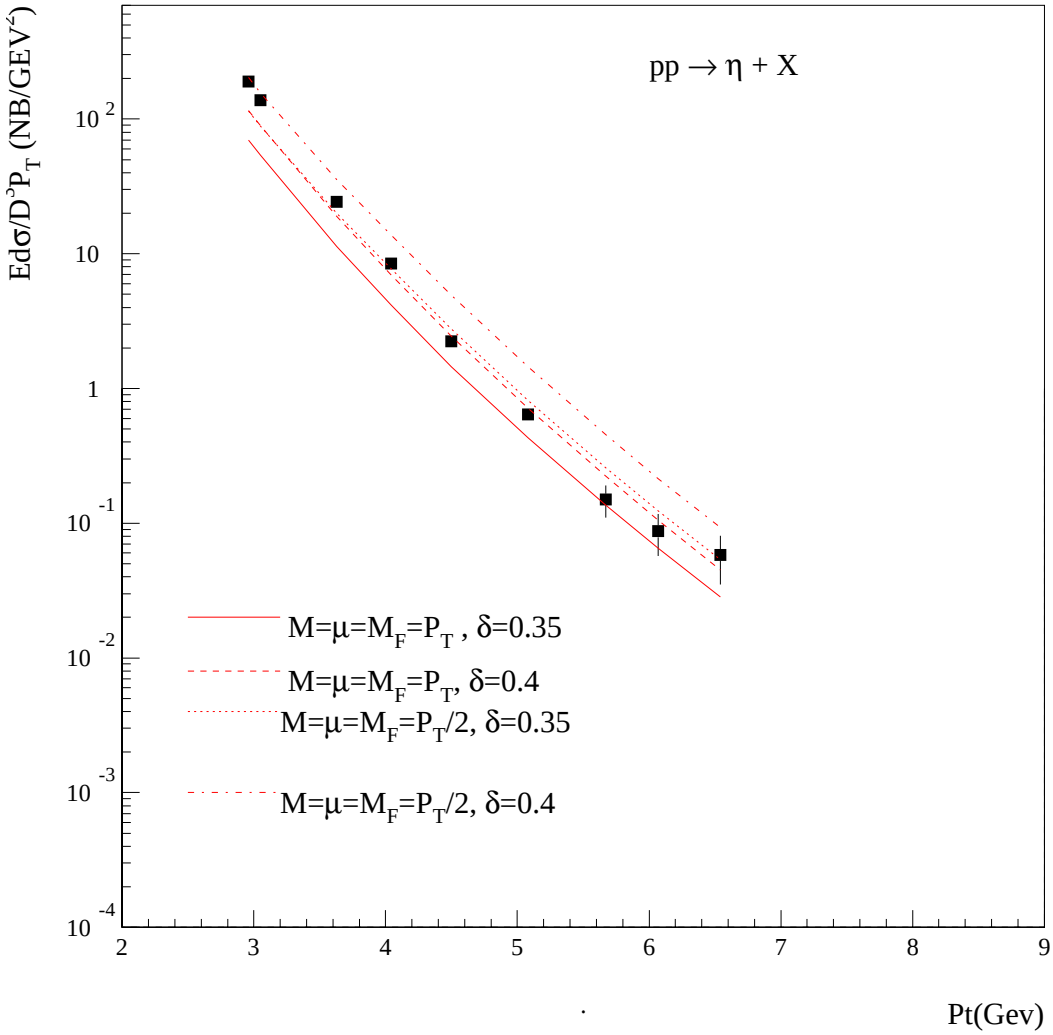

Figure 3.22: η production at ISR at 52.7 GeV

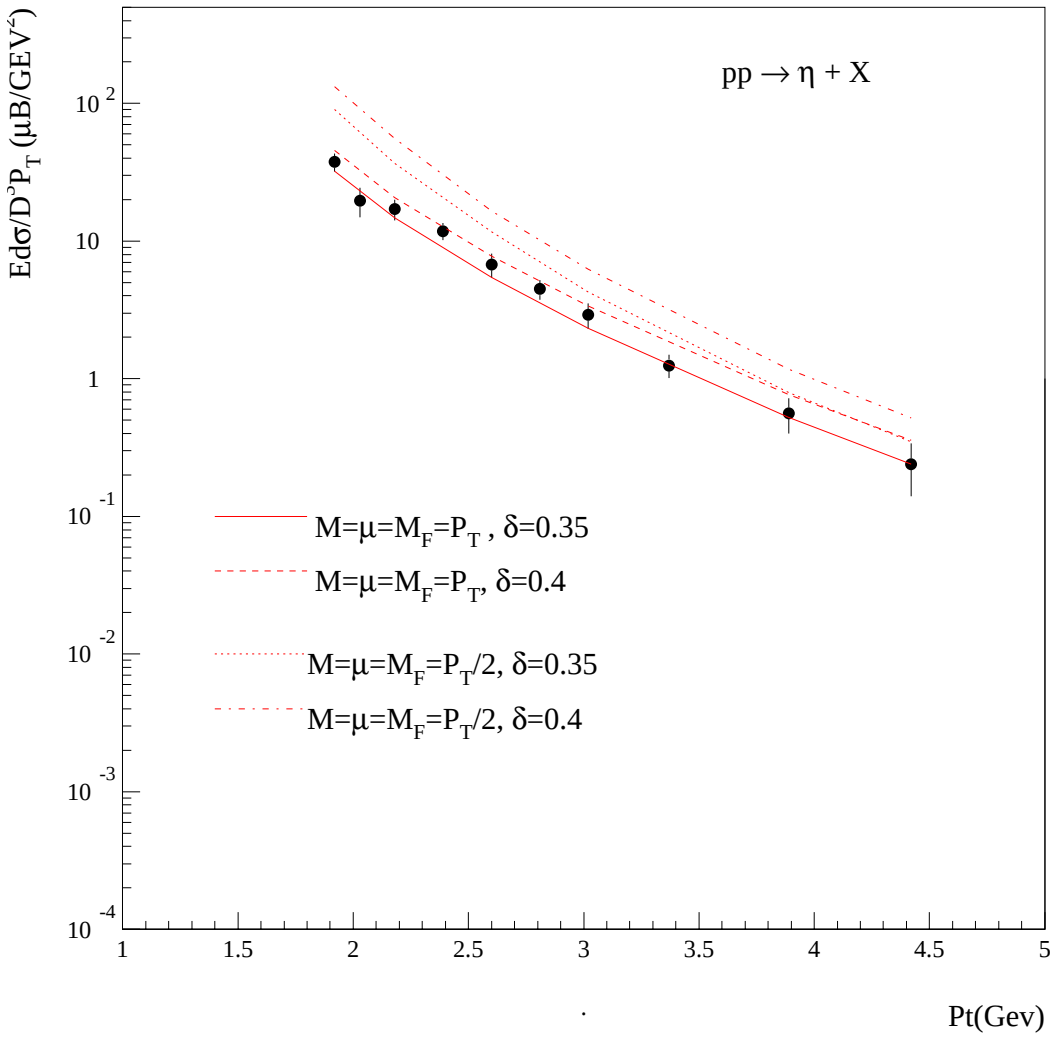

Figure 3.23: η production at UA2 at 540 GeV

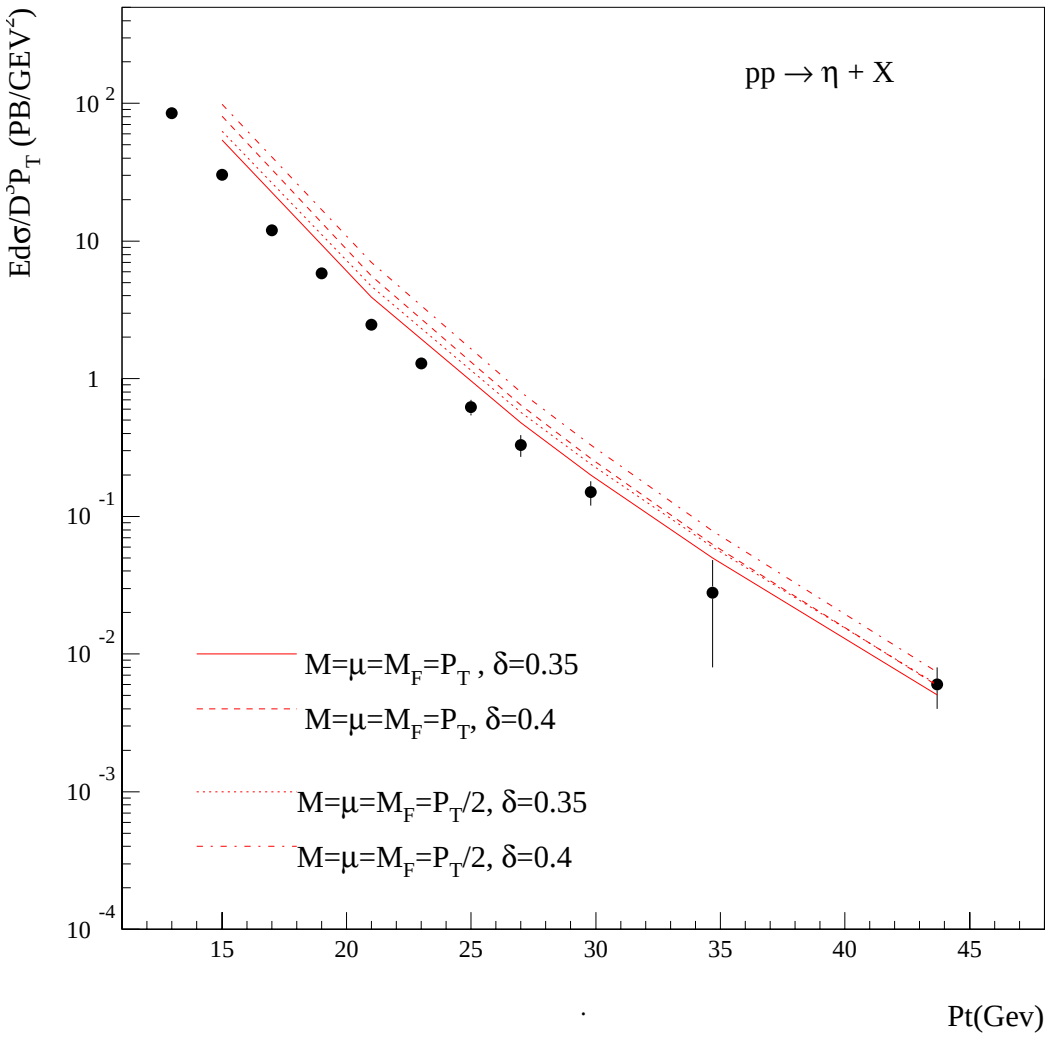

Figure 3.24: η production at UA2 at 630 GeV

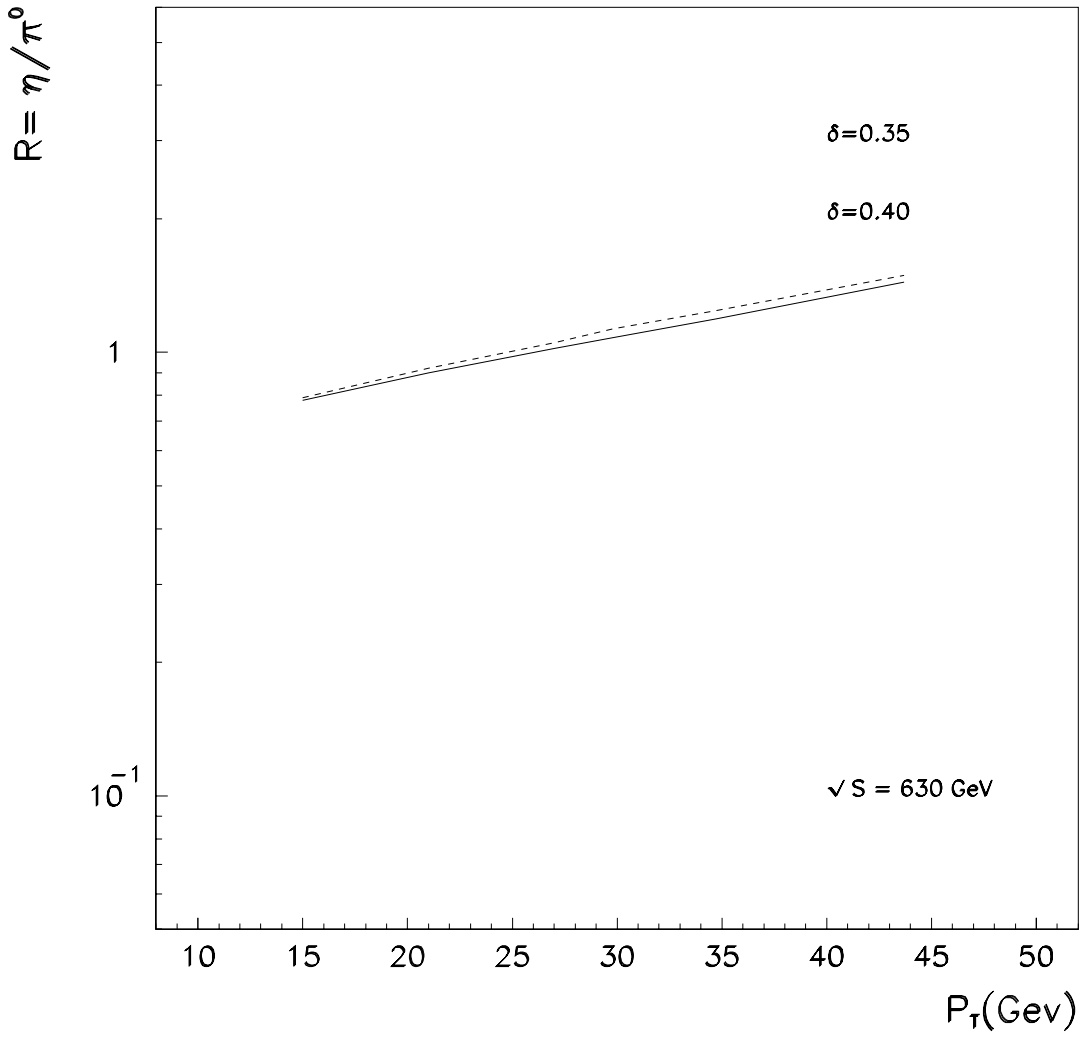

Figure 3.25: theoretical prediction of the ratio η/π^0 as function of p_T at UA2

functions, evolved to NLO accuracy, at $\sqrt{S} = 16$ TeV.

We then calculate the theoretical ratio η/π^0 as evaluated from the π^0 results of the previous subsection. The ratio increases with respect to ISR energies, and shows a dependence on p_t similar to what found at $Sp\bar{p}S$ energies.

The uncertainty due to factorization scheme, especially coming from fragmentation functions is expected to be tiny because the evaluation done for one jet inclusive cross section has shown [23] that at collider energies its magnitude is of the order of 5% and we can reasonably expect the same order of magnitude for one hadron inclusive cross section. Finally, the theoretical uncertainty from the structure functions is much smaller than that coming from fragmentation function.

3.4 Light mesons production at Tevatron

In this section we will show the prediction for light meson production at Tevatron.

In Fig.28 we show the p_t distribution for inclusive single particle production for π^0, η, $\pi^{\pm}$, $K^{\pm}$, integrated in the region of pseudorapidity $\eta = -\ln(\tan(\frac{\theta}{2}))$ between -0.7 and 0.7 and using the Set B-1 of Morfin and Tung [17]. We set all the scales equal to the p_T of the produced hadron.

In Figs. 29-30 we compare our predictions for charged kaons and pions production to those of reference [29]. The difference is seen to be of order of a factor 2 for the kaons.

Finally, in order to disentangle the fragmentation properties and the hadronization mechanism of high p_t jets, we consider the ratio between the single hadron and jet cross sections, for fixed values of the variable $z = E_{hadr}/E_{jet}$. Then, using the jet algorithm of ref. [6, ?] and the NLO

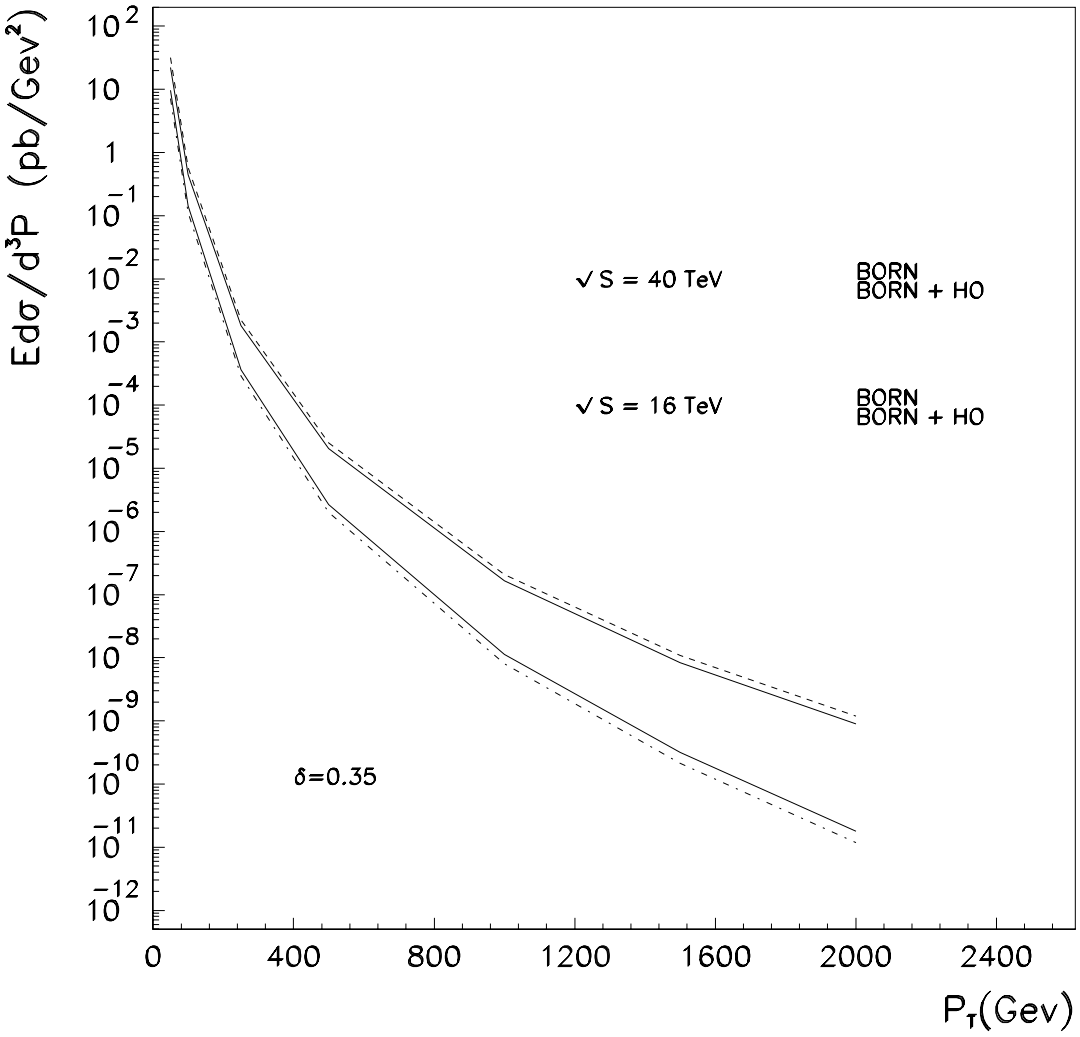

Figure 3.26: NLO inclusive η production in hadronic collisions at LHC and SSC energies at $y = 0$.

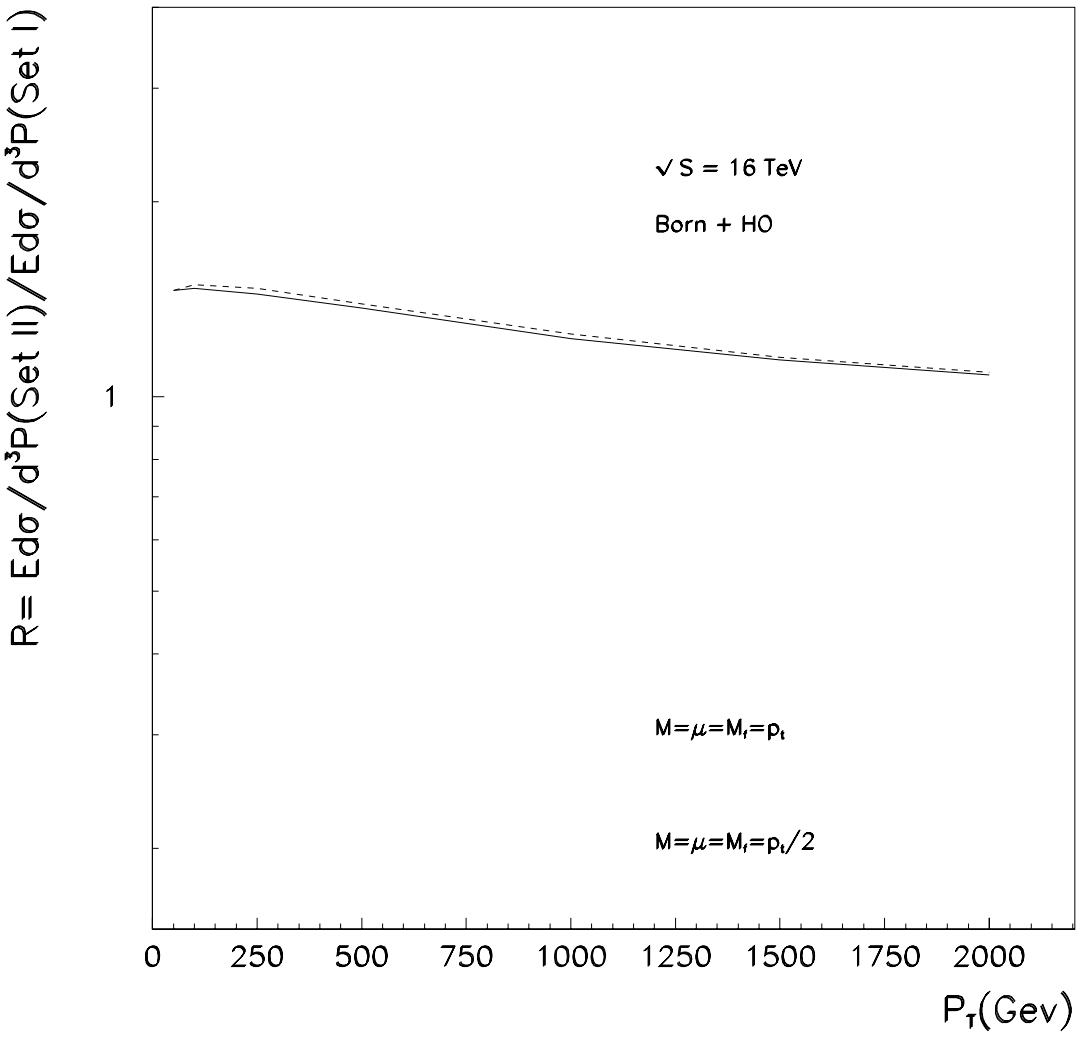

Figure 3.27: ratio of inclusive η cross sections for the two sets of gluon fragmentation functions.

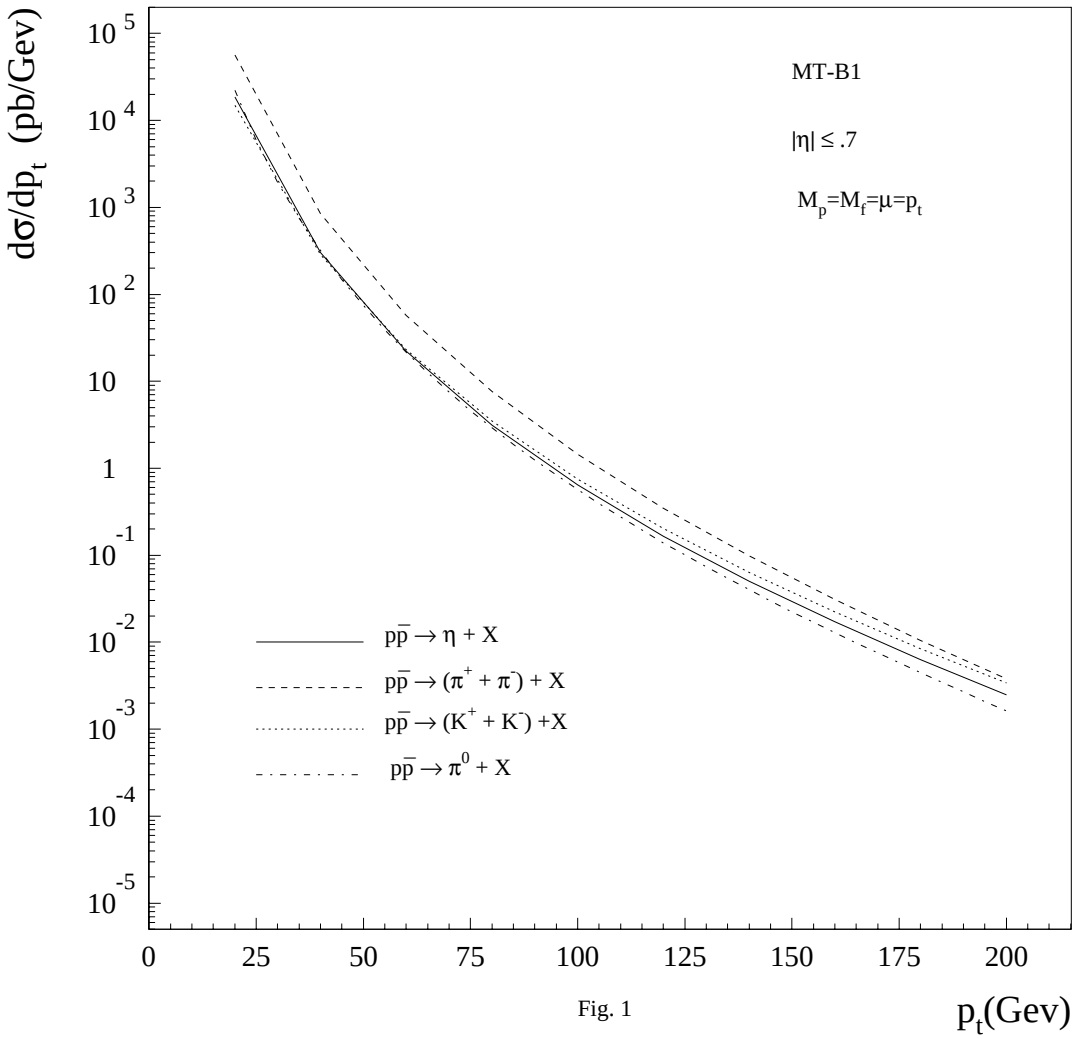

Fig. 1

Figure 3.28: P_t distribution for π^0, η, $\pi^{\pm}$, $K^{\pm}$ production at Tevatron

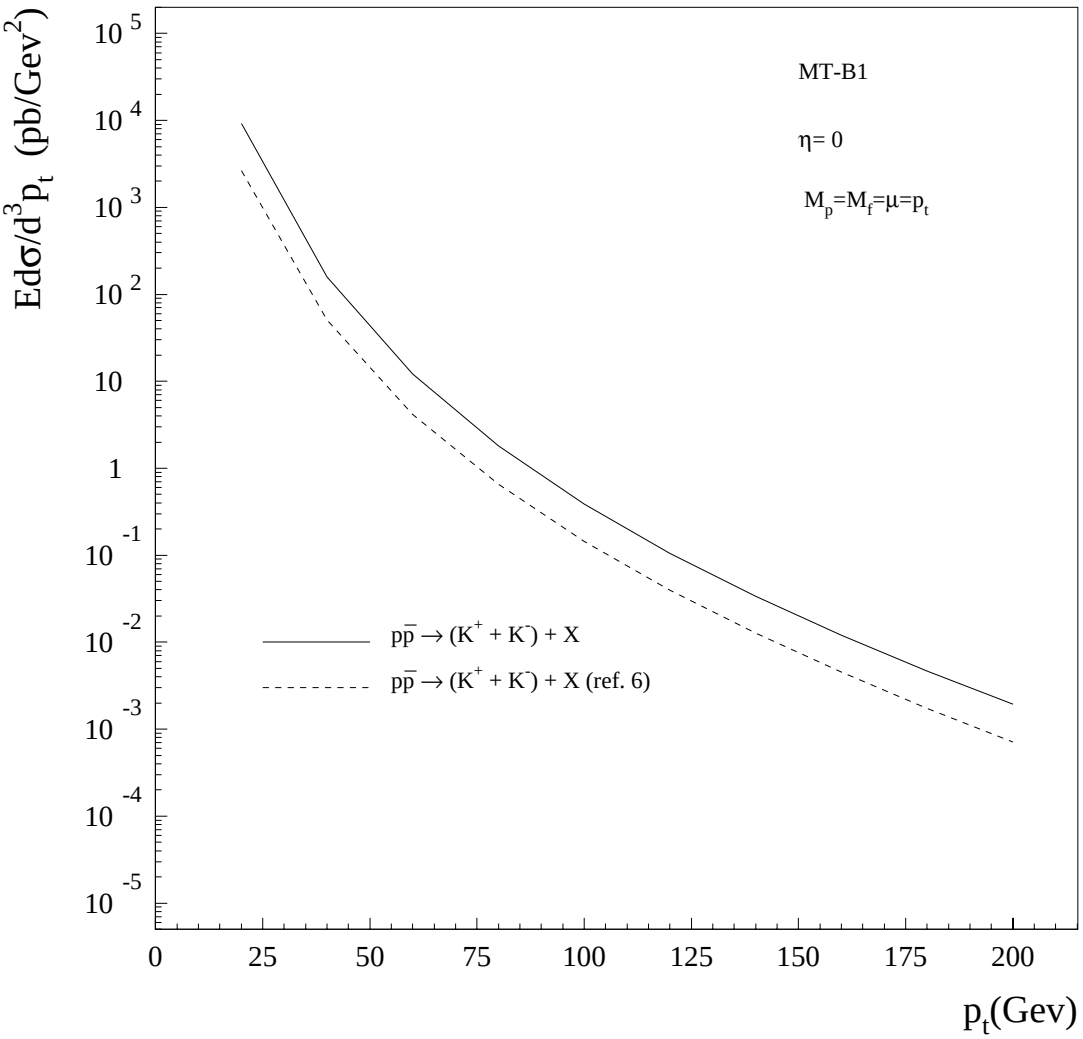

Figure 3.29: Comparison beetwen our predictions and those from Kramer et al.

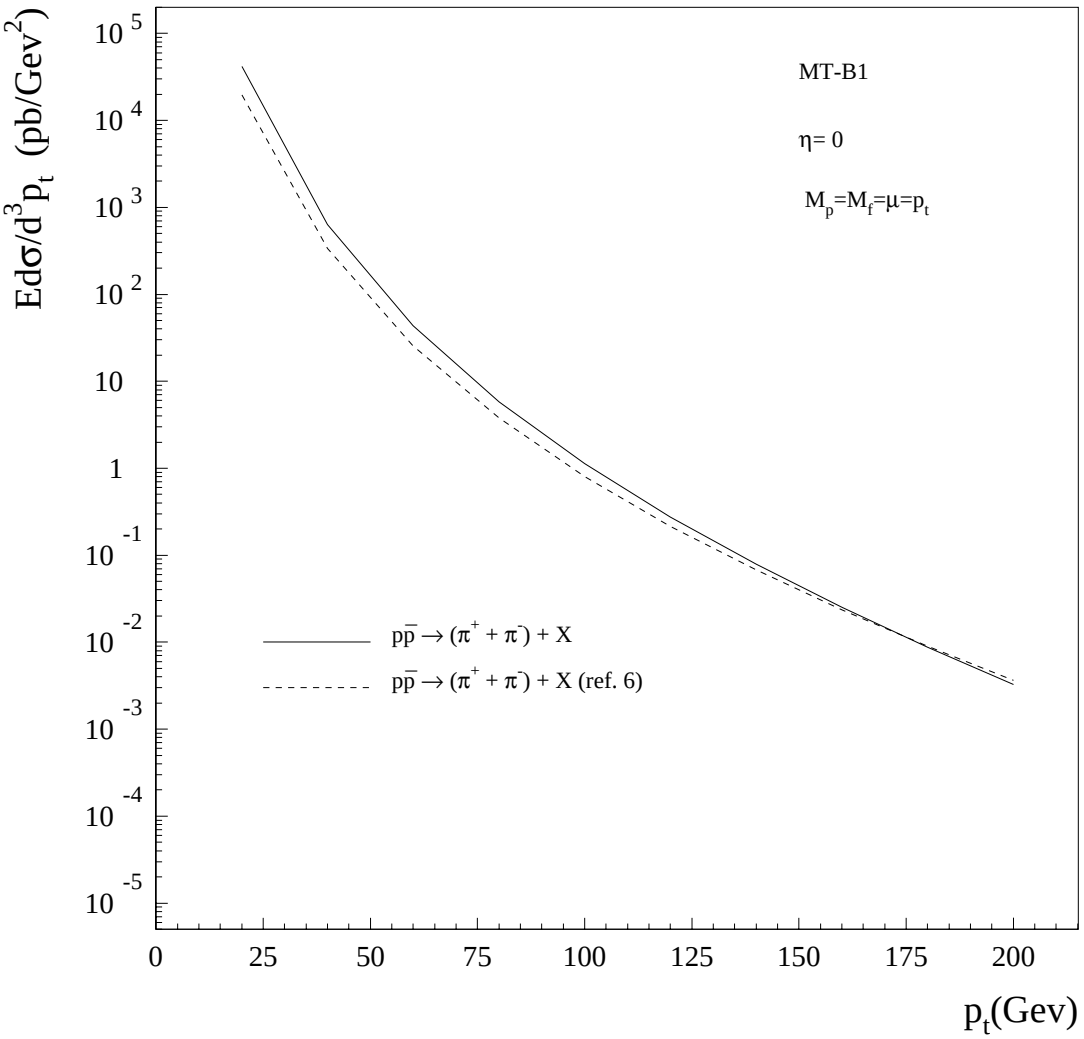

Figure 3.30: Same as Fig. 29

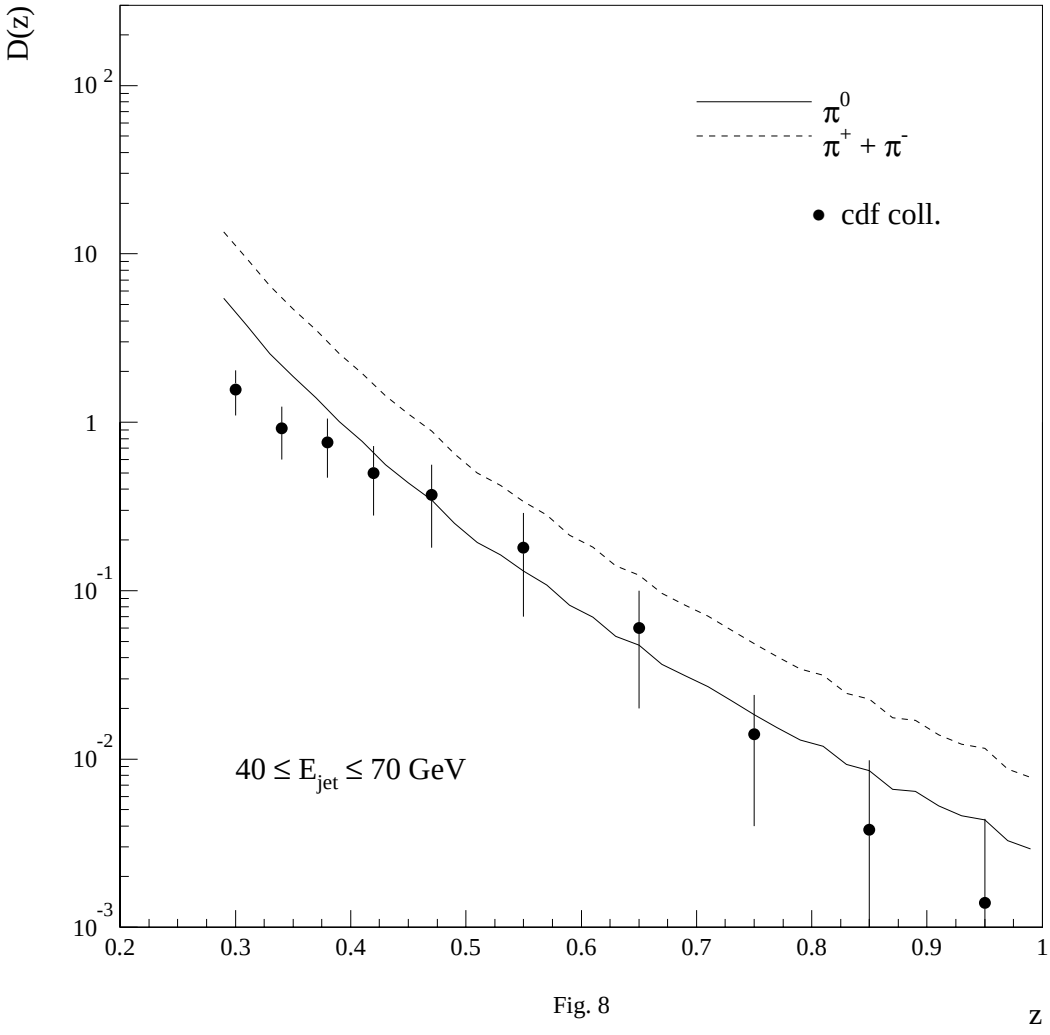

Figure 3.31: jet fragmentation function, into π^0 and $(\pi^+ + \pi^-)$. The experimental points refer to charged hadrons and are from D. Hubbard

evaluation of the jet cross sections of ref. [5], we present in Fig.31 result on jet fragmentation in charged and neutral pions, with the energy of the jet varying between 40 and 70 GeV, and a jet cone radius R=0.7 centered around the $\eta = 0$ direction. The overall theoretical uncertainty -which is not reported in figure- can be estimated to be of order 50%. We also show the analogous experimental result on jet fragmentation in charged hadrons [31], in reasonable agreement with the theoretical prediction.

As a final result we give a mean value for the ratio R=$\eta/\pi^0 = 1.15 \pm .30$, in the range 20 Gev $< p_t <$ 200 GeV which agrees with the recent experimental value of R=$1.02 \pm 0.15 \pm 0.23$ [32]. The theoretical uncertainty is related to the variation of the scales in parton distributions and fragmentation functions.

Appendix C

3.5 Mass divergences factorization in single particle inclusive production

Let us consider the following reaction:

$$H_1(K_1) + H_2(K_2) \to H_3(K_3) + X, \tag{3.14}$$

at parton level it is described by:

$$p_i + p_j \to p_l + X, \tag{3.15}$$

and the inclusive cross section is given by:

$$E_3\frac{d\sigma}{d^3K_3} = \sum_{i,j,l}\int dx_1 dx_2 \frac{dx_3}{x_3^2} F_{p_i}^{H_1}(x_1, M^2) F_{p_j}^{H_2}(x_2, M^2) D_{p_3}^{H_3}(x_3, M_f^2)$$
$$\times [\frac{1}{v}(\frac{d\sigma^0}{dv})_{p_i p_j \to p_l}(s, v)\delta(1-w) + \frac{\alpha_s(\mu^2)}{2\pi} K_{p_i p_j \to p_l}(s, v, w, \mu^2, M^2, M_f^2)] \tag{3.16}$$

where $s = x_1 x_2 S$ and v e w are given in terms of x_1,x_2 and hadronic momenta K_1, K_2 e K_3. F and D are respectively structure and fragmentation functions at factorization scale M and fragmentation scale m_f; $d\sigma^0$ is the Born cross section at order $\alpha_s^2(\mu^2)$ and $K_{ij\to l}$ are the order $\alpha_s(\mu)$ corrections.

In the naïf parton model the inclusive cross section for reaction () is simply given by:

$$E_3\frac{d\sigma}{d^3k_3} = \sum_{i,j,l}\int dx_1 dx_2 \frac{dx_3}{x_3^2} F_{0i}^{H_1}(x_1) F_{0j}^{H_2}(x_2) D_{0l}^{H_3}(x_3) \frac{p_3^0 d\sigma^0(p_1^i p_2^j \to p_3^l)}{d^3p_3} \tag{3.17}$$

As we can see no scale dependence is present in structure and fragmentation functions. If we add QCD corrections we obtain a dependence on the scale for D and F, which we can choose of order of p_t of the scattered parton. The great uncertainty in the choice of the scale (almost a factor two at LO) is greatly reduced if we add order α_s^3 corrections. We can perform this task in the following fashion: we start from the squared matrix elements in n dimensions for the parton subprocesses $(2 \to 3)$ and we integrate on the phase space. The divergences of type $\frac{1}{\epsilon^2}$ are cancelled by adding virtual contributions, while terms of order $\frac{1}{\epsilon}$ due to mass singularities are absorbed into effective fragmentation and structure functions beyond the leading order.

Singularities associated to initial state partons are factorized into the structure functions evolved at scale M^2 while divergencies associated to final state partons are absorbed into a redefinition of fragmentation functions at scale M_f. For every process we add a term proportional to:

$$\frac{\alpha_s}{2\pi} H_{p_i p_j}(y) d\sigma^0_{p_i p_j \to p_l}(ys, z) \tag{3.18}$$

to the sum of Born cross section (order α_s^2) and corrections of order α_s^3.

In the previous equation $H(y)$ has singularities in ϵ and can be rewritten as:

$$\begin{aligned} H_{p_i p_j}(y) &= -\frac{1}{\epsilon} P_{p_i p_j}(y) \left(\frac{4\pi\mu^2}{M^2}\right)^{\epsilon} \frac{,(1-\epsilon)}{,(1-2\epsilon)} + f_{p_i p_j}(y) = \\ &= P_{p_j p_i}(y)\left(-\frac{1}{\bar{\epsilon}}\right) + P_{p_i p_j}(y) \ln\left(\frac{M^2}{\mu^2}\right) + f_{p_i p_j}(y) \end{aligned} \tag{3.19}$$

where $P_{p_i p_j}(y)$ and $f_{p_i p_j}(y)$ are respectively Altarelli-Parisi evolution equations kernels and finite corrections of order $O(\alpha_s)$ to structure functions.

In the same way divergencies associated to final state partons are cured adding terms of type:

$$\frac{\alpha_s}{2\pi} \bar{H}_{p_l p_l}(y) d\sigma^0_{p_i p_j \to p_l}(s, \frac{vw}{y}) \tag{3.20}$$

with $y = 1 - v - wv$ and where, as before:

$$\bar{H}_{p_l p_l}(y) = P_{p_i p_j}(y)(-\frac{1}{\bar{\epsilon}}) + P_{p_i p_j}(y) \ln(\frac{M_f^2}{\mu^2}) + d_{p_i p_j}(y) \tag{3.21}$$

Until now only f_{qq} and d_{qq} have been explicitly calculated and imposing momenta conservation rules we obtain:

$$f_{gg} = 2N \left[x \left(\frac{\ln(1-x)}{1-x} \right)_+ - \frac{x \ln x}{1-x} + \left(\frac{5N_F}{24N} - \frac{1}{6}\pi^2 - \frac{1}{2} \right) \delta(1-x) \right] \tag{3.22}$$

$$d_{gg} = 2N \left[x \left(\frac{\ln(1-x)}{1-x} \right)_+ - \frac{x 2 \ln x}{1-x} + \left(\frac{7N_F}{16N} - \frac{1}{3}\pi^2 - \frac{17}{4} \right) \delta(1-x) \right] \tag{3.23}$$

$$f_{gg}(x) = \frac{1}{2}[x^2 + (1-x)^2] \ln(\frac{1-x}{x}) \tag{3.24}$$

$$d_{gg}(x) = \frac{1}{2}[x^2 + (1-x)^2] \ln[x^2(1-x^2)] \tag{3.25}$$

$$f_{gq}(x) = C_F \left[\frac{1 + (1-x)^2}{x} \ln[(1-x)x^2] - 2 \right] \tag{3.26}$$

For reader's convinience we report the following expressions::

$$f_{qq}(x) = C_F \left[(1-x^2) \left(\frac{\ln(1-x)}{1-x} \right)_+ - \frac{3}{2} \frac{1}{(1-x)_+} - \frac{1+x^2}{1-x} \ln x + 3 + \right.$$
$$\left. + 2x - (\frac{9}{2} + \frac{\pi^2}{3}) \delta(1-x) \right] \tag{3.27}$$

$$d_{qq}(x) = C_F \left[(1-x^2) \left(\frac{\ln(1-x)}{1-x} \right)_+ + 2 \frac{1+x^2}{1-x} \ln x - \frac{3}{2} \frac{1}{(1-x)_+} + \right.$$
$$\left. + \frac{3}{2}(1-x) + (\frac{2}{3}\pi^2 - \frac{9}{2}) \delta(1-x) \right] \tag{3.28}$$

Chapter 4

Inclusive particle photoproduction at HERA

4.1 Introduction

In this chapter we study the inclusive photoproduction of neutral and charged pions and η at HERA, via the resolved photon mechanism, in QCD to next-to-leading order. We present various distributions of phenomenological interest and study the theoretical uncertainties due to the mass scales, and to photon and proton sets of structure functions.

Inclusive production of high p_t particles and jets at HERA plays an important role in testing QCD, providing a detailed source of information on the hadron-like structure of the photon.

For this purpose leading order (LO) perturbative QCD predictions - based on evaluations of partonic cross sections at tree level and evolution of structure and fragmentation functions at one loop level– are not accurate enough, being plagued by the usual theoretical uncertainties associated to the large scale dependence of $O(\alpha_{em}\alpha_S)$ terms. A consistent calculation at next-to-leading order (NLO) needs two loop evolved structure and fragmentation functions and a NLO evaluation of parton-parton subprocesses. As well known, two mechanisms contribute to the inclusive photoproduction of particles or jets at high energies: the photon can interact directly with the partons originating from the proton (direct process), or via its quark and gluon content (resolved process). Previous theoretical analyses have considered both direct photoproduction to NLO, Aurenche et al. [33], and resolved photoproduction, Borzumati et al. [34], the latter having used the NLO corrections to all contributing parton-parton scattering processes of Aversa et al. [5] and LO fragmentation functions for the final hadron. Those results show the dominance of the resolved component at low p_t ($p_t < 10$ Gev), which is the region firstly explored at HERA, the role played by the direct contributions being shifted at higher p_t. The separation of the cross section in two components induces an artificial dependence on the photon factorization mass scale M_γ, which should cancel when the two terms are added up. Indeed this mechanism has been explicitly shown [35] to apply in the inclusive photoproduction of jets, which has been recently studied to NLO accuracy.

Motivated by these results, the photoproduction of single hadrons in electron-proton collisions at HERA energies, based on the NLO fragmentation functions of second chapter, limiting ourselves to the study of the resolved component only. In particular we present a detailed quantitative evaluation of π^0, $\pi^\pm$ and η photoproduction at HERA at moderate p_t, using the hard scattering cross sections of ref. [5], and two loop structure and fragmentation functions.

4.2 Theoretical framework

We give now the relevant formulae for the cross sections. The inclusive cross section for $ep \to h + X$ in an improved next-to-leading-order approximation is:

$$E_h \frac{d^3\sigma(ep \to h + X)}{d^3p_h} = \int_{x_{min}}^{1} dx f_{\gamma/e}(x) \hat{E}_h \frac{d^3\hat{\sigma}(\gamma p \to h + X)}{d^3\hat{p}_h}(x) \quad (4.1)$$

where x_{min} is given in terms of the transverse momentum p_t and of the center-of-mass pseudorapidity η_{cm} of the produced hadron as:

$$x_{min} = \frac{p_t e^{\eta_{cm}}}{\sqrt{s} - p_t e^{-\eta_{cm}}} \quad (4.2)$$

The rapidity η_{lab} measured in the laboratory frame is related to η_{cm} as:

$$\eta_{lab} = \eta_{cm} - \frac{1}{2} \ln \frac{E_p}{E} \quad (4.3)$$

where E and E_p are the energies of the electron and the proton respectively ($E = 27$ GeV and $E_p = 820$ GeV, for the present HERA conditions).

The distribution in the longitudinal momentum fraction y of the outgoing photon has in the NLO approximation the following form [36]:

$$f_\gamma^{(e)}(y) = \frac{\alpha_{em}}{2\pi} \left\{ 2(1-y) \left[\frac{m_e^2 y}{E^2(1-y)^2\theta_c^2 + m_e^2 y^2} - \frac{1}{y} \right] + \frac{1 + (1-y)^2}{y} \log \frac{E^2(1-y)^2\theta_c^2 + m_e^2 y^2}{m_e^2 y^2} + \mathcal{O}(\theta_c^2, m_e^2/E^2) \right\}, \quad (4.4)$$

where $\theta_c = 5^\circ$ is the maximum value of the electron scattering angle and m_e is the electron mass.

Finally the γp inclusive cross section is given by:

$$E \frac{d\sigma^{\gamma p}}{d^3P} = \frac{1}{\pi S} \sum_{i,j,l} \int_0^1 \int_0^1 \int_0^1 dx_1\, dx_2\, \frac{dx_3}{x_3^2} F_i^p(x_1, M_p^2) F_j^\gamma(x_2, M_\gamma^2) D_l^h(x_3, M_f^2) \times$$

$$\times \left(\frac{\alpha_S(\mu^2)}{2\pi}\right)^2 \left[\frac{1}{v}\sigma^0_{ijl}(s,v)\delta(1-w) + \frac{\alpha_S(\mu^2)}{2\pi}K_{ijl}(s,v,w;M_p^2,M_\gamma^2,\mu^2,M_f^2)\right] \tag{4.5}$$

where s, v and w are the partonic variables $s = x_1 x_2 S$, $v = \frac{x_2 - 1 + V}{x_2}$, $w = \frac{x_2 V W}{x_1(x_2 - 1 + V)}$ and $V = 1 + \frac{T}{S}$, $W = \frac{-U}{T+S}$, with S, T, U the hadronic Mandelstam variables. σ^0_{ijl} are the partonic Born cross sections $O(\alpha_S^2)$, while K_{ijl} are the finite higher order corrections $O(\alpha_S^3)$ [5],with i, j, l running on all kinds of partons. As usual, the photon structure functions are expressed in terms of the hadronic and the pointlike contributions as $F^\gamma(x,Q^2) = F^\gamma_{had}(x,Q^2) + F^\gamma_{point}(x,Q^2)$, and obey the appropriate evolution equation with the inhomogeneous term related to F^γ_{point} [37].

As already stated above a consistent calculation to next-to-leading order needs two-loop evolved structure and fragmentation functions and a NLO evaluation of parton-parton subprocesses. In the partonic cross sections to one loop [5], calculated from the squared matrix elements $O(\alpha_S^3)$ of Ellis et Sexton [38], the initial state collinear divergences have been factorized and absorbed into the dressed structure functions in the $\overline{MS}$ scheme. Coherently with this choice, we have used for the proton structure functions set B1 of Morfin & Tung, [17] (set A), set MRS S0 of Martins Roberts & Stirling [18] (set B), and set GRV HO of Glück, Reya & Vogt [39] (set C) and three different NLO parameterizations of the photon structure functions, namely the set of Aurenche et al. [40] with massless charm (set I), that of Glück, Reya and Vogt [41] (set II) (mode=272 in the PDFLIB library) and that of Gordon and Storrow [42] (set III). Sets I and II have been also used in the previous analysis of Borzumati et al. [34].

We have used α_S calculated at 2-loop, with 4 flavors and with $\Lambda_{QCD} = 200\ MeV$. Set A of the proton structure functions has been indeed evolved with $\Lambda_{QCD} = 194\ MeV$, but the error induced by this different choice is negligible. We have also considered 5 flavors in the proton, in the photon and in the final state, but the contribution given by the bottom is clearly negligible in the range of p_t values studied.

We have used the improved expression (4) for the Weiszaecher- Williams photon density in the electron [36]. When comparing our results with those obtained with the usual leading order formula (e.g. see eq.1 in ref. [43]) we found a negative correction which is no larger than 5%.

4.3 Results

We present now various numerical results for the three sets of photon structure functions, studying in particular the uncertainties of the theoretical predictions. We always use set A for the proton and set I for the photon structure functions, except when explicitly mentioned.

Let us consider π^0 photoproduction first. The dependence of the cross section on the various mass scales involved in (5) is shown in figs. 1. As expected, the dependence is very strong at the Born level, as shown in fig.1a for $p_T = 5\ GeV$, for $\eta_{lab} = -2$.

The introduction of higher orders reduces the effect, although the dependence on the photon factorization scale only is still important (figs.1b-1c), unlike to what is observed in the case of hadron-hadron collisions [5, 44]. This behaviour has been also observed in the photoproduction of jets at HERA [42,45,35] and the photon mass scale dependence is reduced when the direct and resolved terms are both considered [35]. The above effect is similar for the three sets of photon structure functions.

More explicitly we have isolated in the K factor in (5) the terms depending on M_p^2 from those depending on M_γ^2, with the following method. We split each term of the K-factors calculated in [5], which is proportional to $\log\left(\frac{s}{M^2}\right)$, where in [5] $M^2 = M_p^2 = M_\gamma^2$, in two pieces and assign a weight factor which takes into account the splitting vertex ($q \to qg$, $g \to gg$) present in the collinear emission. For the subprocesses $qq \to H+X$ and $gg \to H + X$ the weight is $\frac{1}{2}$, due to the symmetry of all possible collinear emission. In the subprocess $q(p)g(\gamma) \to H + X$ and $q(\gamma)g(p) \to H + X$ we

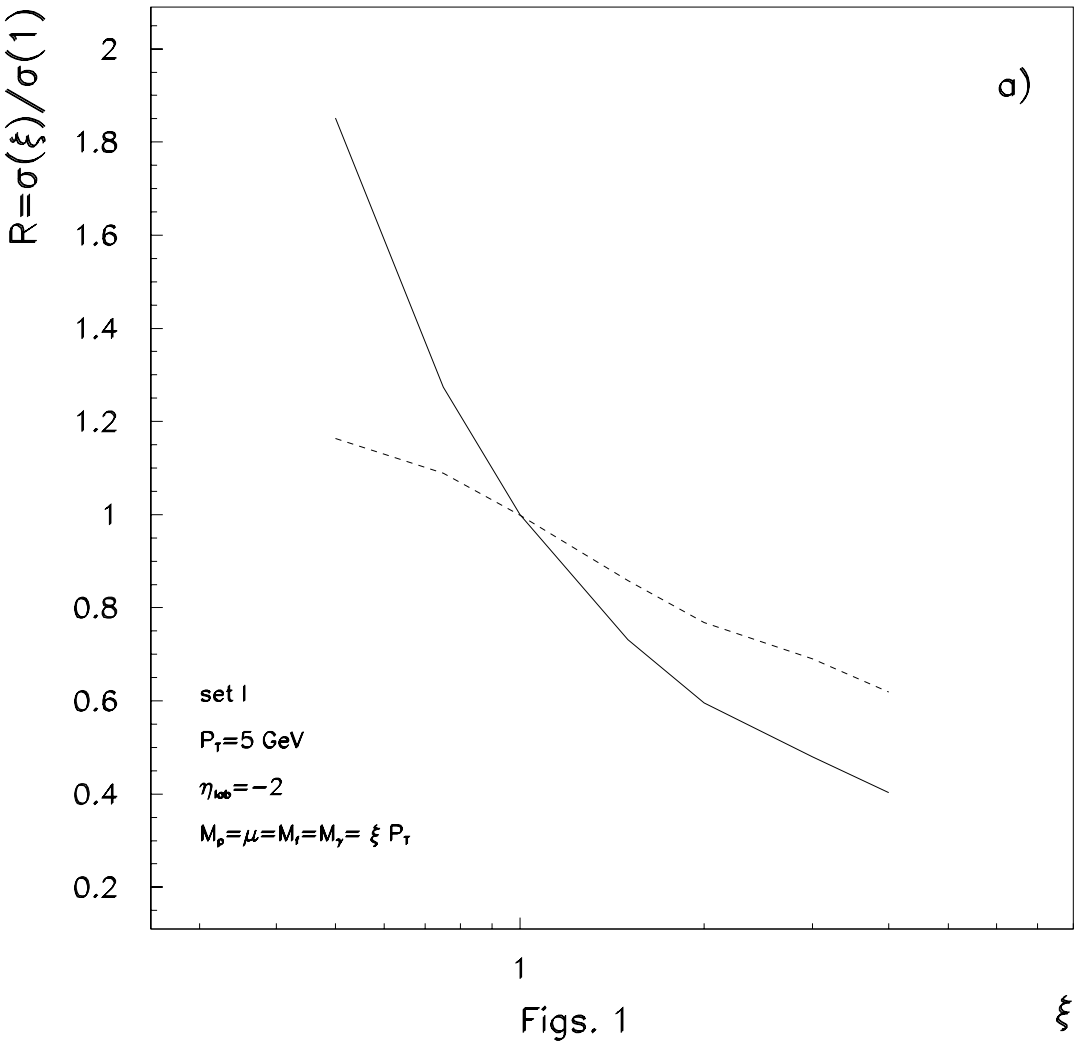
R=σ(ξ)/σ(1)
2
1.8
1.6
1.4
1.2
1
0.8
0.6
0.4
0.2
1
ξ
a)
set I
P_T=5 GeV
η_lab=−2
M_p=μ=M_f=M_γ= ξ P_T

Figs. 1

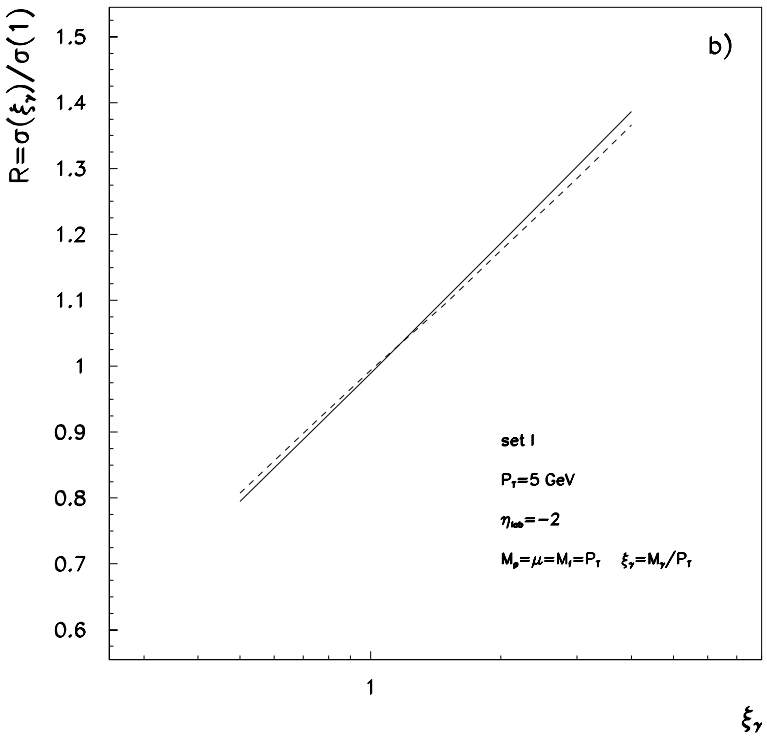
b)
R=σ(ξγ)/σ(1)
1.5
1.4
1.3
1.2
1.1
1
0.9
0.8
0.7
0.6
1
ξγ
set I
PT=5 GeV
ηlab=−2
Mp=μ=Mf=PT ξγ=Mγ/PT

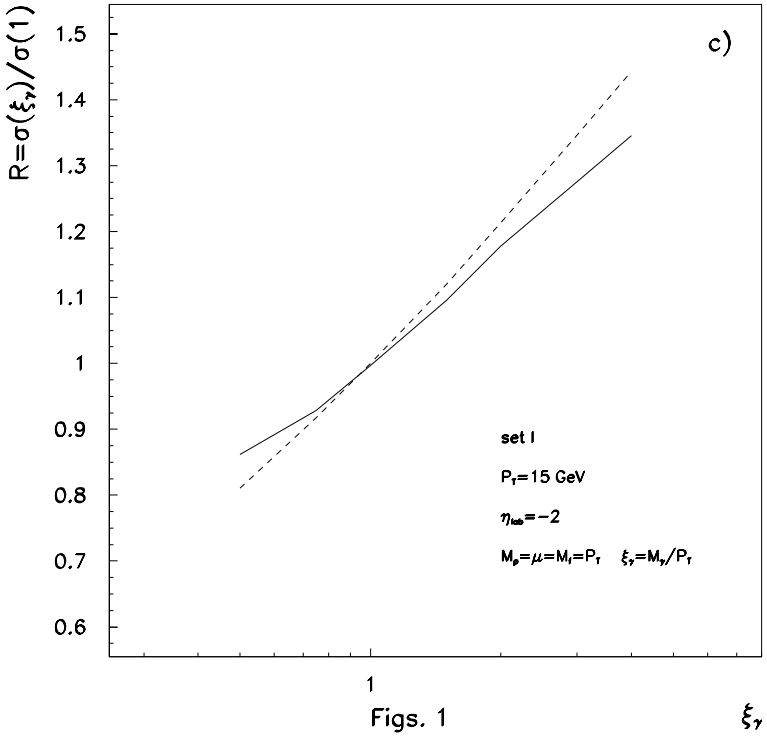
c)
R=σ(ξγ)/σ(1)
1.5
1.4
1.3
1.2
1.1
1
0.9
0.8
0.7
0.6
1
ξγ
set I
PT=15 GeV
ηlab=−2
Mp=μ=Mf=PT ξγ=Mγ/PT

Figs. 1

give a weight $\frac{C_F}{C_F+2C_A+n_F}$ to the quark and $\frac{2C_A+n_F}{C_F+2C_A+n_F}$ to the gluon (C_F and C_A are the usual color factors). Moreover for each subprocess one has to multiply the partonic cross-section for the appropriate combination of structure function.

In order to show the general p_T behaviour of the cross section, $\frac{d\sigma}{d\eta dp_T}$ is plotted in figs. 2 and fig. 3 for different values of η_{lab}, $\mu = M_p = M_\gamma = M_f = p_T$, and for the three sets.

Comparing to the previous analyses of ref [34], we have found differences which we believe are essentially due to the use of out set of fragmentation functions evolved to NLO. On the other hand we are able to reproduce fig.9 of [34], using the same inputs, within a 15% of accuracy but with an almost identical shape. For convenience we show in fig. 4 the comparison between the old set of fragmentation functions [46] and the one used in this thesis.

In figs.5 we present the η_{lab} distribution for fixed $p_t = 5$ GeV. In fig. 5a the contributions is shown by the various partonic subprocesses, while the differential cross-sections $\frac{d\sigma}{d\eta dp_T}$ for the three sets of photon structure functions are compared in fig. 5b. Comparing with ref. [34], as for the case of p_t distributions, the different shapes shown in fig. 5a can be understood firstly because of the different set of fragmentation functions (see fig. 4); furthermore the regions $\eta_{lab} < -3$ and $\eta_{lab} > 1$ lye at the edge of phase space and therefore the numerical convolution of the $\gamma - p$ cross-section with the Weiszaecher- Williams formula is sensitive to slight variations of the parameters.

As in the case of inclusive jet photoproduction [35] the contribution from the gluon content of the photon is too tiny to be observed in most of the phase space available. Indeed from Fig. 5, if one considers the two subpreocesses initiated by the gluon in the photon: $q(p)g(\gamma) \to jet + X$ and $gg \to jet + X$, the first one is clearly dominated by all other reactions, while the second one could be of interest in the region of very negative rapidities ($\eta_{lab} < -3$), where it is however quite difficult to disentangle

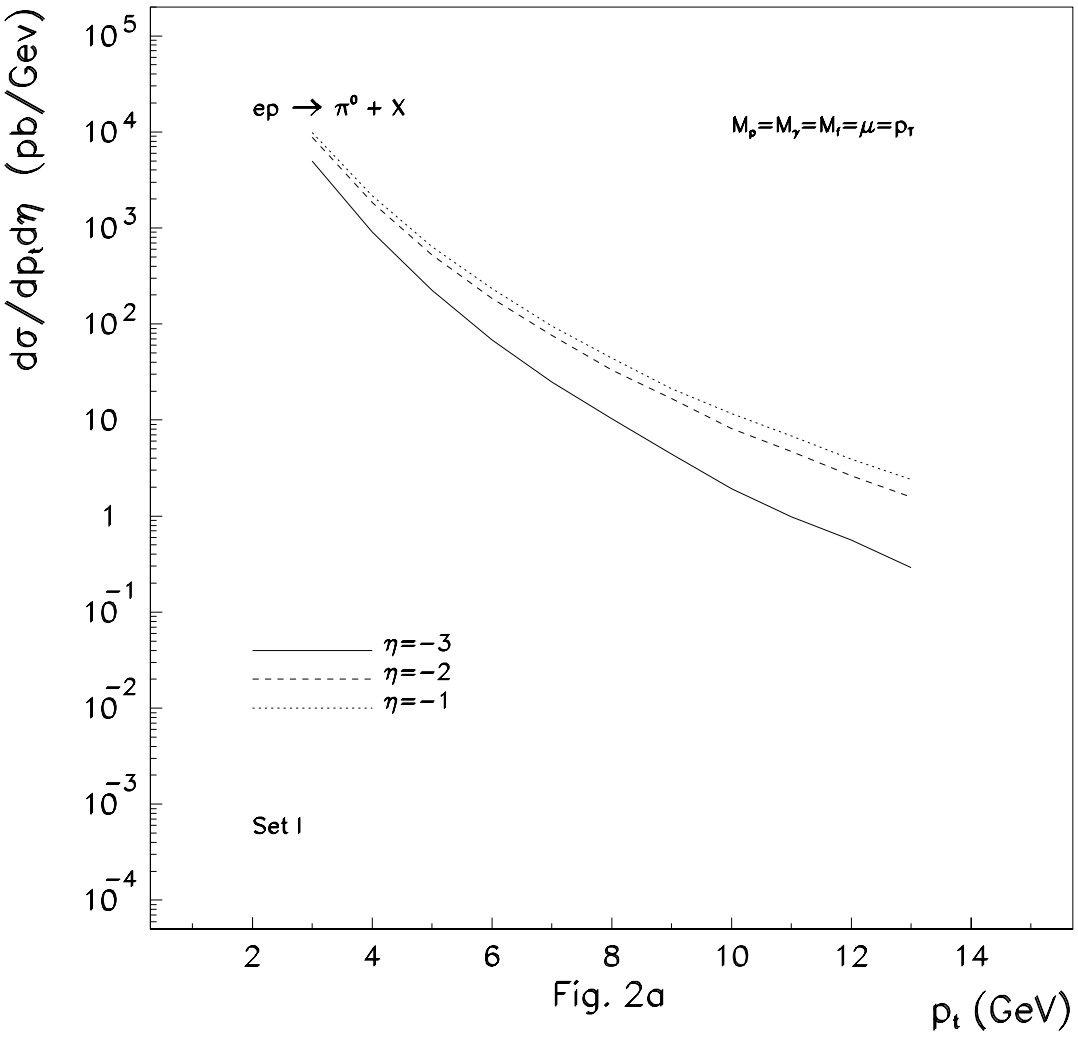
ep → π⁰ + X
M_p=M_γ=M_f=μ=p_T
η=−3
η=−2
η=−1
Set I
dσ/dp_t dη (pb/Gev)
p_t (GeV)
10^5
10^4
10^3
10^2
10
1
10^−1
10^−2
10^−3
10^−4
2
4
6
8
10
12
14

Fig. 2a

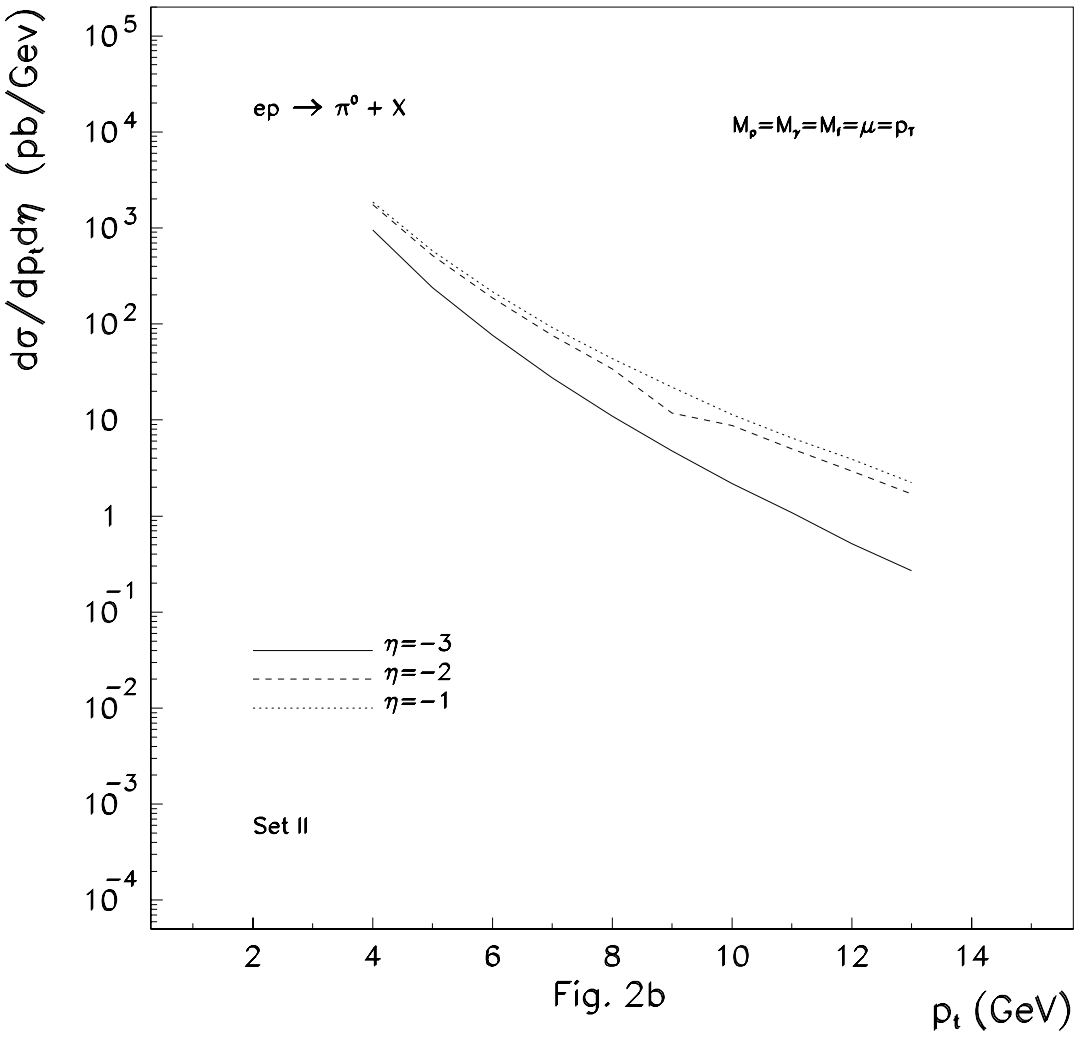
ep → π⁰ + X
M_p=M_γ=M_f=μ=p_T
dσ/dp_t dη (pb/Gev)
10^5
10^4
10^3
10^2
10
1
10^-1
10^-2
10^-3
10^-4
η=−3
η=−2
η=−1
Set II
2
4
6
8
10
12
14
p_t (GeV)

Fig. 2b

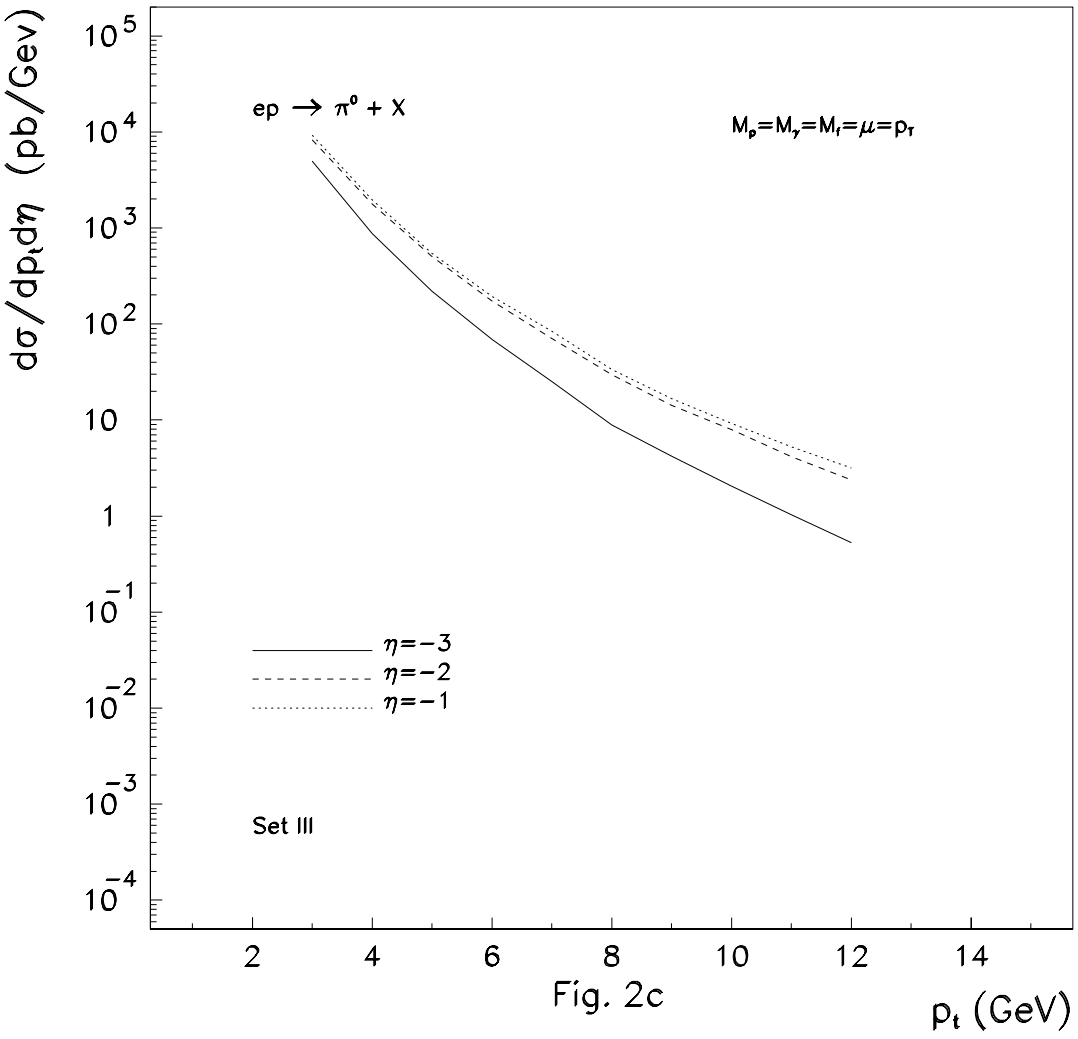
$d\sigma/dp_t d\eta$ (pb/Gev)
10^5
10^4
10^3
10^2
10
1
10^{-1}
10^{-2}
10^{-3}
10^{-4}
$ep \rightarrow \pi^0 + X$
$M_p=M_\gamma=M_f=\mu=p_T$
$\eta=-3$
$\eta=-2$
$\eta=-1$
Set III
2
4
6
8
10
12
14
p_t (GeV)

Fig. 2c

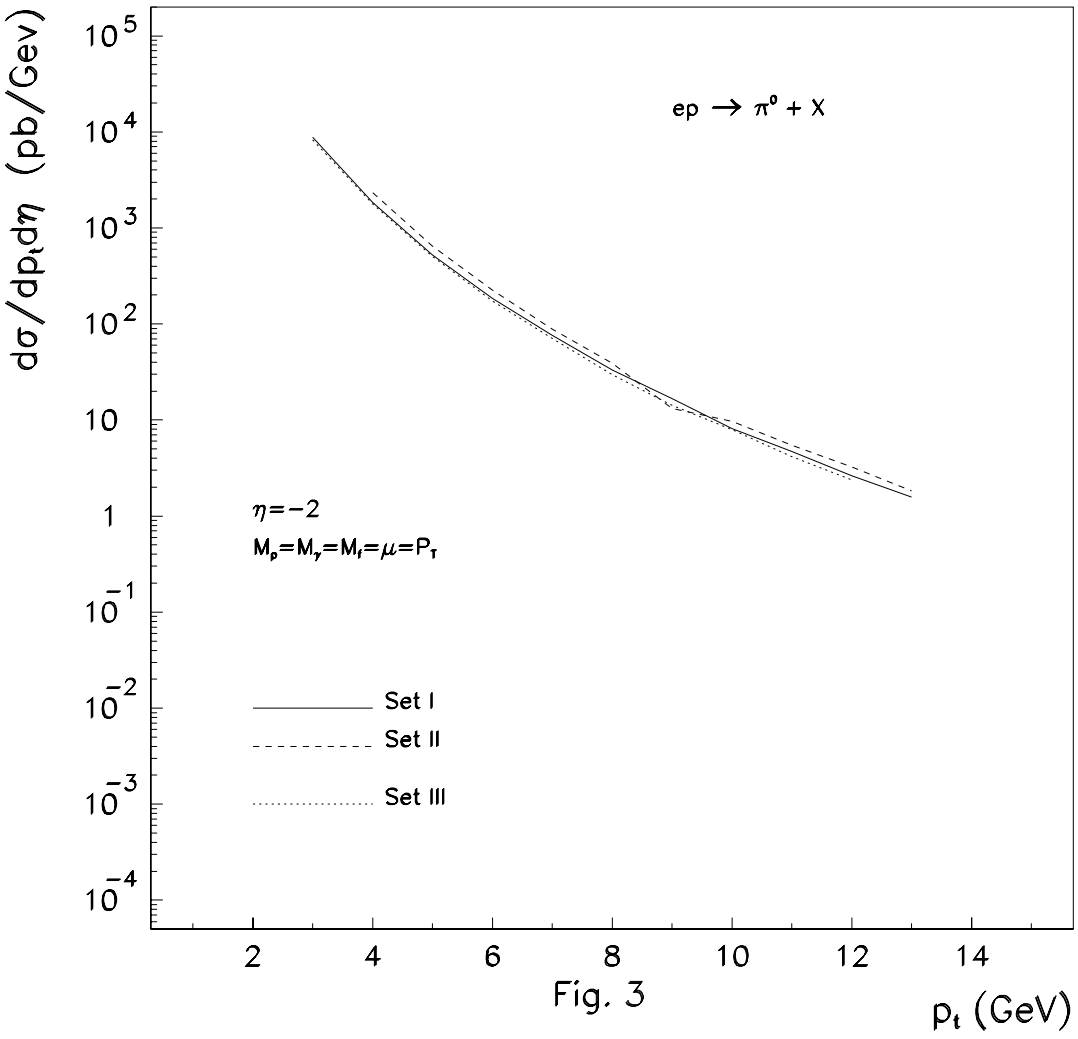
$d\sigma/dp_t d\eta$ (pb/Gev)
10^5
10^4
10^3
10^2
10
1
10^{-1}
10^{-2}
10^{-3}
10^{-4}
$ep \rightarrow \pi^0 + X$
$\eta=-2$
$M_p=M_\gamma=M_f=\mu=P_T$
Set I
Set II
Set III
2
4
6
8
10
12
14
p_t (GeV)

Fig. 3

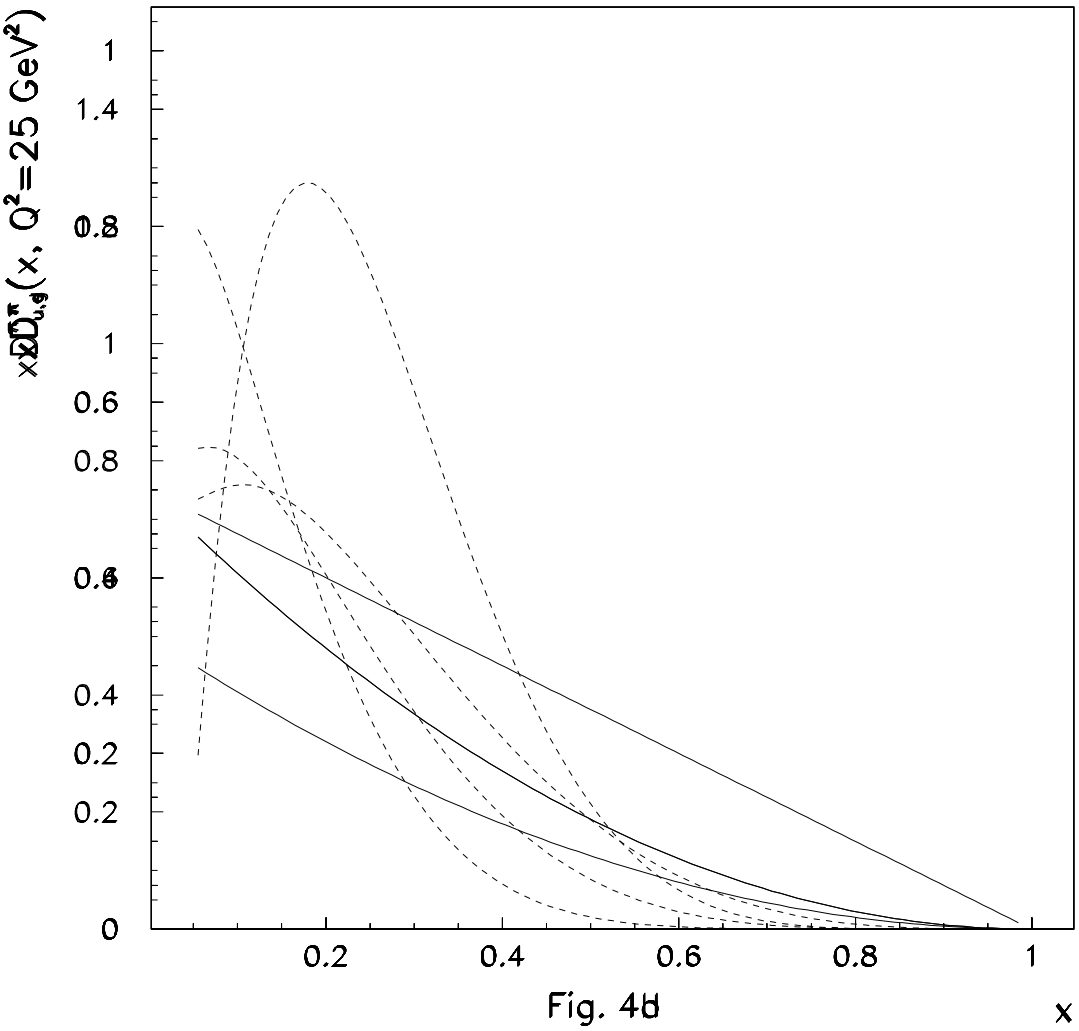

Fig. 4b

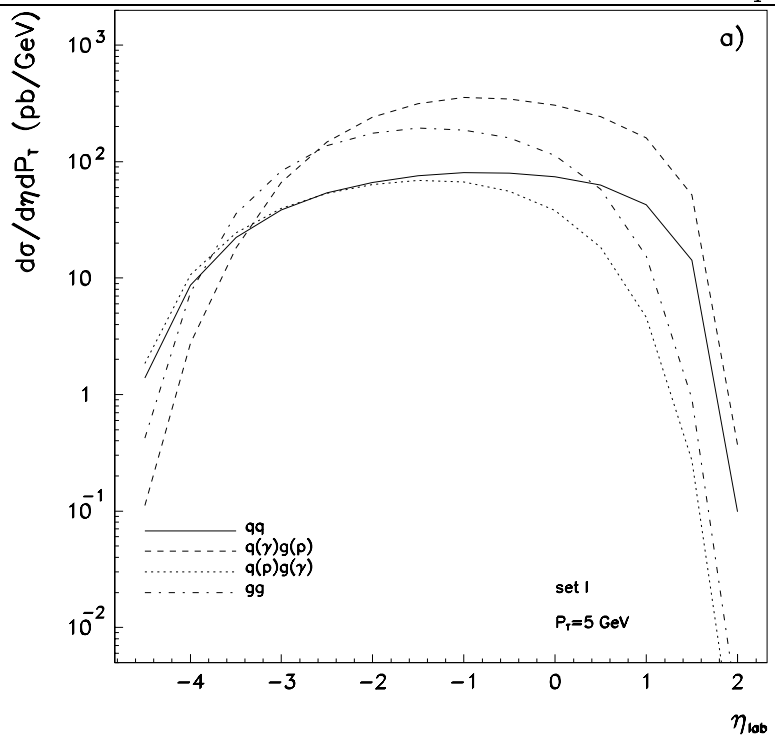
a)
$d\sigma/d\eta dP_T$ (pb/GeV)
10^3
10^2
10
1
10^{-1}
10^{-2}
qq
q(γ)g(p)
q(p)g(γ)
gg
set I
P_T=5 GeV
−4 −3 −2 −1 0 1 2
η_{lab}

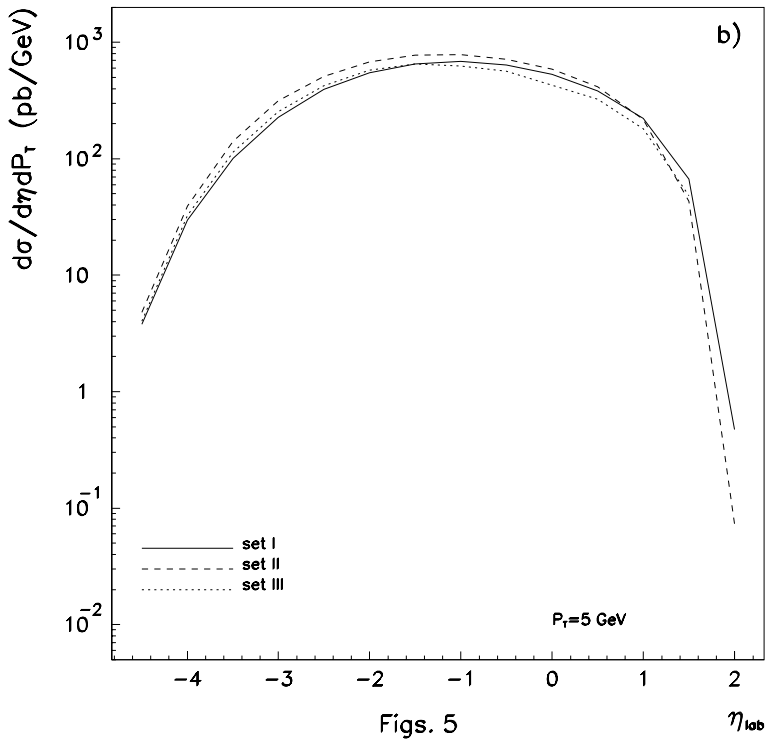
b)
$d\sigma/d\eta dP_T$ (pb/GeV)
10^3
10^2
10
1
10^{-1}
10^{-2}
set I
set II
set III
P_T=5 GeV
−4 −3 −2 −1 0 1 2
η_{lab}

Figs. 5

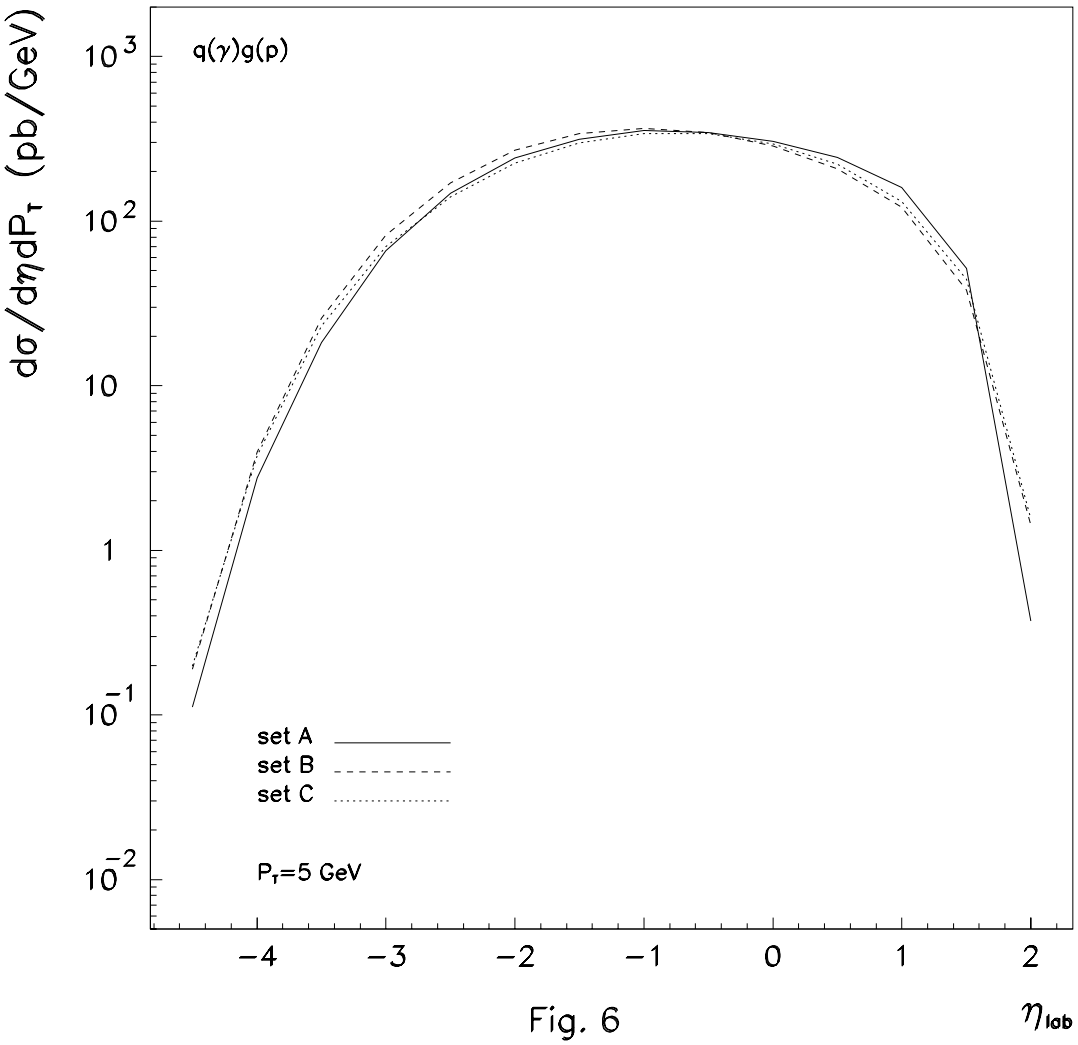
q(γ)g(p)
dσ/dηdP_T (pb/GeV)
10^3
10^2
10
1
10^-1
10^-2
set A
set B
set C
P_T=5 GeV
−4
−3
−2
−1
0
1
2
η_lab

Fig. 6

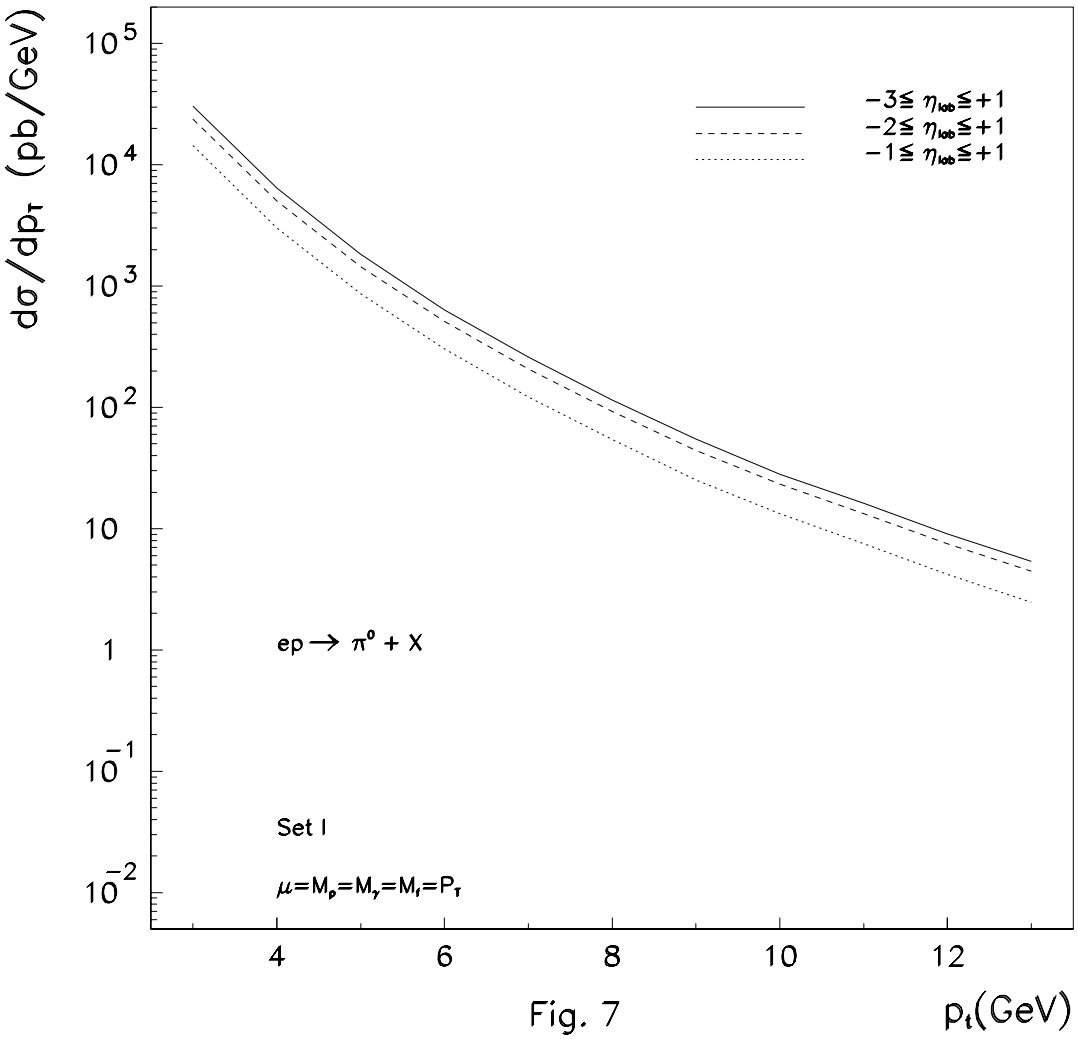
dσ/dp_T (pb/GeV)
10^5
10^4
10^3
10^2
10
1
10^-1
10^-2
−3≦ η_lab≦+1
−2≦ η_lab≦+1
−1≦ η_lab≦+1
ep → π° + X
Set I
μ=M_p=M_γ=M_f=P_T
4
6
8
10
12
p_t(GeV)

Fig. 7

the small-x behaviour of the photon structure function in the actual cross section.

On the contrary, the gluon contribution from the proton structure function plays a relevant role, and is essentially independent from the photon and proton structure functions, as also shown in fig. 6, where the η_{lab} distribution of the subprocess $q(\gamma)g(p) \to \pi^0 + X$ for three different parameterization NLO of proton structure functions.

We finally show the cross section integrated over different ranges of η_{lab} in fig. 7, for the Set I of photon structure functions, which is of immediate phenomenological interest for HERA experiments.

Concerning the photoproduction of η and charged pions, we present in Figs. 8 the p_T distribution for different values of η_{lab}, in Figs. 9 the η_{lab} distributions for $p_t = 5$ GeV and for different subprocesses, and in Figs. 10 the distribution in p_t integrated in η_{lab}. The dependence on the photon structure functions is similar to what found for the π^0 case. Finally we show in Table I our prediction for the ratio η/π^0 where we define R as the ratio of the cross sections $\frac{d\sigma}{d\eta dp_t}$ for the production of eta and pions respectively.

p_t	3	4	5	6	7	8	9	10	11	12	13
R	0.55	0.60	0.64	0.67	0.67	0.72	0.72	0.79	0.80	0.84	0.86

Table I

In Fig. 11 we show the dependence of the cross section on the proton structure functions.

To summarize, in this chapter a next-to-leading order calculation of inclusive neutral and charged pions and η production in electron-proton collisions has been presented, particularly via the resolved photon mechanism. We have studied the effects of the theoretical uncertainties related to the photon structure functions, as well as the dependence from the

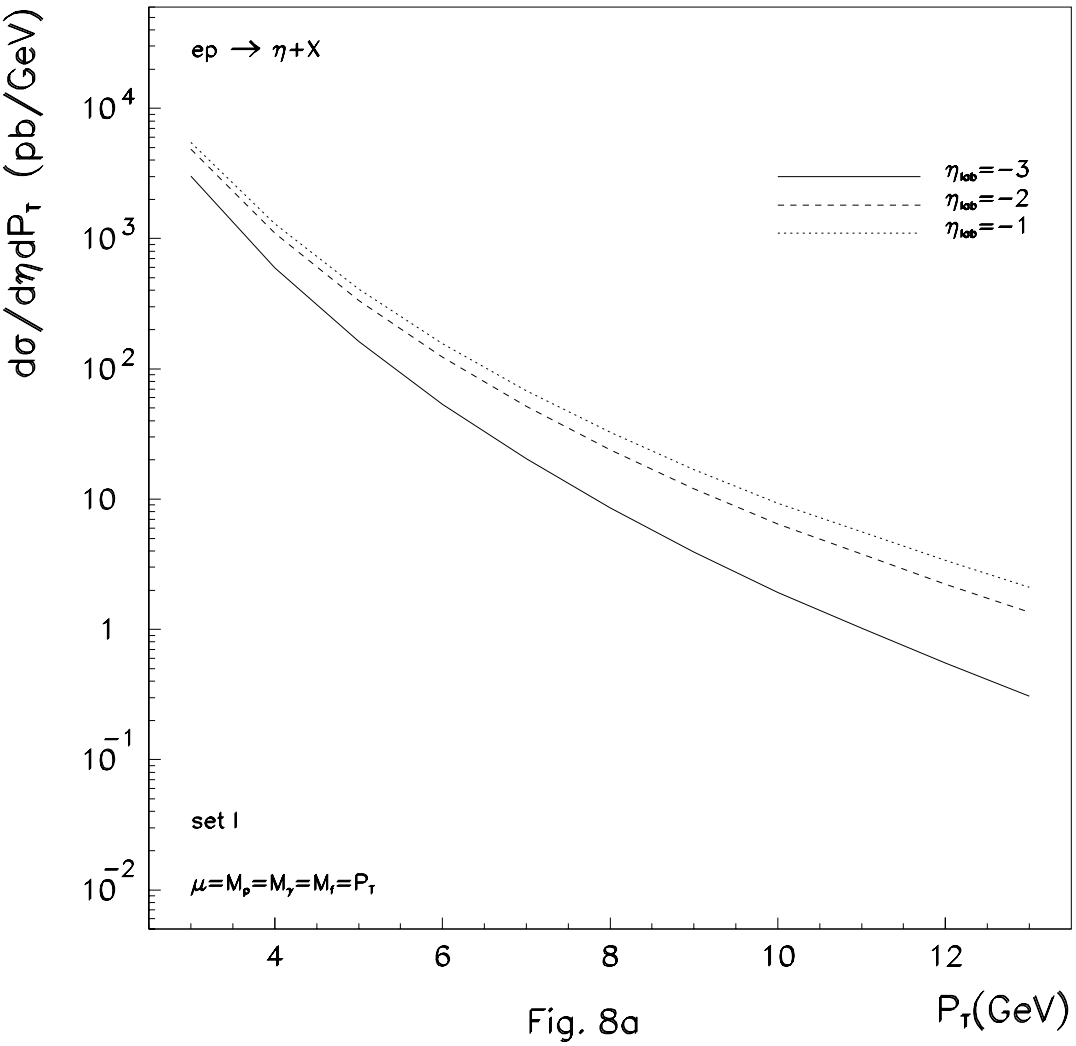
ep → η+X
dσ/dηdP_T (pb/GeV)
10^4
10^3
10^2
10
1
10^-1
10^-2
η_lab=−3
η_lab=−2
η_lab=−1
set I
μ=M_p=M_γ=M_f=P_T
4
6
8
10
12
P_T(GeV)

Fig. 8a

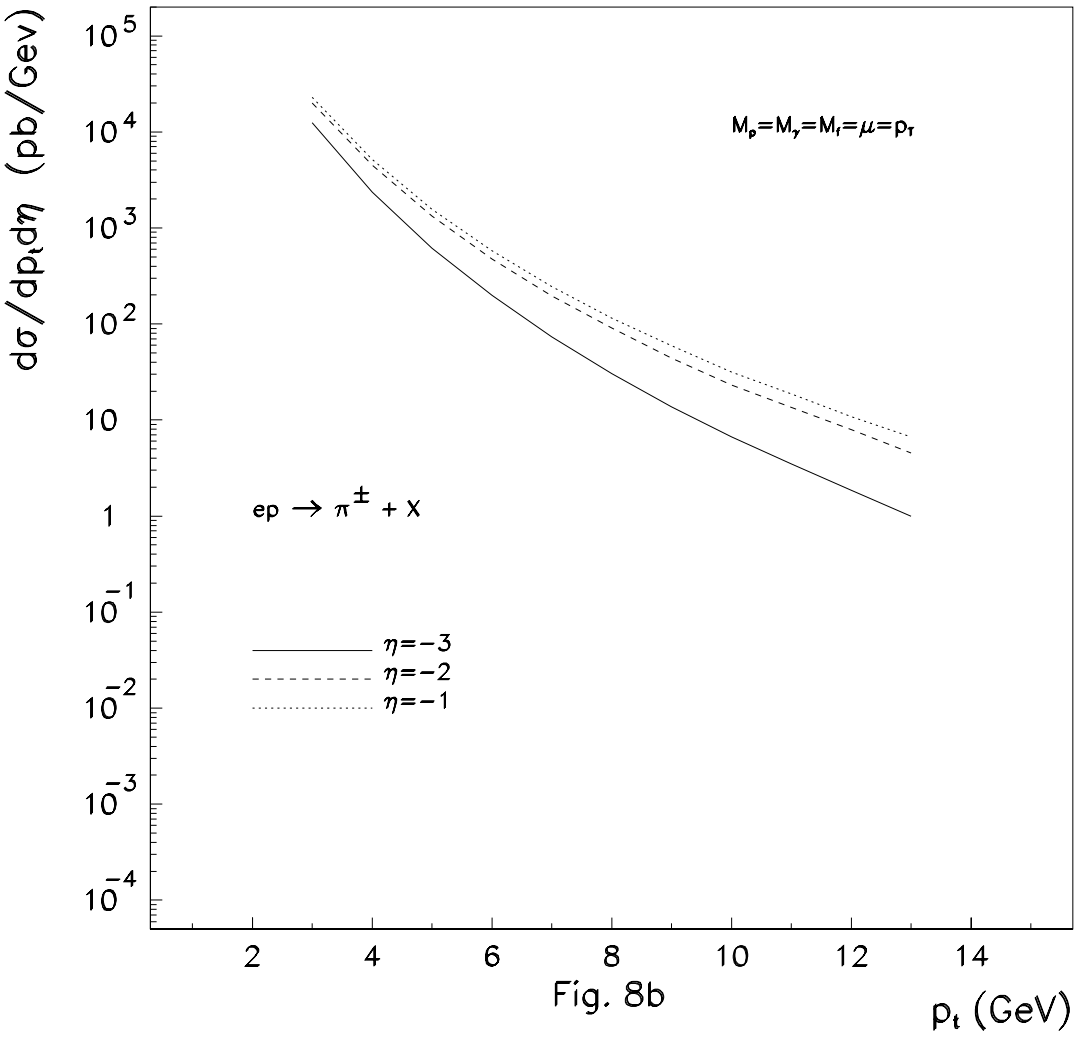
$d\sigma/dp_t d\eta$ (pb/Gev)
10^5
10^4
10^3
10^2
10
1
10^{-1}
10^{-2}
10^{-3}
10^{-4}
$M_p=M_\gamma=M_f=\mu=p_T$
$ep \rightarrow \pi^{\pm} + X$
$\eta=-3$
$\eta=-2$
$\eta=-1$
2
4
6
8
10
12
14
p_t (GeV)

Fig. 8b

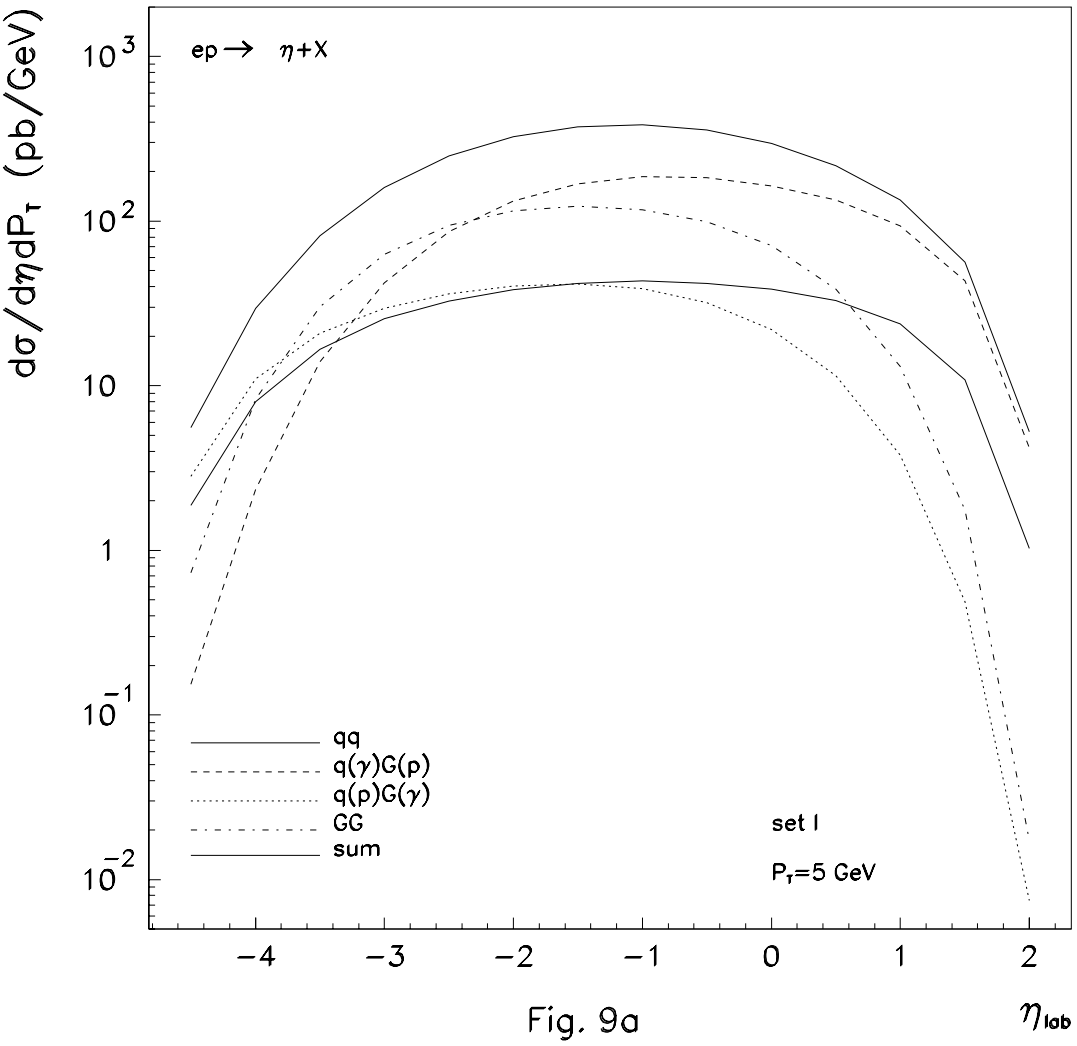
ep → η+X
dσ/dηdP_T (pb/GeV)
10^3
10^2
10
1
10^-1
10^-2
qq
q(γ)G(p)
q(p)G(γ)
GG
sum
set I
P_T=5 GeV
−4
−3
−2
−1
0
1
2
η_lab

Fig. 9a

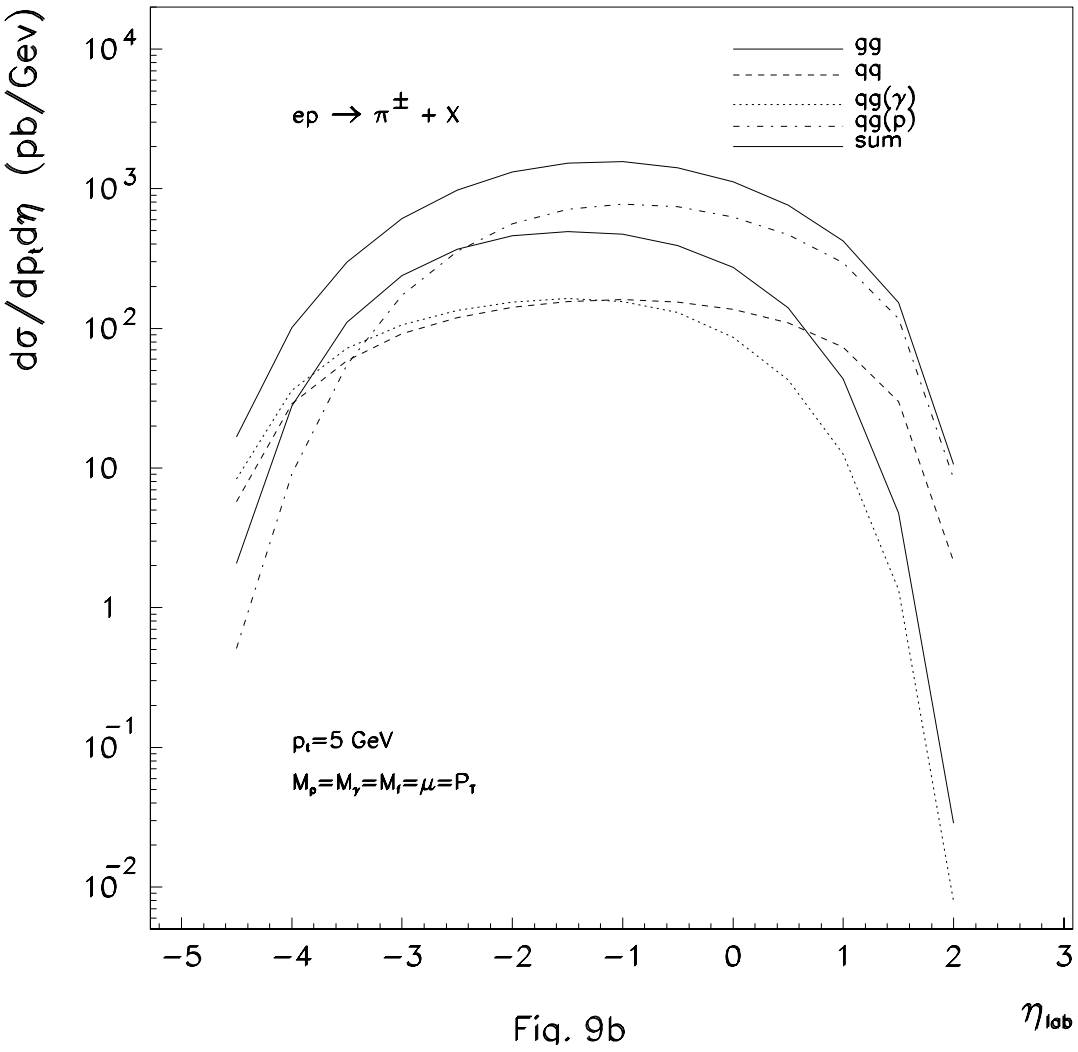
gg
qq
qg(γ)
qg(p)
sum
ep → π± + X
pt=5 GeV
Mp=Mγ=Mf=μ=PT
dσ/dptdη (pb/Gev)
10^4
10^3
10^2
10
1
10^-1
10^-2
−5
−4
−3
−2
−1
0
1
2
3
ηlab

Fig. 9b

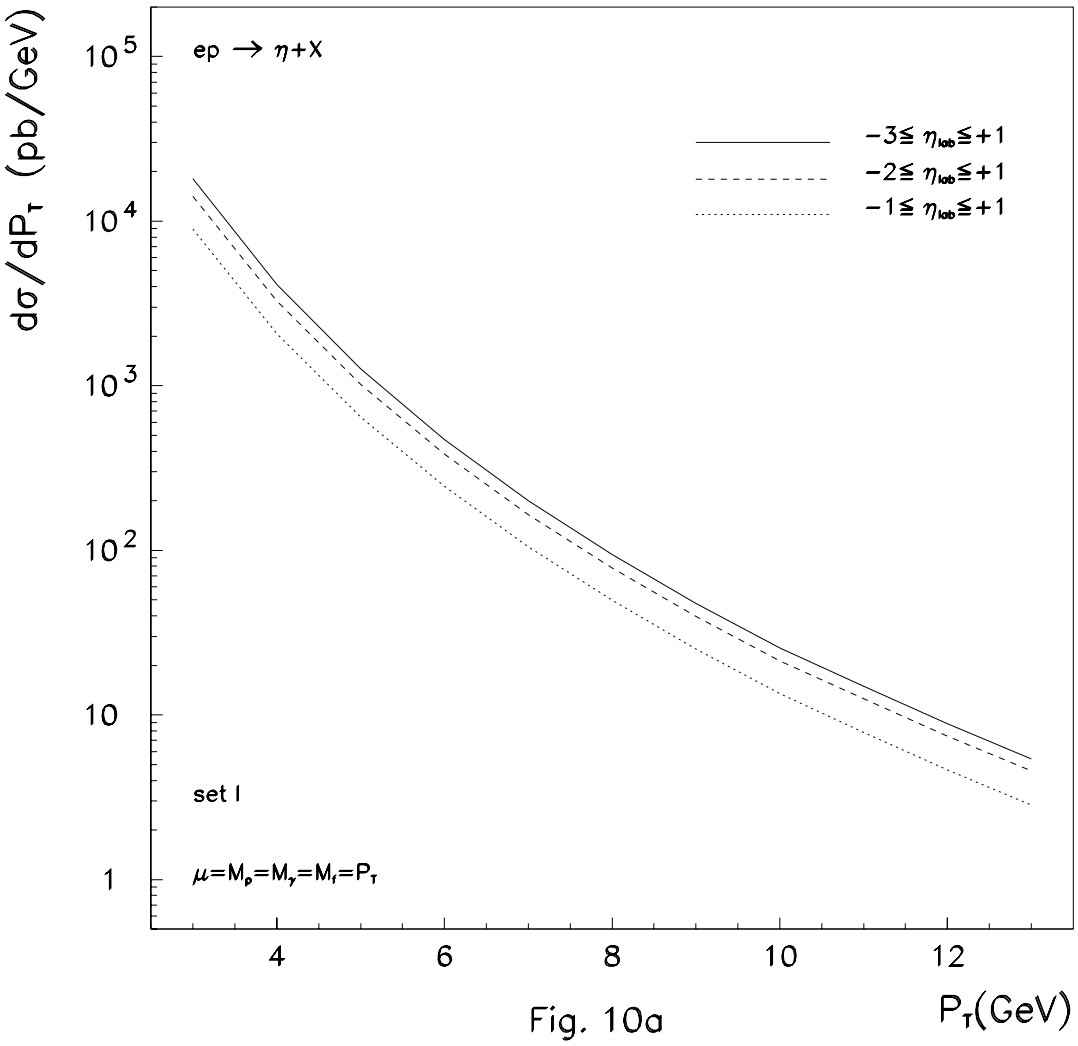
ep → η+X
dσ/dP_T (pb/GeV)
10^5
10^4
10^3
10^2
10
1
−3≦ η_lab≦+1
−2≦ η_lab≦+1
−1≦ η_lab≦+1
set I
μ=M_p=M_γ=M_f=P_T
4
6
8
10
12
P_T(GeV)

Fig. 10a

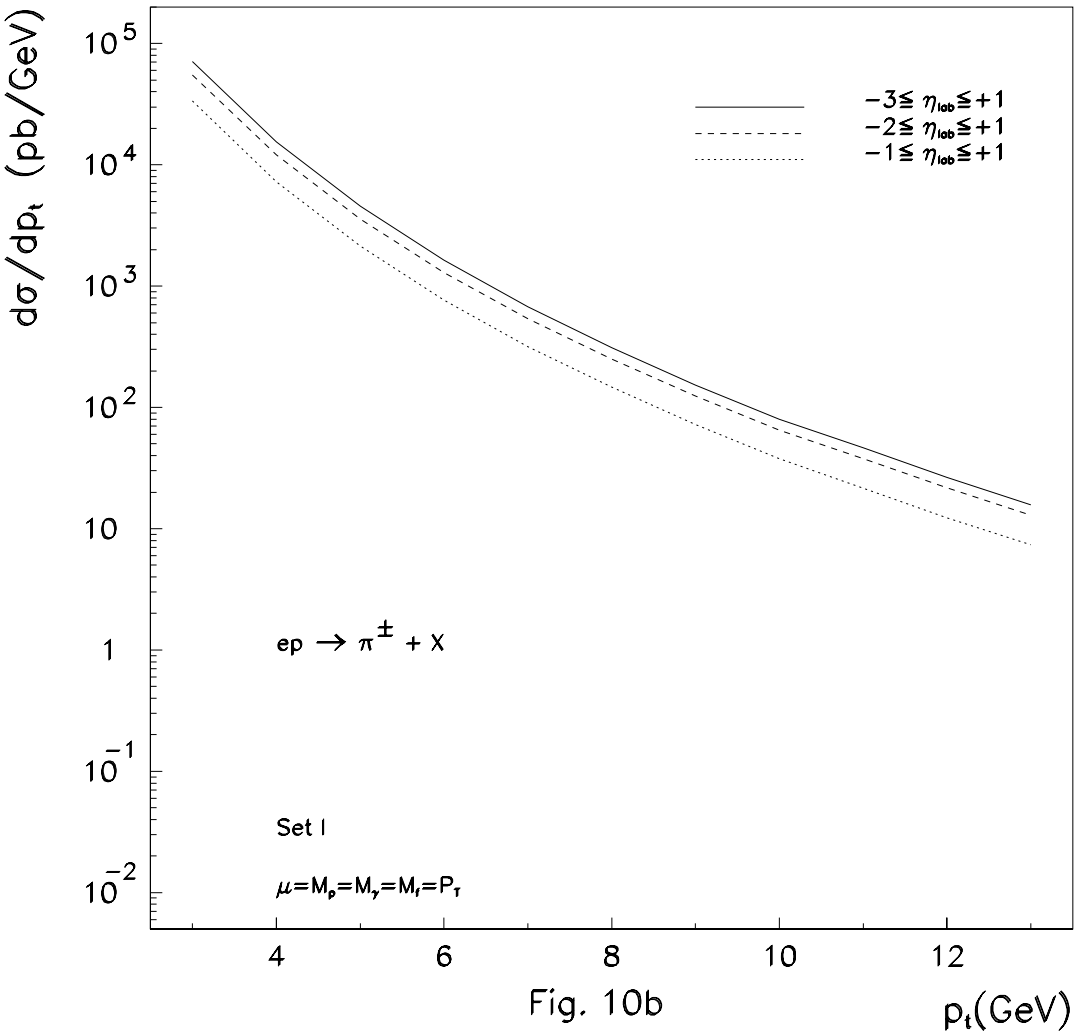
dσ/dp_t (pb/GeV)
10^5
10^4
10^3
10^2
10
1
10^-1
10^-2
−3≦ η_lab≦+1
−2≦ η_lab≦+1
−1≦ η_lab≦+1
ep → π^± + X
Set I
μ=M_p=M_γ=M_f=P_T
4
6
8
10
12
p_t(GeV)

Fig. 10b

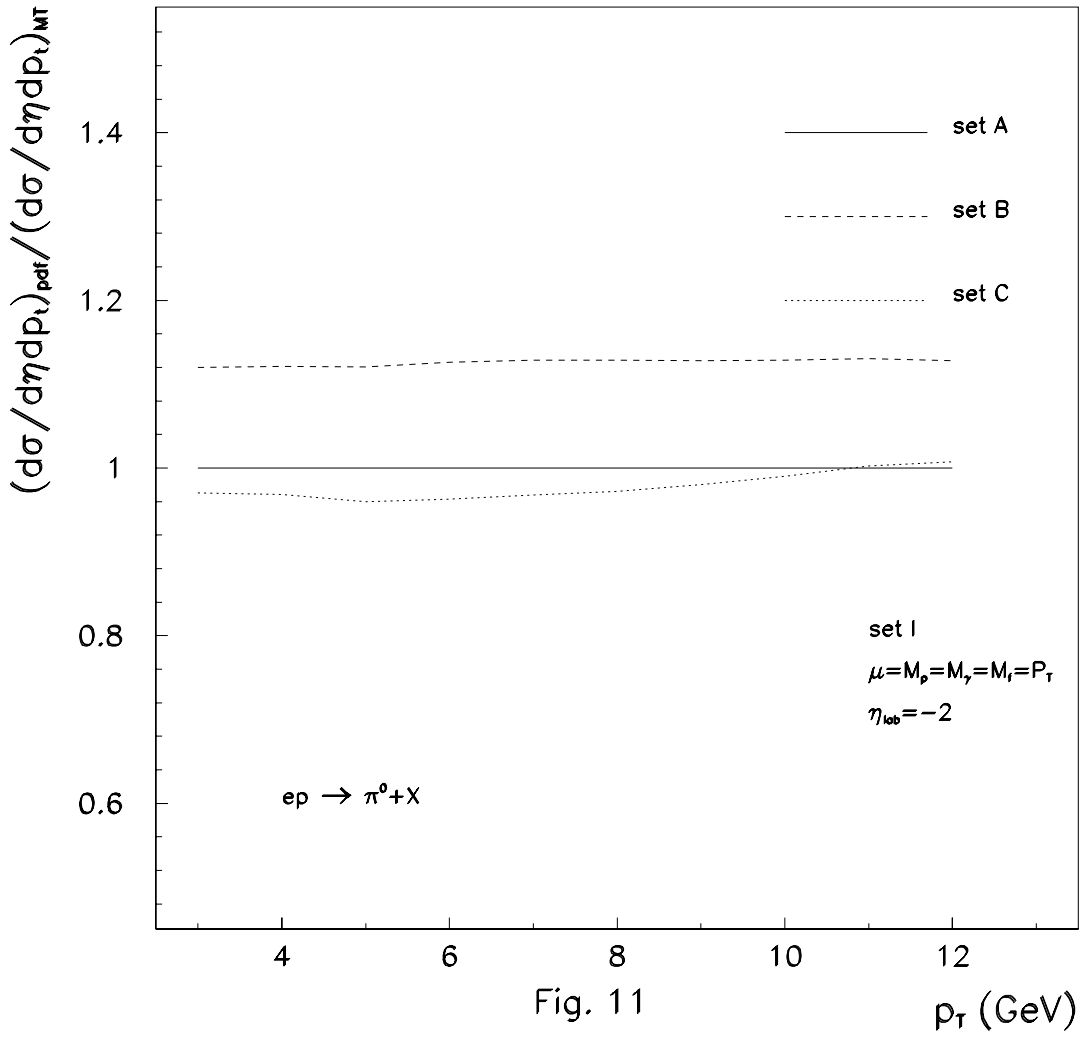
$(d\sigma/d\eta dp_t)_{pdf}/(d\sigma/d\eta dp_t)_{MT}$
1.4
1.2
1
0.8
0.6
set A
set B
set C
set I
$\mu=M_p=M_\gamma=M_f=P_T$
$\eta_{lab}=-2$
$ep \rightarrow \pi^0+X$
4
6
8
10
12
p_T (GeV)

Fig. 11

various mass scales, which is still significative in the considered p_t range. The inclusion of the direct component should make this effect weaker. We stress that the gluon content of the proton can be accurately disentangled via the photoproduction of single particles at HERA.

Chapter 5

Production of $Wb\bar{b}$ plus jets

5.1 Introduction

In this chapter we will study the production of $Wb\bar{b}$ in association with jets, using a parton level matrix elements calculation for production of $Wb\bar{b} + n$ partons in the massless limit and a parton shower MC in order to account for parton fragmentation into jets. We will show that after fragmentation there is not difference between using massless matrix elements and the ones corrected for mass effects, in the particular case of $Wb\bar{b}$ production.

5.2 $Wb\bar{b}$ plus jets and top signal background

The Tevatron experiments CDF and D0 gave evidence for the existence of top quark in 1994-1995 [48,49,51,55]. The production cross section is in agreement with the theoretical calculation [56] while the mass results are quite different: CDF quotes a top mass of 176±8 (stat.)±10 (sys.) GeV/c^2 while D0 gives 199±20(stat.)±22 GeV/c^2. In this range of mass, nevertheless, a produced top decay into a real W and a bottom quark, with the subsequent decay of the W into a lepton or quark pair. Detecting the top required a precise understanding of the possible sources of background to every selected decay channel and this remains true even now, after the discovery of the top quark, when for example one would like to study in detail properties such as mass or angular distributions of decay products.

From the point of view of the background the two most reliable alternatives are certainly the single and double leptonic decays. They have complementary features, the dilepton channel being relatively background free, but with a smaller branching ratio and more difficult possibility to reconstruct both the t, the single lepton having a higher branching ratio and allowing a more precise reconstruction of one of the two t quarks. Unfortunately we know that the background from associated production of W and multijets is rather severe and has a large overall uncertainty in the calculated rate. It is then important to isolate distinct features which could unambiguously separate signal from background. A stronger evidence that could discriminate the signal from background on an event by event basis (rather than on a statistical one) comes from the direct tagging of one of the b quarks in the event via the reconstruction of its decay vertex. Events are initially selected via the leptonic decay of one of the W's and then the presence of a b-tag is requested. The probability that an event with W not coming from a top decay has a b quark is expected to be very small, and therefore the background to the top is substantially reduced. In a previous work [57] M. Mangano studied at which extent this

is true and how well we can determine the sources of background to b-tagging, using an exact calculation of the parton level matrix element for production of $Wb\bar{b}$ with the correct mass effect included and subsequently convoluting it with HERWIG parton shower MC in order to account for the jets activity, owing the fact that the exact matrix elements calculation for $pp \rightarrow Wb\bar{b} + jets$ with the correct b mass effects included does not exist.

In this work we will be in some way complementary to the one of Mangano. We will start infact from the LO partonic matrix elements calculation of $pp \rightarrow Wb\bar{b}+$ partons in the massless limit [62] given by the MC VECBOS and use the parton shower MC HERWIG in order to study the structure of the final state jets after the perturbative evolution and the parton→jet transition. In this way we partially solve the problem of having a massless $b\bar{b}$ by the fact that HERWIG assigns the correct masses to the b's at the beginning of the parton shower evolution. As we know the shower MC will then evolve the partons involved in the hard scattering process via a branching algorithm, in which the emissions probabilities are calculated in accordance to the Altarelli-Parisi splitting functions. The radiation emitted during initial and final state will give rise to additional jets. Owing the fact that in the massless limit we have to request that the b's are hard and well separated (in order to avoid infrared and collinear divergences) and for this reason it is impossible to control the rate of background down to small values of the b momentum as well as small separations, we will check that the necessary parton level cuts are not biasing the prediction in the contest of top analysis. In the case of relatively light top (say around 100-120 GeV) this could be not true, because in this case the b's will be soft and in order not to loose much signal one would not be able to afford requiring the b's to form stiff jets. Of course up to higher top masses b's become less and less soft, and the massless calculation becomes more reliable. Has been shown infact [57] that for 120 GeV $\leq m_{top} \leq$160 GeV, requiring the presence of at least two

jets passing the following cuts : $E_t \geq 20$ GeV , $|\eta| \leq 2$ in $t\bar{t}$ events, with $|\eta_b| \leq 1$, is highly efficient in severely reducing the background. For higher top masses, when the production rate is very small, additional cuts can be placed (for example requiring an higher E_t^{jet} threshold). In this case most of the events passing these cuts, in the signal sample, will have b quarks with $p_t \geq 20$ GeV. And this remove us from the "dangerous" zone of soft b's limit.

We show in figure 1 the p_t distribution for the first b-quark in events in which we request at least 2jets with $E_t \geq 15$ GeV and $|\eta| \leq 2$. We also request that the lepton cuts are the following: $P_t^{lep} \geq 20$ GeV and $|\eta_{lep} \leq 2$. Solid line is the result obtained using $Wb\bar{b}$ massless matrix element +HERWIG, while dashed line is the one from $Wb\bar{b}$ massive matrix element +HERWIG and dotted is for HERWIG $t\bar{t}$ production at $m_{top} = 175$ GeV. The three distribution have been normalized to the unit area. In Figure 2 we see the same distribution compared with HERWIG $t\bar{t}$ production with m_{top}=140 GeV.

We can safely say, that with the actual top mass we are far from the soft b's limit and then we can use the massless matrix element calculation.

The outline of the chapter is the following: in section 2 we will briefly describe the VECBOS MonteCarlo along with the interface to the parton shower and the selection of the subprocesses needed to produce $Wb\bar{b}$. Then in section 3 we will show some results compared with the ones obtained using the matrix elements for $Wb\bar{b}$ corrected for mass effects [57]. We will conclude in section 4.

5.3 VECBOS, HERPRT and the jet fragmentation

VECBOS is a parton level MonteCarlo that performs production of $W+n$ partons with $n \leq 4$, in the massless limit. It is based on a tree level

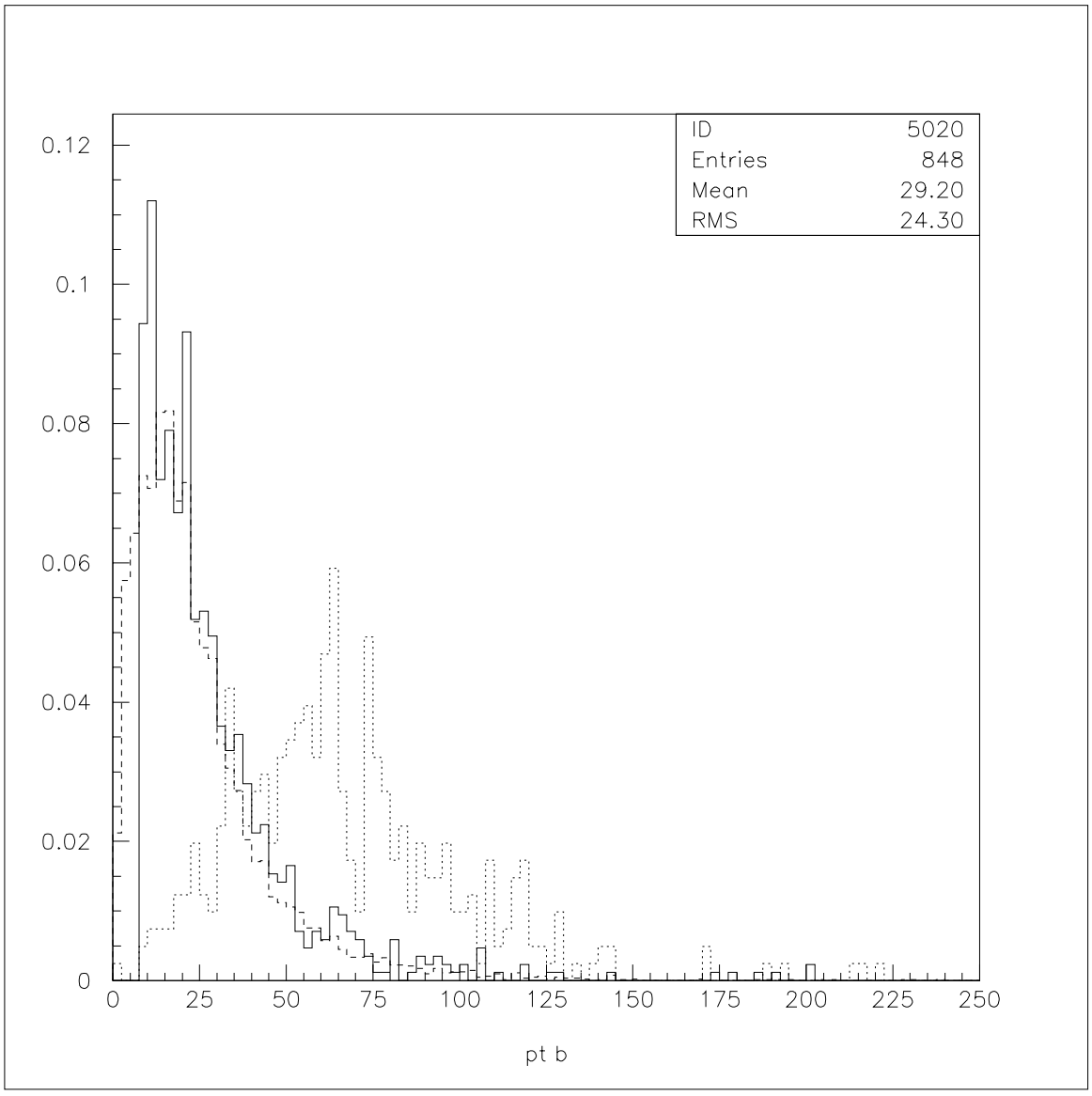

Figure 5.1: p_t distribution for the first b-quark in events in which we request at least 2jets with $E_t \geq 15$ GeV and $|\eta| \leq 2$. Solid line is the result obtained using VECBOS $Wb\bar{b}$ massless +HERWIG, dashed line is the one from Mangano $Wb\bar{b}$ massive +HERWIG and dotted is for HERWIG $t\bar{t}$.

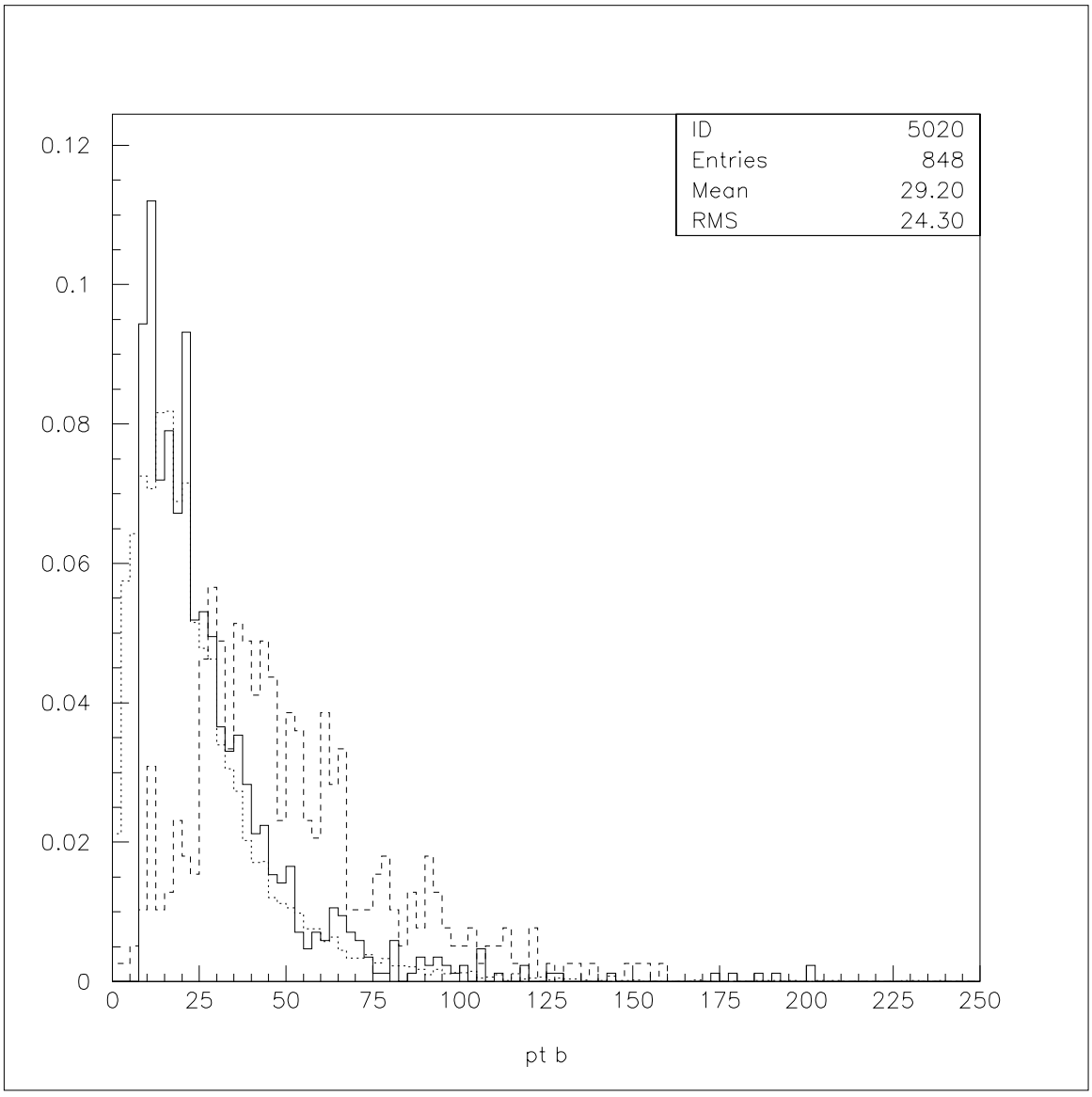

Figure 5.2: p_t distribution for the first b-quark in events in which we request at least 2jets with $E_t \geq 15$ GeV and $|\eta| \leq 2$. Solid line is the result obtained using VECBOS $Wb\bar{b}$ massless +HERWIG, dashed line is the one from Mangano $Wb\bar{b}$ massive +HERWIG and dotted is for TOP 140.

evaluation of the matrix elements obtained using elicity amplitudes techniques [62, 58]. In this calculations is of course necessary to apply cuts on the phase space of the outgoing partons in order to avoid infrared and collinear divergences. In a more experimental-oriented language this means that two of the outgoing partons will create a single jet, or that the jet is too close to the beam, or is not energetic enough to be observed. As we know adding virtual and real gluon emission diagrams will cancel the infrared divergences, while the collinear ones are absorbed in a redefinition of the parton density functions. Of course, the cross section will depend on how jets are defined, for example on what angle of separation is required to identify two partons as two different jets.

The calculation for W+ partons production is indeed at parton level. It gives infact the transition probabilities between quark and/or gluon states (with some additional particles which interact weakly, such as leptons and electroweak bosons). As we know quarks and gluons are not the observable of the experiment. The problem of "translating" a theoretical prediction at parton level to a simulation which gives as output quantities like jets that are directly measured in an experiment has been solved by CDF collaboration that has developed a simple algorithm (called HERPRT [59]) which transforms partons into jets. This algorithm is based on the parton shower fragmentation model and having assigned a partonic configuration it develops each of the partons into a radiation cascade, with the angular and energy spectrum of the emitted gluon or $q\bar{q}$ pairs determined by given probability distributions. The choice of the probability distributions is what makes the difference between the different MC's available (say ISAJET [60],HERWIG [47],PYTHIA [61]). The algorithm takes an arbitrary parton level configuration and turns it into a configuration with a definite assignment of flavors and colors. Once this is done, the event can be passed to the shower MC which will evolve it (both initial and final state radiation), hadronize the final gluons and quarks, decay unstable hadrons and include the interaction of the beam fragments.

In our case we started from the production of $W + n\ partons$ ($n \geq 2$) of which two are requested to be b's as performed by VECBOS MC. This is equivalent to considering a particular set of subprocesses contributing to the normal $W + n\ partons$ events. To be precise, asking for a $b\bar{b}$ massless pair in the final state means that we have to consider just those diagrams with two or more quark pairs, one pair representing the $b\bar{b}$ and the other representing the isospin doublet which couples to the W. In the case of $W + 2\ partons$ the only contribution comes from $q\bar{q} \rightarrow Wb\bar{b}$,while in the case of $W + 3\ partons$ we need to add the contributions coming from $gq(g\bar{q}) \rightarrow Wb\bar{b}q$, $qg(\bar{q}g) \rightarrow Wb\bar{b}q$ and finally in the case of 4 partons we have to consider also the contributions from $gg \rightarrow Wb\bar{b}q\bar{q}$ and $q\bar{q} \rightarrow Wb\bar{b}q\bar{q}$. We modified the routine that assigns flavour and color connections to the partons, in order to implement the case of a $b\bar{b}$ massless pair in the final state. In this way we can study the production of $Wb\bar{b}$ plus jets.

5.4 Results

In this section we present some distributions that can be of interested in comparing whenever possible the massless and massive approach after the fragmentation process. In order to reconstruct jets we used an algorithm developed by F. Paige to simulate standard jet clustering performed by hadron collider experiments [63]. This algorithm defines seed towers as regions of area $0.1 \times 15^\circ$ in $\eta\phi$ space containing more than 1 GeV of transverse energy. The transverse energy flowing in a cone of radius R_{jet} around a seed tower is collected to define a jet. We use R_{jet}=0.7, 1.0 and consider jets satisfying the following cuts: $p_t^{jet} > 15$ GeV and $|\eta| < 2.0$. We use set MRS Set (A) (L230-MSb) for structure functions, with $\Lambda_{QCD} = 230$ MeV. At the VECBOS stage of generation we have the following set of cuts: $p_t^{jet} \geq 8$ GeV, $|\eta_{jet}| \leq 3.5$, ΔR=0.4. We didn't place cuts on leptons.

In Table I we report the jet multiplicity for tho different choices of the

cone R_{jet}: 0.7, 1.0 after parton shower evolution of $W + b\bar{b}$ (massless b's) sample, $Wb\bar{b}$ massive sample and $Wb\bar{b} + 1$ parton sample.

Sample	jet multiplicity $R_{jet} = 0.7$	jet multiplicity $R_{jet} = 1.0$
$Wb\bar{b}$ massless	2.23	2.27
$Wb\bar{b}$ massive	1.87	1.92
$Wb\bar{b}$ massless +1 parton	2.82	2.87

Table I

In Figure 3, we show the correlation in $\eta\phi$ space between the first b and all the jets in the event. The solid line is obtained with VECBOS $Wb\bar{b}$ massless, while the shaded one is from the corrected matrix element calculation. Dotted line is the same correlation for top events.

In Figure 4 we show the correlation between the two leading jets, for reconstructed cones of 0.7 (upper) and 1.0. The different behaviour in the first bin is due to the fact that the b's are separated at parton level in the massless case while they are not in the massive case.

In Figure 5 we show the p_t distribution of the two leading jets for the massless (solid) and massive case (shaded). We found that starting with massive matrix element gives spectra a little bit softer, but this is in agreement with the fact that even the p_t^b spectrum is slightly softer in the massive than in the massless case (see Figure 1). The spectra are in any case in reasonable agreement.

In order to better understand the possible difference between the massive and massless cases, we calculate the number of times that, in events where we reconstruct two or more jets with p_t=15 GeV and $|\eta| \leq 2$, and the lepton satisfying the following cuts: $p_t^{lep} \geq 20$ GeV and $|\eta_{lep}| \leq 2$, the two b's belong each to the one of the two leading jets, the case in which b or $\bar{b}$ belongs to the leading jet, while $\bar{b}$ and b does not, the case in which both b's don't belong to the two leading jets and finally the case

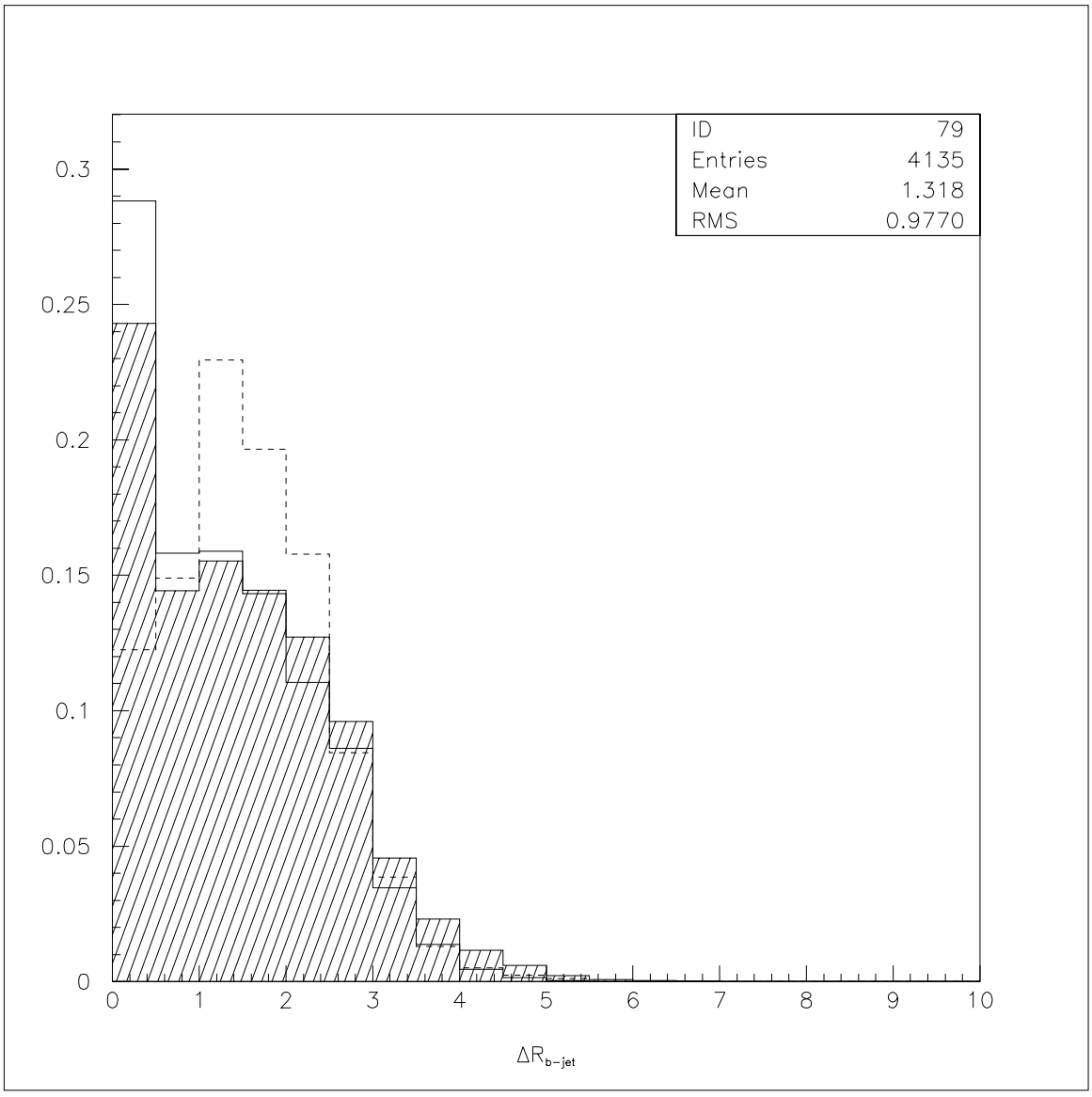

Figure 5.3: Correlations in $\eta\phi$ space between the first b and all the jets in the event. See text for explanations

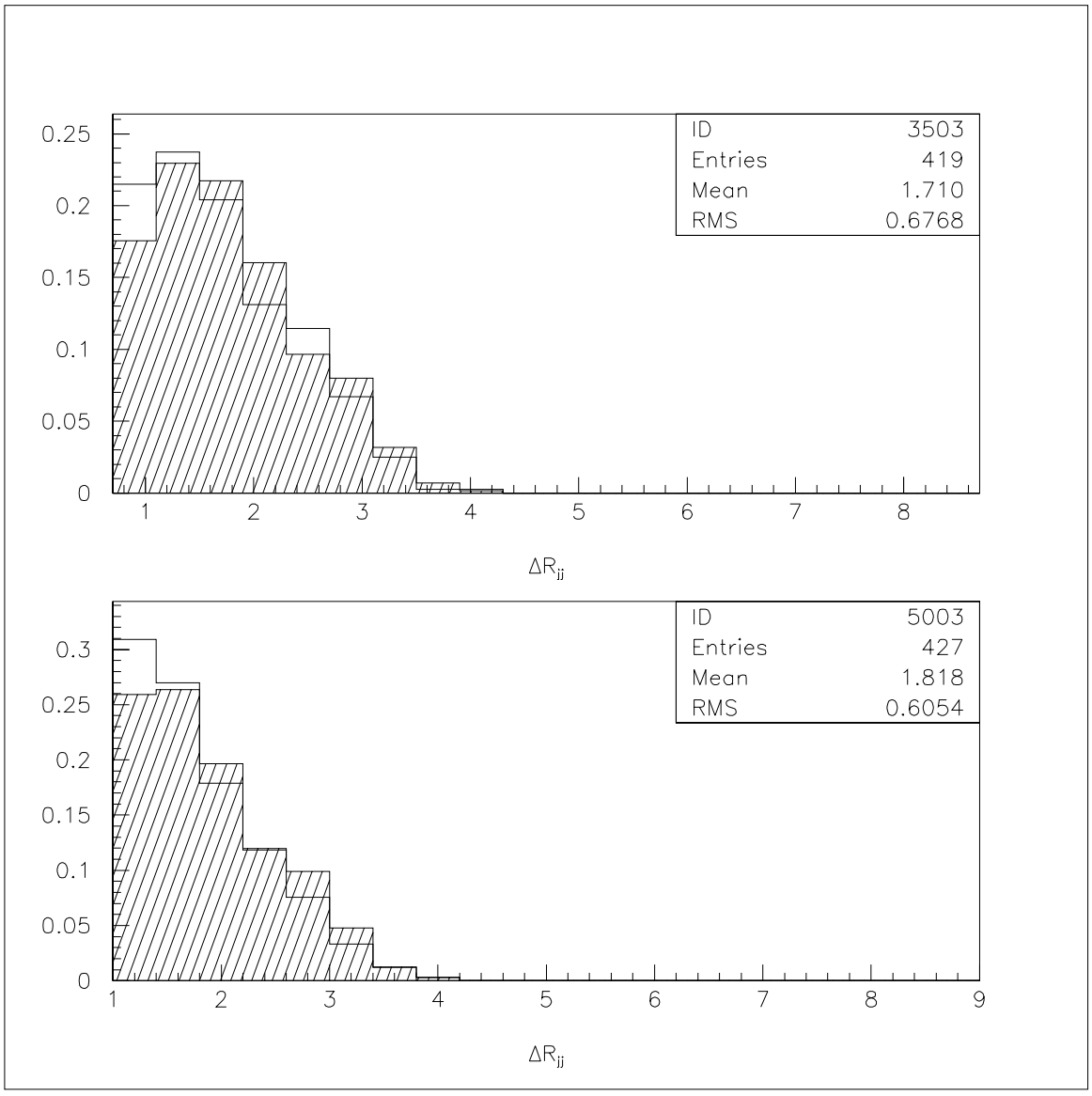

Figure 5.4: Correlation in $\eta\phi$ space of the two leading jets, after the fragmentation. Massive matrix element (shaded), massless (solid)

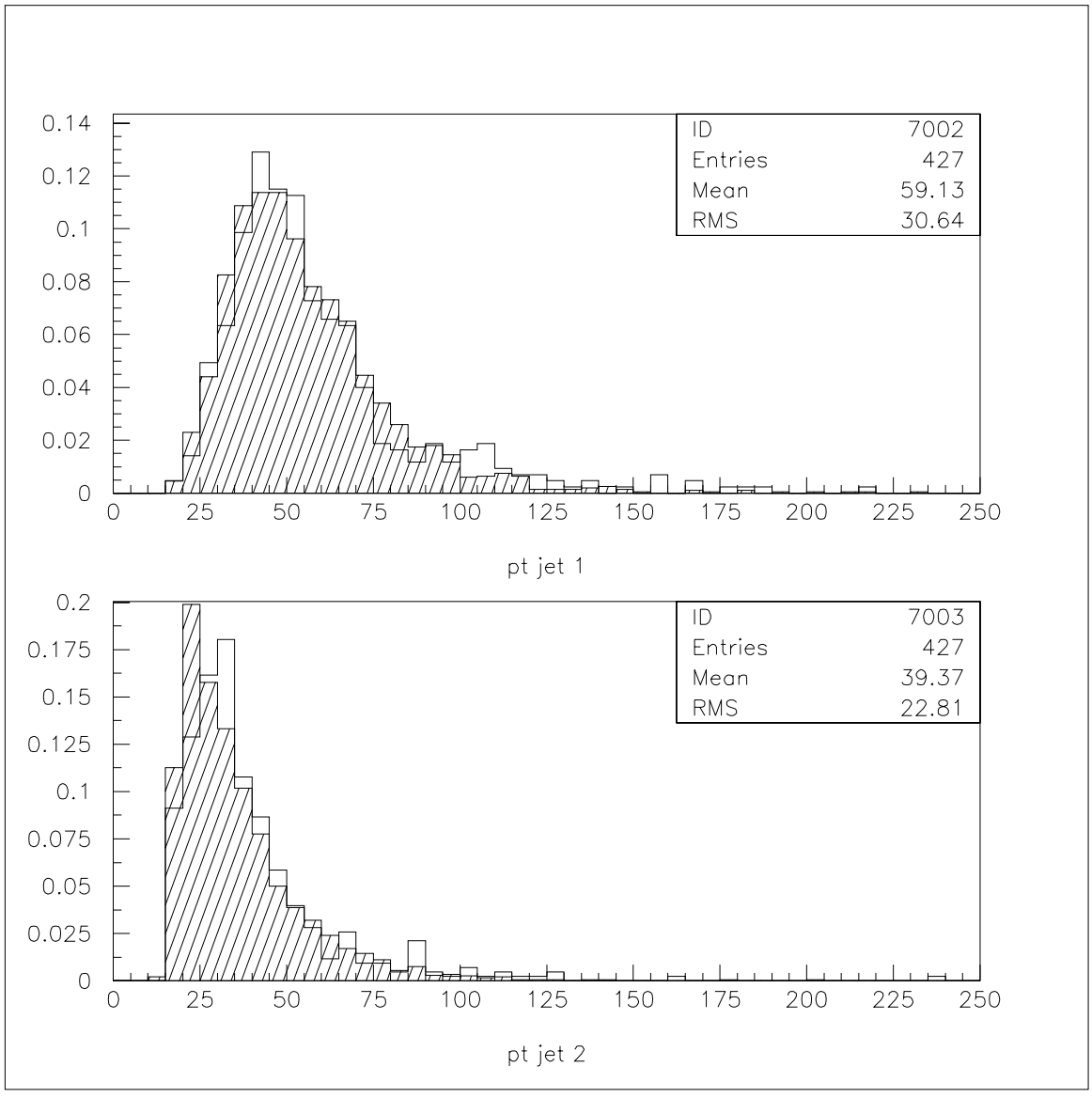

Figure 5.5: p_T distribution for the two leading jets, after fragmentation. Massive matrix element (shaded), massless (solid)

in which they belong to the same jets. The results is reported in Table II for VECBOS/HERPRT W+2jets and Mangano+HERWIG.

Combinations	VECBOS/HERPRT	Mangano/HERWIG
$b \in jet1\ \bar{b} \in jet2$	12%	11%
$b \in jet1(jet2)\ \bar{b} \notin jet1(jet2)$	60%	53%
$b\bar{b} \notin jet1(jet2)$	21%	15%
$b\bar{b} \in jet1(jet2)$	20%	22%

Table II

We can see that the results are quite similar in the case of VECBOS/HERPRT and $Wb\bar{b}$ massive+HERWIG. b and $\bar{b}$ give rise to separate jets, with almost the same frequency. We also plot in fig 6-7 the p_t distribution for the b-quark in the case it belongs to the leading or second leading jet, while the $\bar{b}$-quark does not, for VECBOS/HERPRT W+2jets and Mangano/HERWIG W$b\bar{b}$. In Fig 8-9 are the p_t distributions of the two leading jets in this case. The distributions look quite similar and the means are very close.

In Fig 10-11 we have the p_t distribution for b-quark and $\bar{b}$-quark in the case that both does not belong to the two leading jets. As we can see these are soft b's and the jets are given by initial state radiation.

To conclude, in this chapter we reported about the study on production of $Wb\bar{b}$ in association with jets. The calculation is complementary to the one performed using massive matrix element for $Wb\bar{b}$ production. In the case of top analysis, where we required high p_t b's we can reliably use the massless matrix element calculation. We showed some comparisons with distribution from the massive calculation and did not find substantial disagreement. We are then quite confident on the possibility to use VECBOS/HERPRT as a tool to study the $Wb\bar{b} + \ jets$ background to top.

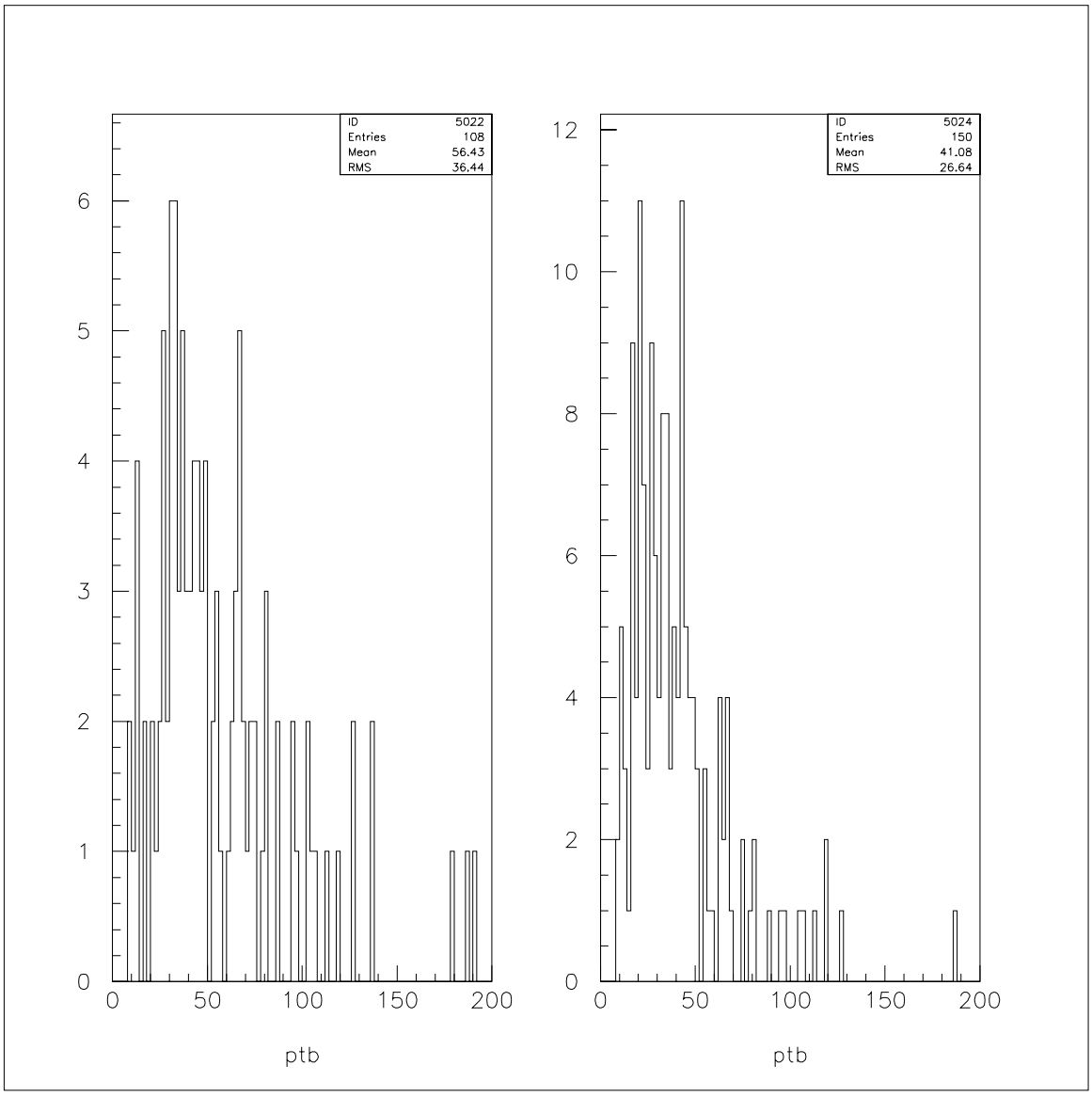

Figure 5.6: p_t distribution of the b-quark in events with two or more jets with p_t^{jet} $\geq$15 GeV and $|\eta|_{jet} \leq 2$, whit the b-quark belonging to the leading jet or second leading and the $\bar{b}$-quark not. VECBOS/HERPRT W+2jets

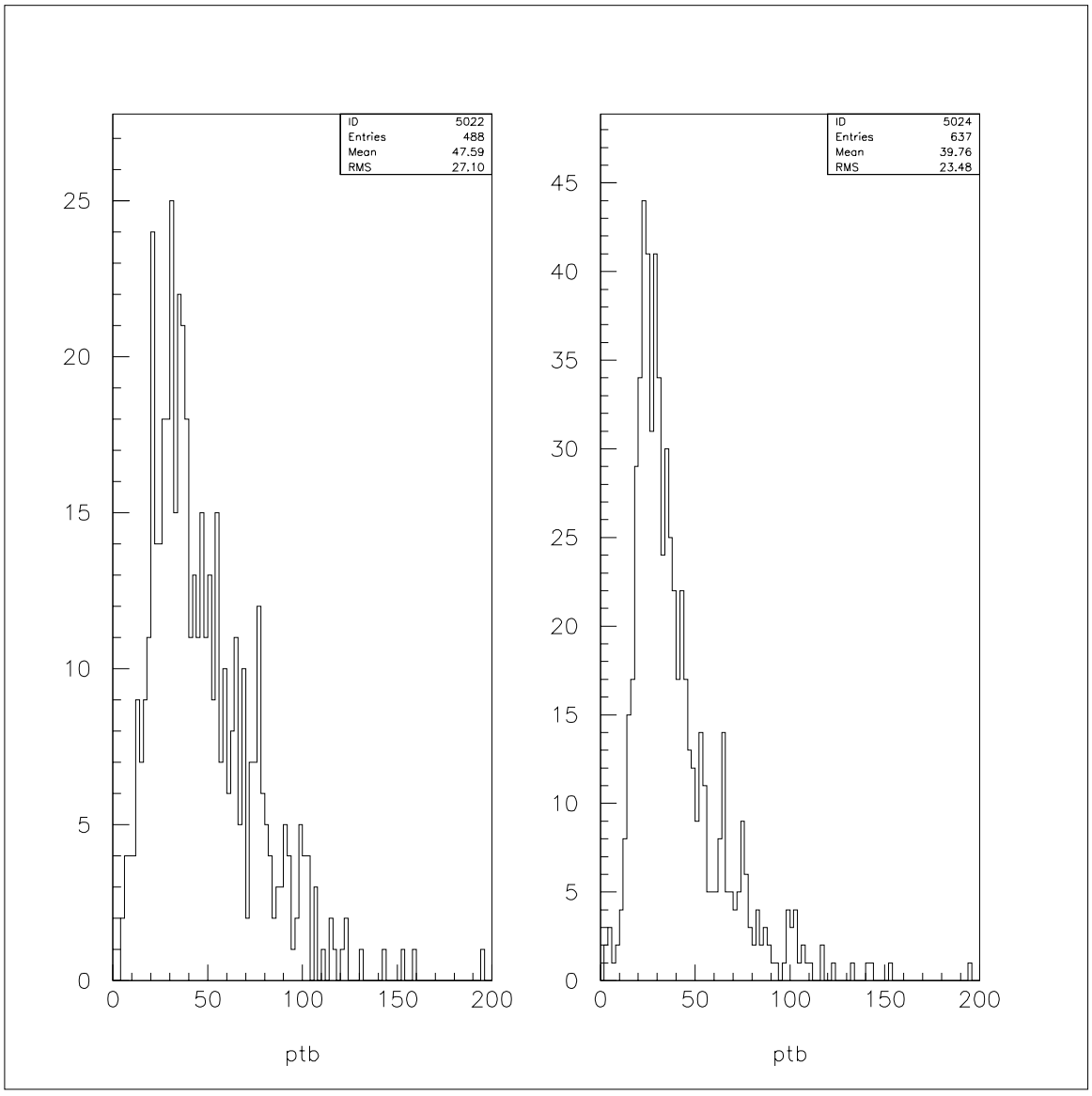

Figure 5.7: p_t distribution of the b-quark in events with two or more jets with p_t^{jet} $\geq$15 GeV and $|\eta|_{jet} \leq 2$, with the b-quark belonging to the leading jet or the second leading and the $\bar{b}$-quark not. Mangano+HERPRT+QFL

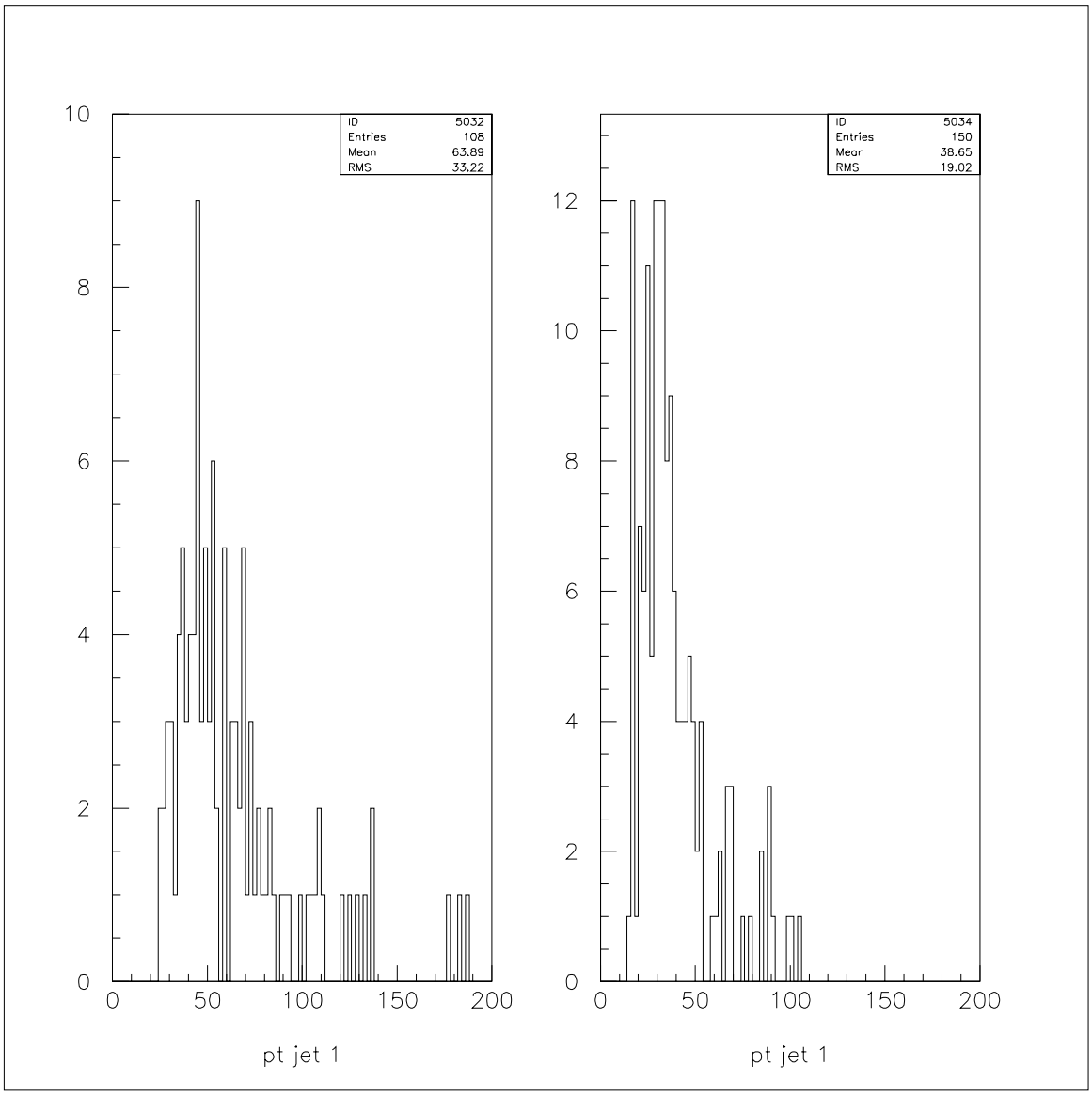

Figure 5.8: p_t distribution of the two leading jets in events with two or more jets with $p_t^{jet} \geq$15 GeV and $|\eta|_{jet} \leq 2$, whit the b-quark belonging to the leading jet or second leading and the $\bar{b}$-quark not. VECBOS/HERPRT W+2jets

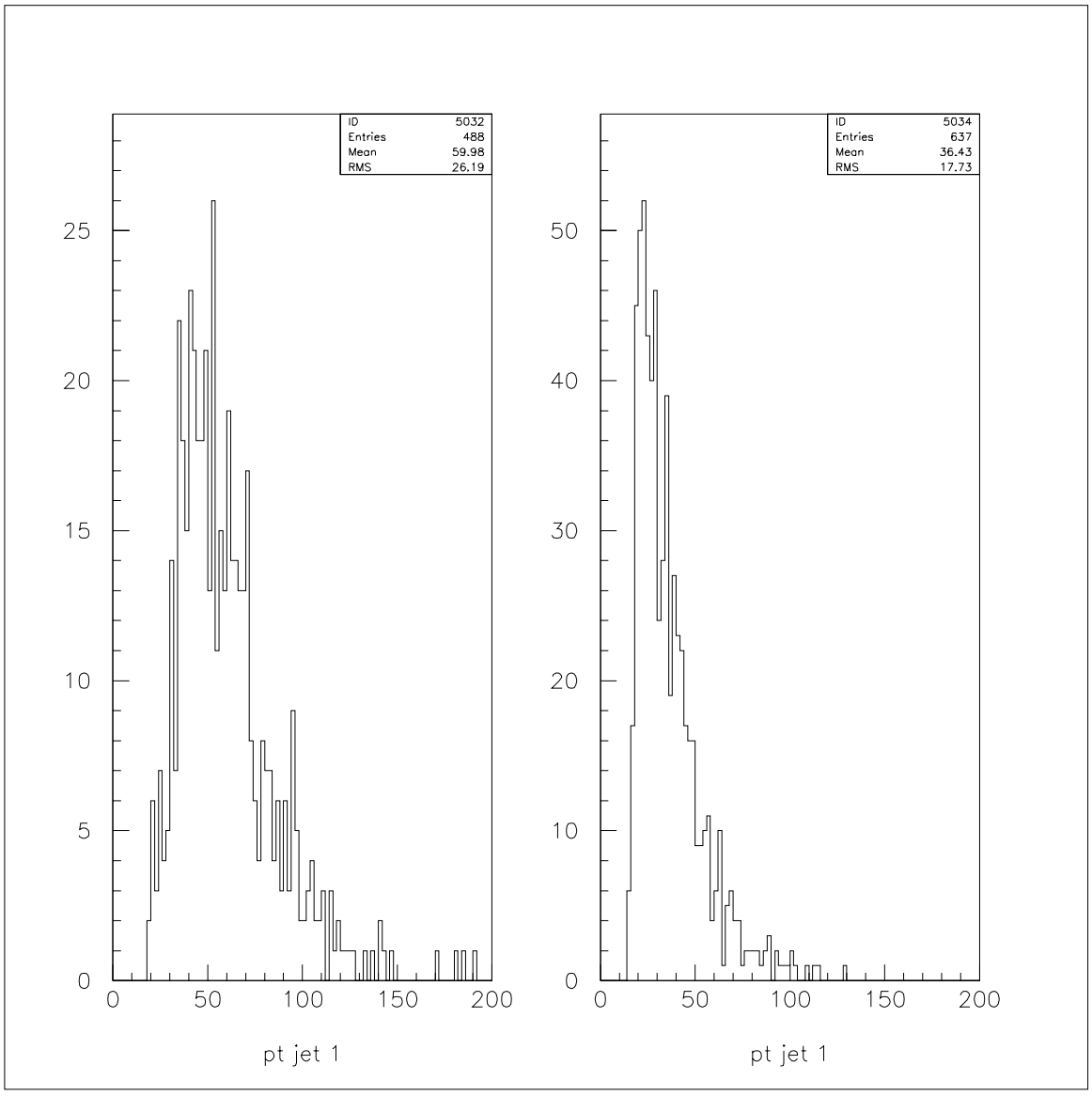

Figure 5.9: p_t distribution of the two leading jets in events with two or more jets with $p_t^{jet} \geq 15$ GeV and $|\eta|_{jet} \leq 2$, with the b-quark belonging to the leading jet or the second leading and the $\bar{b}$-quark not. Mangano+HERPRT+QFL

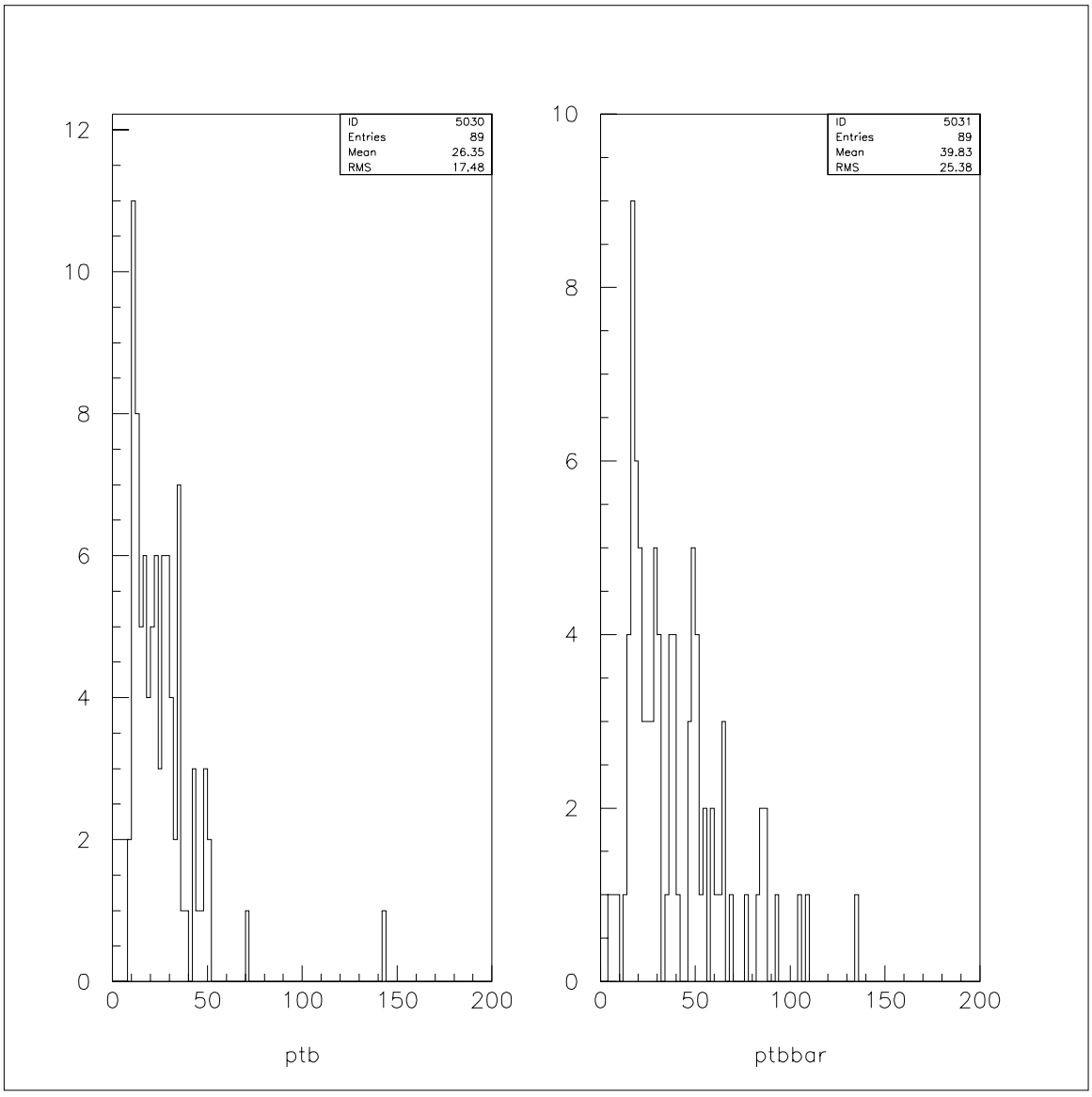

Figure 5.10: p_t distribution of the b-quark and $\bar{b}$-quark in events with two or more jets with $p_t^{jet} \geq$15 GeV and $|\eta|_{jet} \leq 2$, when the two quarks does not belong to either the leading or second leading jet. VECBOS/HERPRT W+2 jets

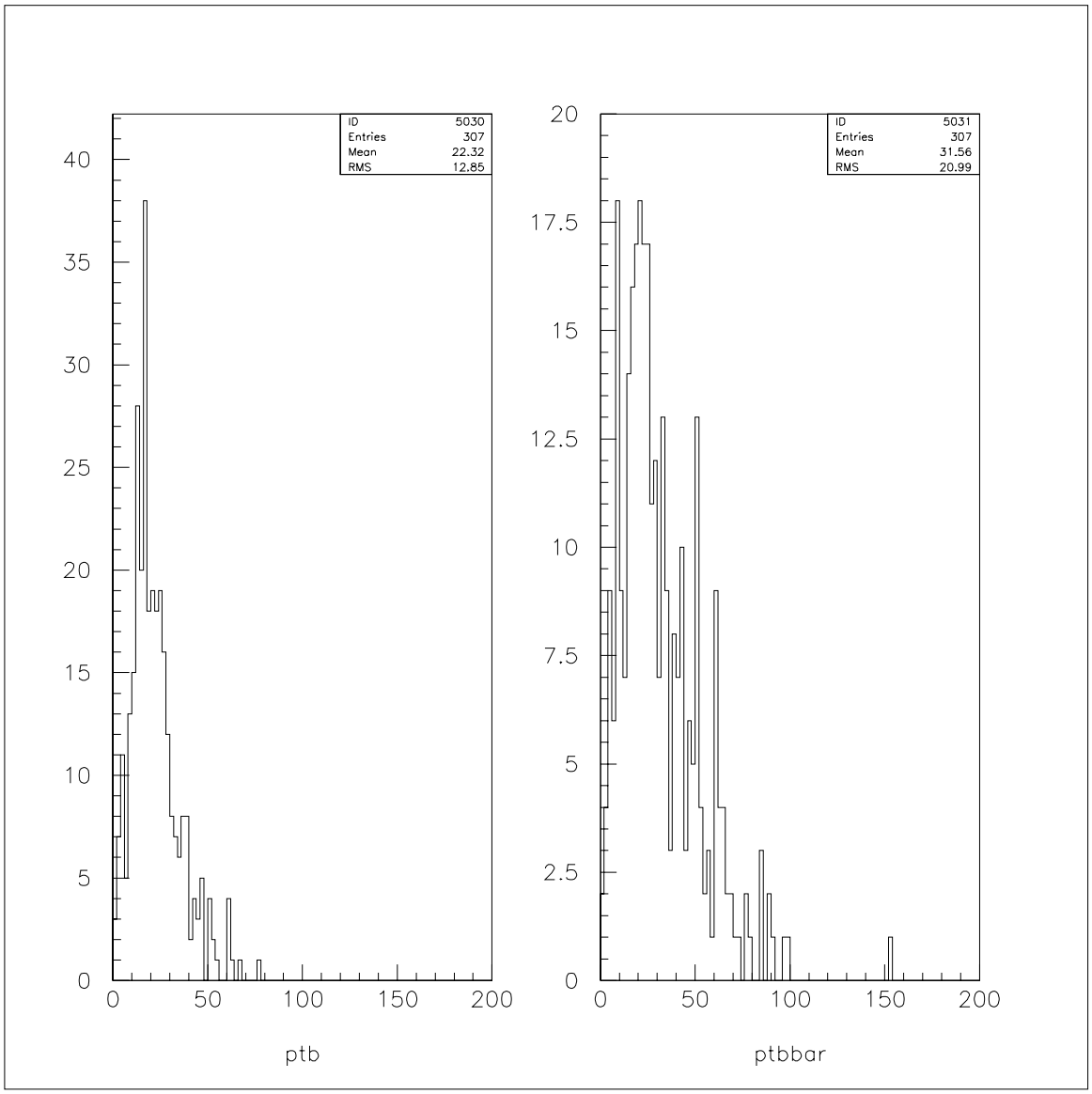

Figure 5.11: p_t distribution of the b-quark and $\bar{b}$-quark in events with two or more jets with $p_t^{jet} \geq$15 GeV and $|\eta|_{jet} \leq 2$, when the two quarks does not belong to either the leading or second leading jet. Mangano-HERWIG

Bibliography

[1] G. Altarelli, Phys. Rep. 81 (1982) 1

[2] M. Breidenbach et al. ,Phys. Rev. Lett. 23 (1969) 935

[3] G. Altarelli, G. Parisi, Nucl. Phys. B126 (1977) 298

[4] G. Altarelli, R. K. Ellis, G. Martinelli e S. Y. Pi, Nucl. Phys. B160 (1979) 301

[5] F. Aversa, P. Chiappetta, M. Greco e J. Ph. Guillet, Nucl. Phys. B327 (1989) 105

[6] S. Ellis, D. Soper, Z. Kunzst, Phys. Rev. Lett 62 (1989) 726; S. Ellis, D. Soper, Z. Kunszt, Phys. Rev D40 (1989) 2188

[7] J.F.Owens, Phys. Lett. B76 (1978) 85, T.Uematsu, Phys. Lett. B79 (1978) 97

[8] B. Mele, P. Nason, Nucl. Phys. B361 (1991) 626

[9] JADE collab.: W. Bartel et al., Z. Phys. C28, 343 (1985).

[10] TPC collab.: H. Aihara et al., Z. Phys. C27, 187 (1985).

[11] TASSO collab.: W. Braunschweig et al., Z. Phys. C33, 13 (1986).

[12] CELLO collab.:H. J. Behrend et al., Z. Phys. C47, 1 (1990).

[13] CELLO collab.: H. J. Behrend et al., Z. Phys. C20, 207 (1983). H. J. Behrend et al., Z. Phys. C47, 1 (1990). W. Braunschweig et al., Z. Phys. C33, 13 (1986).

[14] ARGUS collab.: H. Albrecht et al., Z. Phys. C46, 15 (1990).

[15] L3 Collaboration, Phys. Lett. B259, 199 (1991).

[16] B.R. Webber, CERN-TH 6706/92 (1992).

[17] J. G. Morfin and W. K. Tung, Z. Phys. C52, 13 (1989).

[18] A. D. Martin, R. G. Roberts and W. J. Stirling, Phys. Rev. D37, 1161 (1988); Mod. Phys . Lett A4, 1135 (1989); P. N. Harriman, A. D. Martin, R. G. Roberts and W. J. Stirling, Phys. Rev. D42, 798 (1990) and Phys. Rev. D42, 3645 (1990).

[19] P. Aurenche, R. Baier, M. Fontannaz, J.F. Owens and M. Werlen, Phys. Rev. D39, 3275 (1989).

[20] P.M.Stevenson and H.D.Politzer, Nucl. Phys. B277, 758 (1986). P.Aurenche, R.Baier, M.Fontannaz and D.Schiff, Nucl. Phys. B286, 509 (1987).

[21] TPC collaboration, LBL23737 (1988);

[22] R.Baier and K.Fey, Z. Phys. C2 (1979) 339.

[23] F.Aversa, P.Chiappetta, M.Greco and J.Ph.Guillet, Nucl. Phys. B327, 105 (1989).

[24] WA70 collab.: M. Bonesini et al., Z. Phys. C38, 371 (1988).

[25] E706 collab.: G. Alverson et al., Phys. Rev. D45, 3899 (1992).

[26] AFS collab.: T. Akesson et al., Sov. J. Nucl. Phys. 51, 836 (1990).

[27] C. Kourkoumelis et al., Z. Phys. C5, 95 (1980).

[28] UA2 collab. 630 GeV: R. Ansari et al., Z. Phys. C41, 395 (1988); UA2 collab. 540 GeV: M. Banner et al., Z. Phys. C27, 329 (1985). ; M. Banner et al., Phys. Lett. B115, 59 (1982).

[29] J. Binnewies, B. A. Kniehl and G. Kramer; Z. Phys. **C 65** 471 (1995)

[30] J.E.Huth et al., Fermilab-Conf-90/249-E (1990).

[31] CDF Collaboration, Phys. Rev. Lett. 65 968 (1990).

[32] CDF Collaboration, Phys. Rev **D48** 2998 (1993).

[33] P.Aurenche et al.; Nucl.Phys. B 286 (1987) 553.

[34] F. M. Borzumati, B. A. Kniehl, G. Kramer; Z.Phys. C 59 (1993) 341.

[35] M. Greco and A. Vicini; Nucl. Phys. B 415, 386 (1994);

[36] S. Frixione, M. Mangano, P. Nason, G. Ridolfi; Phys. Lett. B 314 (1993) 339.

[37] E. Witten, Nucl. Phys. B 120 (1977) 189.

[38] R.K.Ellis and J.C.Sexton; Nucl.Phys.B 269 (1986) 445.

[39] M. Glück, E. Reya, A. Vogt; Z.Phys. C 53 (1992) 127

[40] P.Aurenche, P.Chiappetta, M.Fontannaz, J.Ph.Guillet and E.Pilon; Z.Phys. C 56 (1992) 589.

[41] M.Glück, E.Reya and A.Vogt; Phys.Rev. D45 (1992) 3986.

[42] L.E.Gordon and J.K.Storrow; Phys.Lett. B 291 (1992) 320, L.E.Gordon and J.K.Storrow Z.Phys. C 56 (1992) 307.

[43] H.Baer, J.Ohnemus and J.F.Owens; Z.Phys. C 42 (1989) 657.

[44] R.K.Ellis,P.Nason and S.Dawson; Nucl.Phys.B 303 (1988) 724.

[45] G. Kramer and S. G. Salesch; Z.Phys. C 61 (1993) 277.

[46] R. Baier, J. Engles, B. Petersson: Z. Phys. C 2 (1979) 265; M. Anselmino, P. Kroll, E. Leader: Z. Phys. C 18 (1983) 307.

[47] G. Marchesini et al., Comp. Phys. Comm. 67(1992)465

[48] CDF collaboration, Phys. Rev D50 (1994) 2966

[49] CDF collaboration, Phys. Rev. Lett.74 (1995) 2626

[50] "Calibration stability and Jet energy scale; Run 0 and Run 1A compared" by B. Flaugher, S. Berhends, A. Bhatti, P. Derwent, S. Kuhlmann, T. LeCompte, P. Schlabach, CDF-2902, December, 1994.

[51] CDF collaboration, Phys. Rev. Lett.70 (1993) 714

[52] "S. B. Kim, S. Vejcik, "Evidence for additional underlying Event Energy from multiple interactions in Z + jets events", CDF-3247, July 1995.

[53] W.M. Yao, L. Galtieri, M. Garcia-Sciveres, J. Lys in " Studies of Gluon Radiation systematics with $b\bar{b}$ events and a Proposal for multiple underlying event correction on the Jet Energy" CDF-3257, July 1995.

[54] L. Galtieri, M. Garcia-Sciveres, J. Lys, W. Yao, S. Rolli in "Gluon Radiation Studies using the W+$\geq$1 jet sample", CDF-3253, July 1995.

[55] DZero Collaboration, Phys. Rev. Lett.74 (1995) 2632;

[56] E. Lenen, J. Smith and W. L. van Nerven, Nucl. Phys. B369 (1992) 543; E. Lenen, J. Smith and W. L. van Nerven, Phys. Lett. B321 (1994) 254;

[57] M. Mangano, Nucl. Phys. B405 (1993) 536;

[58] S. Rolli, B. Drucker, L.Galtieri "The CDF VECBOS manual" CDF/DOC/MONTECARLO/CDFR/3185;

[59] J. Bennloch, Alessandra Caner, Teresa Rodrigo and Michelangelo Mangano. "On transforming partons into jets: HERPRT, a new interface between ME MC and fragmentation models". CDF/DOC/MONTECARLO/1823;

[60] F. Paige and S.D. Protopopescu, Brookhaven report BNL-38034 (1986);

[61] T. Sjöstrand and M. Bengtsson, Comp. Phys. Comm. 43(1987)367;

[62] F. A. Berends, W. T. Giele, H. Kuijf, Nucl. Phys. B321(1989) 39; F. A. Berends, H. Kuij, B. Tausk and W. T. Giele, f, Nucl. Phys. B357(1991) 32;

[63] M. Mangano, private communication;